Use of Microelectrochemical Devices to Study Diffusion of Electroactive Species in Nonfluid Media and Photoelectrochemistry of Surface-Confined Metallocenes

by

Helen B. Tatistcheff

B.S., University of Puget Sound
(1988)

Submitted to the Department of Chemistry
in Partial Fulfillment of the Requirements for the
Degree of Doctor of Philosophy

at the

Massachusetts Institute of Technology
May 1994

Signature of Author _____
Department of Chemistry
April 28, 1994

Certified by _____
Mark S. Wrighton
Thesis Supervisor

Accepted by _____
Glenn A. Berchtold
Chairman, Departmental Committee on Graduate Students

This doctoral thesis has been examined by a Committee of the Department of Chemistry as follows:

Professor Stephen J. Lippard _____ Chairman

Professor Mark S. Wrighton _____ Thesis Supervisor

Professor Hans-Conrad zur Loye _____

USE OF MICROELECTROCHEMICAL DEVICES TO STUDY DIFFUSION OF ELECTROACTIVE SPECIES IN NONFLUID MEDIA AND PHOTOELECTROCHEMISTRY OF SURFACE-CONFINED METALLOCENES

by

Helen B. Tatistcheff

Submitted to the Department of Chemistry on April 28, 1994 in partial fulfillment of the requirements for the Degree of Doctor of Philosophy in Chemistry

Abstract

CHAPTER 1: GENERAL INTRODUCTION: THE BEHAVIOR OF ULTRAMICROELECTRODES AND THEIR VALUE IN INVESTIGATING DIFFUSION PHENOMENA

The importance of electrodes with small dimensions for diffusion measurements is described. An overview of various types of ultramicroelectrodes is given.

CHAPTER 2: A COMPARISON OF DIFFUSION COEFFICIENTS OF ELECTROACTIVE SPECIES IN AQUEOUS FLUID ELECTROLYTES AND POLYACRYLATE GELS

We report electrochemical measurement of diffusion coefficients, D, and operation of electrochemical devices using potential step generation-collection on arrays of closely spaced microelectrodes in aqueous polyacrylate gels formed by neutralization of poly(acrylic acid), MW = 4×10^6 Da. Aqueous solutions form gels with viscosities as high as 5×10^4 cP. For 1,1'-*bis*(hydroxymethyl)ferrocenium D was found to be $5.8(\pm 0.4) \times 10^{-6}$ cm^2/s in the gel electrolyte (aqueous 0.5% poly(acrylic acid) at pH 7) and $8.8(\pm 0.8) \times 10^{-6}$ cm^2/s in the aqueous fluid electrolyte 0.1 M $NaCH_3CO_2$ (pH 7). The small decrease observed in D for the gel vs. the fluid with such a large increase in viscosity is unusual, but is in accord with the structure of polyacrylate gels which consists of two phases. Electrochemical transistors based on ruthenium oxide exhibit similar operating characteristics in both polyacrylate gel and aqueous fluid electrolytes. Response times of electrochromic polymer films made from *N,N'-bis*[*p*-(trimethoxysilyl)benzyl]-4,4'-bipyridinum are slower in gel by about a factor of ten compared to aqueous fluid electrolytes.

CHAPTER 3: PULSE GENERATION-COLLECTION MEASUREMENT OF DIFFUSION OF SILVER IONS IN FROZEN PERCHLORIC ACID HYDRATE: EVIDENCE FOR TWO-PHASE BEHAVIOR

We report the measurement of diffusion of Ag^+ through frozen $HClO_4 \cdot 5.5H_2O$ at temperatures ranging from -45 to -85°C using a pulse generation-collection technique [*J. Phys. Chem.* **1990**, *94*, 2680]. Because movement of the Ag^+ can be verified, we can state unequivocally that the signals observed are due to physical diffusion of the Ag^+. For each temperature in the range -45 to -85°C we find that the measured diffusion coefficient, D, will be one of two values. At -20°C we found D to be 1.2(±0.1) x 10^{-6} cm^2/s, yet at -60°C we found D's of 7.3(±1.6) x 10^{-7} and 1.9(±0.6) x 10^{-7} cm^2/s. Annealling or thawing and refreezing a sample sometimes induces a change from one value of D to the other. A histogram of the D's from data collected at a given temperature is bimodal. We attribute the two different values of D to the presence of one of two different forms of the acid in the vicinity of the microelectrode array used in the diffusion measurement. Activation energies of diffusion for the two phases are 0.33(±0.03) eV and 0.19(±0.02) eV. That this biphasic behavior has not been observed in previous electrochemical studies in $HClO_4 \cdot 5.5H_2O$ may be due to the fact that our pulse generation-collection technique probes a relatively small (~100 μm) region of the electrolyte.

CHAPTER 4: CHARGE TRANSFER TO SOLVENT PHOTOCHEMISTRY OF ELECTRODE-CONFINED, FERROCENE- AND COBALTOCENE-BASED POLYMERS: PHOTOELECTROCHEMICAL REDUCTION OF HALOCARBONS

Metallocenes and metallocene-based polymers exhibit near-UV (280-370 nm) charge-transfer-to-solvent (CTTS) absorption in the presence of CCl_4, $CHCl_3$, CH_2Cl_2, CBr_4 and $CHBr_3$. The photoelectrochemistry of charge transfer complexes of poly(2-ferrocenylethyl methacrylate), poly-(3-(octamethylferrocenyl)propyl methacrylate), and poly(1,1'-bis[((3-(triethoxysilyl)propyl)amino)carbonyl]cobaltocene has been studied. Photoexcitation of metallocene-halocarbon complexes yields oxidation of the metallocene and reduction of the halocarbon. When a metallocene-based polymer is confined to the surface of an electrode that is held at a potential negative of the formal potential of the redox polymer, near-UV excitation results in sustained cathodic current in electrolyte solutions containing halocarbons.

Thesis Supervisor: Dr. Mark S. Wrighton
Title: Ciba-Geigy Professor of Chemistry

For from him and through him and to him are all things.

To him be the glory forever! Amen.

-Romans 11:36 (NIV)

Acknowledgment

First I wish to thank the people who helped me get to MIT. I am grateful to my parents who always encouraged me to pursue what interested me with all of my energy (James 5:16). I thank Mark Purdy who is a truly inspiring teacher and who first sparked my interest in chemistry. I am also grateful to the chemistry faculty at the University of Puget Sound for making my time there interesting and fun, and for doing an excellent job of preparing me for graduate school.

I am grateful to my advisor, Mark Wrighton, for teaching me how to think critically about my work and my own capabilities, for giving me the freedom to pursue what interested me, and for that last motivational push at the end.

Larry "Bud" Hancock and Clark "the animal" Early were "useful postdocs" - thanks for all you taught me. I thank Ingrid Fritsch-Faules and Hal van Ryswyck for teaching me a lot about electrochemistry and collaboration. I thank Vince Cammarata for leaving an informative and accurate thesis that helped me start to understand diffusion. Thanks to Martin "relax! have a coffee" Schloh, Guillermo "Gadgidee" Mülhmann, Dave "the Oaf" Ofer and Chris "whoever this is, let's kill them" McCoy for making my time here lots of fun. Eric, we had a few good years. Thanks for all you added to my life; I hope I have added as much to yours. Thanks to Melinda Cerney for helping me over the rough spots.

I thank the women of Joy Unspeakable Dance Troupe and everyone else at Parkway Christian Center for being my friends and standing beside me. I thank Araz, Rob, Eliza and every one in my extended family at Tree of Life City Church for being relentless in your faith. I am grateful to Dale and Karen for helping "the least of these" in very tangible ways that always included dessert and purple stuff. You have made me understand what it means to be apart of this Body. Thanks to Sandy and Andrew for being my partners in prayer and accountability. I have grown a lot from knowing both of you.

Table of Contents

List of Figures

Chapter Two

List of Schemes

Chapter One

Chapter Two

Chapter Three

Chapter One

General Introduction: The Behavior of Ultramicroelectrodes and Their Value in Investigating Diffusion Phenomena

The most common electrochemical measurements involve oxidation or reduction of a species in solution at the surface of a solid electrode. As with many heterogeneous reaction, the reaction rate is affected by how rapidly the solution species is brought into contact with the solid reactant. Because the reaction rate (current) may be governed, at least partially, by mass transport in an electrochemical system, it is important to understand and measure diffusion.

Diffusion results from Brownian motion of molecules in a liquid. The movement of a single molecule or ion follows a completely random path. This motion is described on a microscopic scale by the random walk model in one dimension as shown in Scheme I. If a molecule in 1-D space can move in steps of length ℓ and moves at a rate of one step for every time interval t_i, then the location of the molecule at a given time is described in terms of the probability of finding the molecule at a given distance from its starting point (see part B of Scheme I). After each time interval the molecule moves $\pm\ell$ from its current location and at long times the probability of finding the molecule is a Gaussian distribution centered around the molecule's location at $t = 0$. This model gives us the relation in equation (1) for the average displacement of a molecule where d is distance, t is time, and D is diffusion coefficient. This relationship

$$d = \sqrt{2Dt} \qquad (1)$$

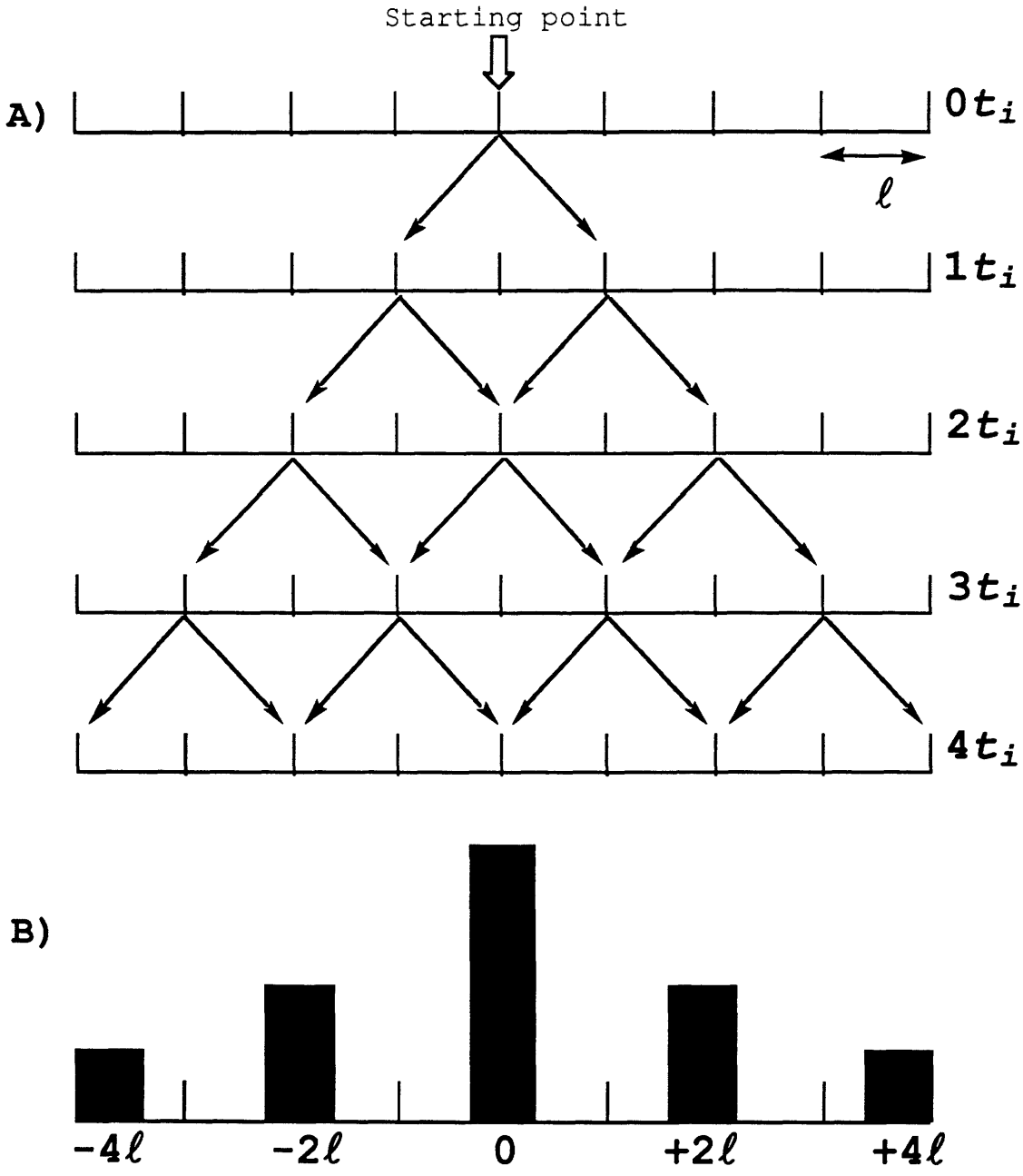

Scheme I. Random walk model in one dimension

can be used to provide a rule of thumb for estimating the thickness of the diffusion layer in an experiment.

On a macroscopic scale we discuss diffusion in terms of concentrations instead of probabilities of finding single molecules and diffusion is described by differential equations known as Fick's laws. Fick's first law is given in equation (2), for a situation as depicted in Scheme II. When a concentration gradient is present, the random motion of individual molecules results in a net flux of material from the region of high concentration to the region of low concentration. The magnitude of this flux is proportional to

$$-J(x,t) = D\frac{\partial C(x,t)}{\partial x} \qquad \text{Fick's first law} \qquad (2)$$

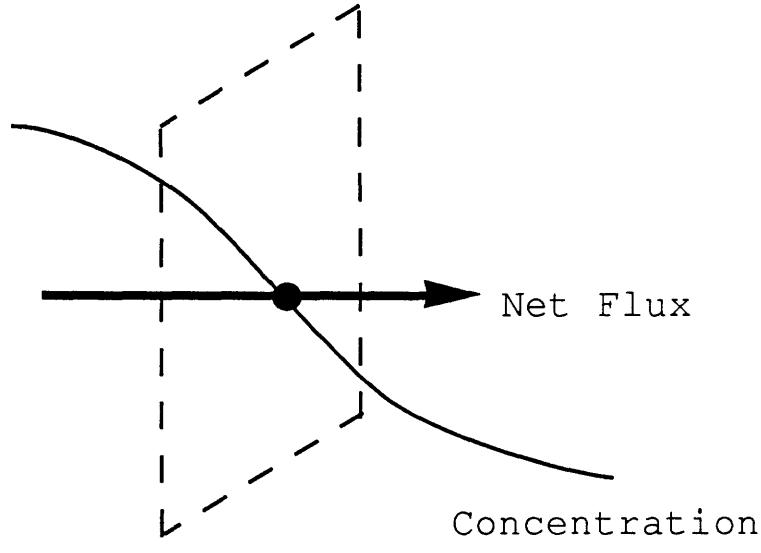

Scheme II. Fick's first law

the magnitude of the concentration gradient and the diffusion coefficient. J is flux of material per unit time per unit area, C is concentration. The idea of a flow being proportional to a gradient is a common physical occurrence. Equations (3)-(5) are the analogous laws governing the flow

$$J = -K_T \frac{\partial T}{\partial x} \qquad \text{Fourier's Law} \quad (3)$$

$$J = -K \frac{\partial \phi}{\partial x} \qquad \text{Ohm's Law} \quad (4)$$

$$J = -C \frac{\partial p}{\partial x} \qquad \text{Poiselle's Law} \quad (5)$$

of heat, fluids and electrical current. These analogies between diffusion and other physical phenomena have had important consequences because some of the electrode geometries for which electrochemists wish to describe diffusion have already been studied by engineers interested in heat conduction.[1] This understanding eliminates unnecessary duplication of efforts.

If we examine a case similar to that shown in Scheme II where instead of an arbitrary plane in space we have the surface of a large planar electrode, and the concentration gradient that exists has been setup by a reaction at the electrode surface, the current at the electrode will be governed by the flux of material to the surface. As time goes on and diffusion continues to occur, the shape of the concentration profile will change. The change is described

by Fick's second Law, given in equation (6). Solution of equation (6) for a planar electrode gives equation (7), the

$$\frac{\partial C(x,t)}{\partial t} = D\frac{\partial^2 C(x,t)}{\partial x^2} \qquad \text{Fick's second law} \quad (6)$$

$$i = \frac{nFAD^{1/2}C^*}{\pi^{1/2}t^{1/2}} \qquad \text{Cottrell equation} \quad (7)$$

Cottrell equation, which describes diffusion controlled current at a planar electrode following a potential step. (F is the Faraday constant, n is the number of electrons in the redox reaction, A is electrode area and C^* is bulk concentration.) The notable features of the Cottrell equation are that it describes an electrode sufficiently large that its edges need not be taken into consideration and at infinite time, current decays to zero.

Ultramicroelectrodes

Recently there has been a growing interest in electrodes with very small dimensions.[2] Lithographic techniques have made fabrication of electrodes in various shapes with micron dimensions routine, and other strategies have produced electrodes with dimensions as small as 10 Å.[3] Electrodes which are small enough that on the timescale of a few seconds the diffusion layers are larger than the electrode dimensions are referred to as ultramicroelectrodes. Using equation (1) to estimate diffusion layer thickness, and given D = 10^{-6} cm^2/s we see that for a 1 s experiment the crossover to the ultramicroelectrode regime is at electrode dimensions of

10 μm. In the case of ultramicroelectrodes the electrode areas are sufficiently small that the edges cannot be ignored, and because diffusion layers are large compared to electrode dimensions they have circular (spherical) instead of linear (planar) shapes.

Scheme III shows the evolution of the diffusion profile at an ultramicroelectrode over time. Initially, the diffusion layer conforms to the planar shape of the electrode surface, then becomes spherical. At the initial stage, diffusion perpendicular to the electrode surface dominates. The Cottrell equation describes the case where diffusion only occurs perpendicular to the electrode surface; the situation becomes more complex for spherical diffusion, and electrodes of different shapes must be treated separately. Since

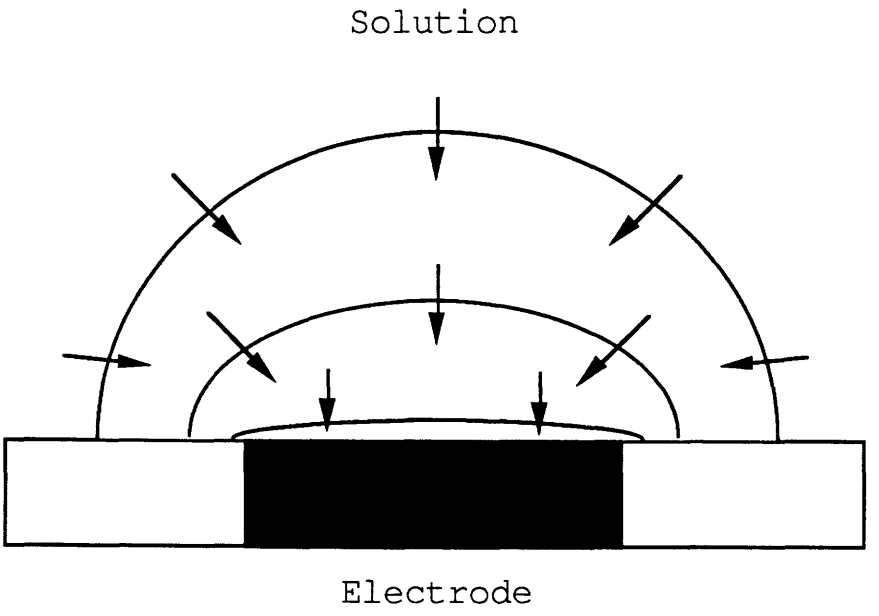

Scheme III. Evolution of diffusion profile with time.

diffusion is linear at short times even for very small electrodes, a guideline for determining whether a system is expected to exhibit micro or macro behavior should include a time element as well as a size element. The value of Dt/a^2, or some multiple thereof, (where a is the smallest electrode dimension) is commonly used as an estimate transition between macroscopic and microscopic behavior. When Dt/a^2 is large (long times or small electrodes) spherical diffusion is expected, whereas, when Dt/a^2 is small (short times, large electrodes) linear or Cottrell behavior will dominate. Because there is a change from one type of behavior to another, the equations describing the response of ultramicroelectrodes are typically the sum of two terms - one term that resembles the Cottrell equation for short times, and one term describing spherical diffusion at longer times.

There are several reasons why ultramicroelectrodes are preferable to larger electrodes. One reason is a reduction in interference from capacitive or charging current. In the case of a disk electrode surface area, and thus capacitance, is proportional to r^2, while faradaic current (as will be seen later) is proportional to r. The ratio of faradaic to charging current (i_f/i_c) will be proportional to 1/r. Interference from capacitance diminishes with smaller electrodes making faster experimental timescales accessible[4] and lowering detection limits.[5] Because ultramicroelectrodes exhibit smaller currents, distortion of signals from solution iR drop will be reduced (this advantage is further enhanced

by the drop in charging current). The development of ultra-microelectrodes has opened the door for electrochemistry in solids, solvents without added electrolyte and other resistive media where the performance of large electrodes is significantly affected by iR drop.[6] Spherical diffusion profiles lead to higher current densities due to diffusive transport which, in combination with shorter experimental timescales, reduces interference from convection in solutions. Finally, as electrodes become smaller and flux becomes very high, electrode reaction rates become limited by kinetics instead of mass transport. High flux and low capacitance allow the study of kinetics of fast electrode reactions.[3,7]

Disk Ultramicroelectrodes

The most common shape of ultramicroelectrodes is the disk; this is because disk electrodes are easy to fabricate. Although there is an analytical solution for the current at a spherical ultramicroelectrode following a potential step, its adaptation to disk shaped electrodes is complicated by the nonuniform accessibility of a flat electrode to a spherical diffusion profile. Nonetheless, there are numerical solutions for the current at microdisks for potential step and potential sweep experiments.[8] The current at a disk for potential step experiments is given by equations. (8) and (9). At long times, rather than decaying to zero, the current at an ultramicrodisk or sphere decays to a steady state value. (Under steady-state conditions Fick's second

law is set to zero, which means that the concentration gradients cease to change.) The steady state current, $i_{d,ss}$ at a ultramicrodisk is given by equation (10) (this is an analytical solution). The fact that ultramicrodisks reach steady state is useful because it provides a regime where current is not time dependent which simplifies its measurement.[9] Denault, Mirkin and Bard have developed an expression for the ratio of current at a disk to the steady state current (equations (11) and (12)).[10] By using this expression D can be determined without knowledge of C*.

Equations for disk electrodes:

$$\frac{i}{4nFDrC^*} = \frac{\pi^{1/2}}{2\tau^{1/2}} + \frac{\pi}{4} - \frac{3\pi\tau}{2^{10}} + \ldots \qquad \text{short times} \quad (8)$$

$$\frac{i}{4nFDrC^*} = 1 + \frac{4}{\pi^{3/2}\tau^{1/2}} + 32\left(\frac{1}{9} - \frac{1}{\pi^2}\right)\left(\frac{1}{\pi\tau}\right)^{3/2} + \ldots \quad \text{long times} \quad (9)$$

$$\tau = \frac{4Dt}{r^2}$$

$$i_{d,ss} = 4nFdC^*r \qquad (10)$$

$$\frac{i_d}{i_{d,ss}} = 0.7854 + \frac{\pi^{1/2}}{4} r(Dt)^{-1/2} \qquad t < 0.04\frac{r^2}{D} \qquad (11)$$

$$\frac{i_d}{i_{d,ss}} = 1 + \frac{2}{\pi^{3/2}} r(Dt)^{-1/2} \qquad t > \frac{r^2}{D} \qquad (12)$$

Band Ultramicroelectrodes

Band shaped ultramicroelectrodes usually have one dimension that falls in the microscopic regime and one

dimension in the macroscopic regime. They thus exhibit the diffusion characteristics of ultramicroelectrodes, but with larger (and more easily measured) currents.[11] As with disk electrodes the flat profile of band electrodes makes exact solution for their behavior difficult, but Szabo, *et. al.* have developed an empirical expression for the potential step experiment at a band electrode.[12] This is given in equations

Equations for band electrodes:

$$\frac{i}{nFDC^{*}l} = \frac{1}{(\pi\tau'')^{1/2}} + 1 \qquad \tau'' < \frac{2}{5} \quad (13)$$

$$\frac{i}{nFDC^{*}l} = \pi \frac{\exp\left[-\frac{2}{5}(\pi\tau'')^{1/2}\right]}{4(\pi\tau'')^{1/2}} + \frac{\pi}{\ln\left[\left(64e^{-\gamma\tau''}\right)^{1/2} + e^{5/3}\right]} \qquad \tau'' > \frac{2}{5} \quad (14)$$

$$\tau'' = \frac{Dt}{a^2} \qquad \gamma = 0.5772156$$

(13) and (14) where l is length and a is the width of the band. In the same way that the Cottrell equation does not take the electrode edges into account, this expression ignores the variation in diffusion profiles at the ends of the bands (the ends of the bands are assumed to be blocked or the band is assumed to be infinitely long). As with disks, it is necessary to divide the behavior of bands into two time regimes. At short times diffusion is largely linear, and the

response is similar to that of a macroelectrode, but at long times the diffusion profile is more spherical (hemicylindrical). Unlike disks, bands do not reach an actual steady state, but reach a quasi-steady state where the current decays very slowly.

Arrays of Ultramicroelectrodes

Band electrodes (and to a lesser extent disks) have been fabricated in arrays where they are separated by distances of a few microns. Thus, an electrode can be placed within the diffusion layer of a neighboring electrode. Another type of electrode array is the interdigitated array electrode (IDA). These are electrodes with a large number of interdigitated fingers that give the electrodes a high degree of communication (Scheme IV). When ultramicroelectrodes are placed far apart, their combined response is equivalent to the sum of their individual responses. Widely spaced arrays are used to combine ultramicroelectrode characteristics with larger currents.[13] The combined current from electrodes in an array decreases as the electrodes are brought sufficiently close together that their diffusion layers overlap. At very long times, the response of a closely spaced array will approach that of a single electrode whose area is equal to the sum of the areas of the electrodes *and* the intervening insulator.

When electrodes are placed in close proximity, the effect that one electrode has on its immediate environment can be detected by a second electrode. One type of

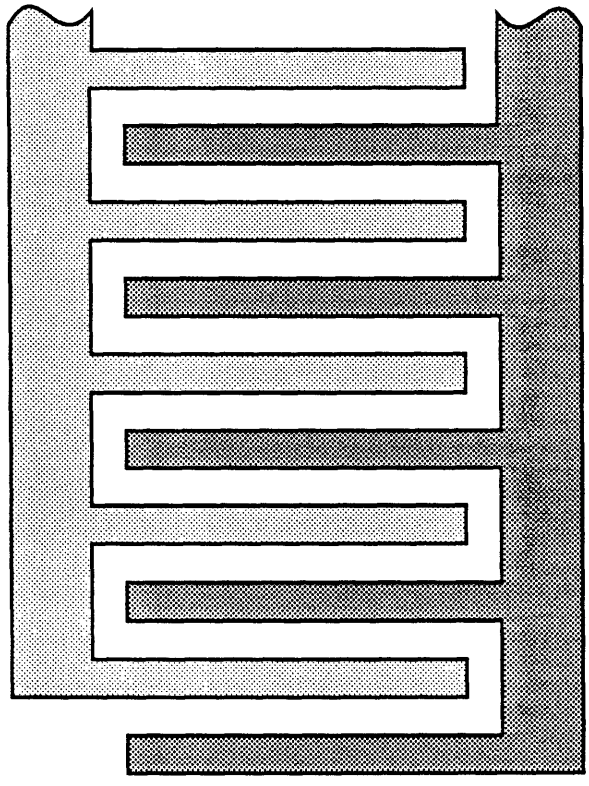

Scheme IV. Interdigitated Array Electrodes

experiment that is possible with arrays of electrodes is a generation-collection experiment. In this case one electrode (usually band or IDA) generates an oxidized or reduced species which is re-reduced, or re-oxidized at an adjacent electrode. There are three general types of information that can be gained from generation-collection experiments: 1) the rate at which species move between electrodes, 2) spatial mapping of potential or detection of diffusing species, 3) rates of reactions of generated species.

The time dependence and magnitude of the generator and collector currents give information about diffusion or

electron hopping in the intervening electrolyte medium.[14] One consequence of the presence of a collector electrode is that the "collected" species are free to diffuse back to the generator electrode and thus may undergo more than one generation-collection cycle. This feedback effect gives the current observed at the generator a larger magnitude than it would have in the absence of collection. IDAs reach steady state at long times during generation-collection experiments, while arrays of bands generally reach a quasi-steady state.

Electrodes in an array can be used as probes for the potential of a particular location. Arrays of several band electrodes have been used to map the potential (and thus, concentration) gradient between generator and collector electrodes.[15] Generation-collection experiments can be carried out using plated metals that are stripped off in the generation step and re-plated onto another electrode in the collection step. The movement of the diffusing species can then be verified following the experiment by analyzing the collector electrode for the presence of the plated metal. Cammarata, *et. al.* showed movement of Ag^+ through a polymer electrolyte by the presence of an Ag stripping wave on the collector electrode following collection.[16]

If a generated species undergoes a homogeneous reaction, generation-collection can give information about the reaction kinetics.[17] If the generated species is consumed by the homogeneous reaction then both generator and collector currents will decrease, but if the reaction regenerates the

collected species there will be an increase in generator current accompanied by a decrease in collector current. It is also possible to generate two reacting species at different electrodes. Electrogenerated chemiluminescence at IDAs and arrays of bands has been shown in solutions of Ru(2,2'-bipyridine)$_3^{2+}$. The Ru(2,2'-bipyridine)$_3^{2+}$ is reduced at one electrode and simultaneously oxidized at the adjacent electrode. The two generated species react in the space between the electrodes to give the luminescent excited state of Ru(2,2'-bipyridine)$_3^{2+}$.[14a,18]

Arrays of microelectrodes have been used as the platform for fabrication of several types of electrochemical devices based on conducting polymers.[19] The utility of their small dimensions lies in the fact that the switching speed of a device decreases with increasing quantities of the conducting polymer. Thus, smaller electrodes and spacings facilitate construction of devices with faster response times.[20]

The bulk of this thesis describes the use of arrays of band ultramicroelectrodes to measure diffusion as a probe of the properties of nonfluid electrolyte media. Pulse and step generation-collection techniques are used to measure diffusion of a probe molecule through aqueous poly(acrylic acid) gel and through frozen $HClO_4 \cdot 5.5H_2O$. In both cases the ability to measure diffusion over controllable distances lends insight into the structure of the electrolyte medium.

References

1. H. S. Carslaw and J. C. Jaeger, *Conduction of Heat in Solids* (2nd. Ed.), Clarendon Press: Oxford, 1959.

2. (a) Wightman, R. M. *Anal. Chem.* **1981**, *53*, 1125A. (b) Wightman, R. Mark, and Wipf, David O. in *Electroanalytical Chemistry: A Series of Advances*; Bard, Allen J., Ed.; Marcel Dekker: New York, 1989, Vol. 15, Chapter 3.

3. Penner, R. M.; Heben, M. J.; Longin, T. L.; Lewis, N. S. *Science* **1990**, *250*, 1118.

4. Bowyer, W. J.; Engleman, E. E.; Evans, D. H. *J. Electroanal. Chem.* **1989**, *262*, 67.

5. Schuette, S. A.; McCreery, R. L. *J. Electroanal. Chem.* **1985**, *191*, 329.

6. (a) Bond, A. M.; Fleischmann, M.; Robinson, J. *J. Electroanal. Chem.* **1984**, *180*, 257. (b) Whiteley, L. D.; Martin, C. R. *J. Phys. Chem.* **1989**, *93*, 4650. (c) Watanabe, M.; Longmire, M.; Wooster, T. T.; Zhang, H.; Barbour, C.; Murray, R. W. In *Microelectrodes: Theory and Applications*; Montenegro, M. Irene; Queiros, M. Arlete; Daschback, John L. (Eds.); NATO ASI Series E, 197 (Microelectrodes); Kluwer Academic Publishers: Boston, 1991. (d) Bond, A. M.; Fleischmann, M.; Robinson, J. *J. Electroanal. Chem.* **1984**, *168*, 299. (e) Bond, A. M.; Fleischmann, M.; Robinson, J. *J. Electroanal. Chem.* **1984**, *172*, 11. (f) Karpinski, Z. J.; Osteryoung, R. A. *J. Electroanal. Chem.* **1993**, *349*, 285.

7. (a) Bowyer, W. J.; Engelman, E. E.; Evans, D. H. *J. Electroanal. Chem.* **1989**, *262*, 67. (b) Montenegro, M. I.; Pletcher, D. *J. Electroanal. Chem.* **1986**, *200*, 371.

8. Michael, A. C.; Wightman, R. M.; Amatore, C. A. *J. Electroanal. Chem.* **1989**, *267*, 33.

9. Oldham, K. B.; Zoski, C. G.; Bond, A. M.; Sweigart, S. A. *J. Electroanal. Chem.* **1988**, *248*, 467.

10. Denuault, G.; Mirkin, M. V.; Bard, A. J. *J. Electroanal. Chem.* **1991**, *308*, 27.

11. Bond, A. M.; Henderson, T. L. E.; Thormann, W. *J. Phys. Chem.* **1986**, *90*, 22911.

12. Szabo,A.; Cope, D. K.; Tallman, D. E.; Kovach, P. M.; Wightman, R. M. *J. Electroanal. Chem.* **1987**, *217*, 417.

13. (a) Strohben, W. E.; Smith D. K.; Evans, D. H. *Anal. Chem.* **1990**, *62*, 1709. (b) Caudill, W. L.; Howell, J. O.; Wightman, R. M. *Anal. Chem.* **1982**, *54*, 2532.

14. (a) Chidsey, C. E.; Feldman, B. J.; Lundgren, C.; Murray, R. W. *Anal. Chem.* **1986**, *58*, 601. (b) Feldman, B. J.; Murray, R. W. *Anal. Chem.* **1986**, *58*, 2844. (c) Geng. L.; Longmire, M. L.; Reed, R. A.; Parcher, J. F.; Barbour, C. J.; Murray, R. W. *Chem. Mater.* **1989**, *1*, 58. (d) Feldman, B. J.; Feldberg, S. W.; Murray, R. W. *J. Phys. Chem.* **1987**, *91*, 6558. (e) Licht, S.; Cammarata, V.; Wrighton, M. S. *J. Phys. Chem.* **1990**, *94*, 6133. (f) Licht, S. Cammarata, V.; Wrighton, M. S. *Science*, **1988**, *243*, 1176.

15. Fritsch-Faules, I.; Faulkner, L. R. *Anal. Chem.* **1992**, *64*, 1118.

16. Cammarata, V.; Talham, D. R.; Crooks, R. M.; Wrighton, M. S. *J. Phys. Chem.* **1990**, *94*, 2680.

17. Shea, T. V.; Bard, A. J. *Anal. Chem.* **1987**, *59*, 2101.

18. Bartelt, J. E.; Drew, S. M.; Wightman, R. M. *J. Electrochem. Soc.* **1992**, *139*, 70.

19. (a) Peng, X.; Horowitz, G.; Fichon, D.; Garnier, F. *Appl Phys. Lett.* **1990**, *57*, 2013. (b) Tsumura, A.; Koezuka, H.; Ando, T. *Synth. Met.* **1988**, *25*, 11. (c) Burroughes, J. H.; Friend, R. H.; Allen, P. C. *J. Phys. D: Appl. Phys.* **1989**, *22*, 956. (d) Kittlesen, G. P.; White, H. S.; Wrighton, M. S. *J. Am. Chem. Soc.* **1984**, *106*, 7389. (e) Thackeray, J. W.; White, Henry, S.; Wrighton, M. S. *J. Phys. Chem.* **1985**, *89*, 5133.

20. (a) Lofton, E. P.; Thackeray, J. W.; Wrighton, M. S. *J. Phys. Chem.* **1986**, *90*, 6080. (b) Jones, E. T. T.; Chyan, O. M.; Wrighton, M. S. *J. Am. Chem. Soc.* **1987**, *109*, 5526.

Chapter Two:

A Comparison of Diffusion Coefficients of Electroactive Species in Aqueous Fluid Electrolytes and Polyacrylate Gels: Step Generation-Collection Diffusion Measurements and Operation of Electrochemical Devices

Introduction

We report direct measurement of diffusion of 1,1'-*bis*(hydroxymethyl)ferrocenium ($Fc(CH_2OH)_2^+$, **I**) in polyacrylate gel, **II**, in order to probe transport properties and usefulness of the gel electrolyte in electrochemical devices. Diffusion measurements were made at arrays of band microelectrodes using a transient generation-collection method developed in our laboratory[1] that is similar to transient measurements made at interdigitated array (IDA) electrodes[2,3] and to electrochemical "time-of-flight" experiments.[4] We demonstrate the use of polyacrylate gel as an electrolyte for a microelectrochemical transistor based on ruthenium oxide, RuO_x,[5,6] and an electrochromic device based on a polymer film of *N,N'-bis*[*p*-(trimethoxysilyl)benzyl]-4,4'-bipyridinum, (viologen, **III**).[7]

Poly(acrylic acid) was obtained commercially with an

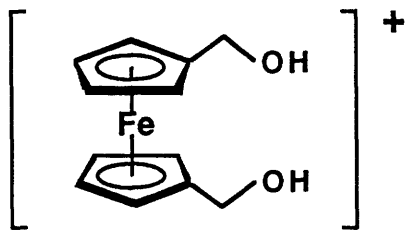

I

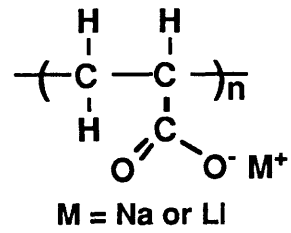

M = Na or Li

II

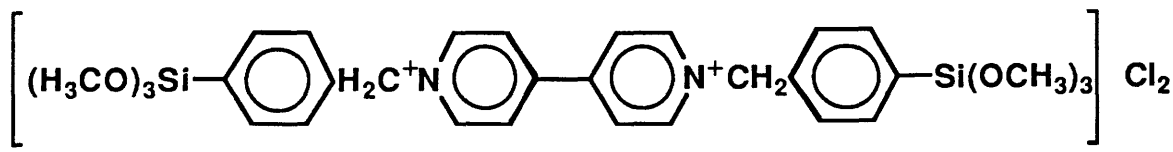

III

average molecular weight of 4 x 10^6 Da. Upon neutralization (pH 6 to 8), mucilages of polyacrylate in H_2O form gels with viscosities as high as 5 x 10^4 cP.[8] Polyacrylate gels are described by Taylor and Bagley[9] as suspensions of solvent-swollen particles in close contact which exhibit non-Newtonian (pseudoplastic) flow properties. The gel can be thought of as a two phase system consisting of a highly viscous discontinuous phase, the gel particles, and a less viscous continuous phase.[10] Applications of polyacrylate include thickening agents for cosmetics and pharmaceuticals and media for drug delivery systems.[8,11] Because of its ionic nature and resistance to flow, the polyacrylate gel electrolyte is an interesting, non-fluid medium for electrochemical experiments.

Non-fluid electrolytes are potentially useful for certain electrochemical devices because they are more easily contained than conventional liquids. This convenience is desirable in designing microelectrochemical transistors and electrochromic devices. Assembly of electrochemical transistors and diodes on arrays of band microelectrodes has been described by our laboratory.[5] Some electrochemical transistors may find use as sensors[12] and their operation in solid electrolytes has been aimed at improving the practicality of such devices.[13,14] Solid electrolytes have been used as a medium for operation of electrochemical transistors based on conducting polymers and metal oxides.[13] The switching speeds of electrochemical devices are usually

reduced in solid electrolytes,[14c] however, due to low ion mobility in the solid.

Gel electrolytes have been used as the medium for operation of electrochromic displays based on organic materials.[15] This application requires an electrolyte that is optically transparent and able to support the counterion motion necessary for rapid oxidation and reduction of the electrochromic material.

Diffusion of a species in an ideal solution is described by the Stokes-Einstein equation, equation (1),where D is the diffusion coefficient, k is the Boltzman constant, T is the temperature, η is the solution viscosity and r_A is the hydrodynamic radius.[16] This relation shows that D is

$$D = \frac{kT}{6\pi\eta r_A} \qquad (1)$$

inversely proportional to the viscosity of an ideal solution. However, in nonideal systems such as solutions of polymers, increases in global viscosity can be effected without the corresponding decrease in D. A model of one such nonideal system has been described for solutions of polystyrene in cyclohexane-benzene.[17]

We have made our diffusion measurements using potential step generation-collection at arrays of microelectrodes, Scheme I.[1b] The microelectrode arrays consist of eight individually addressable band microelectrodes made of Au or

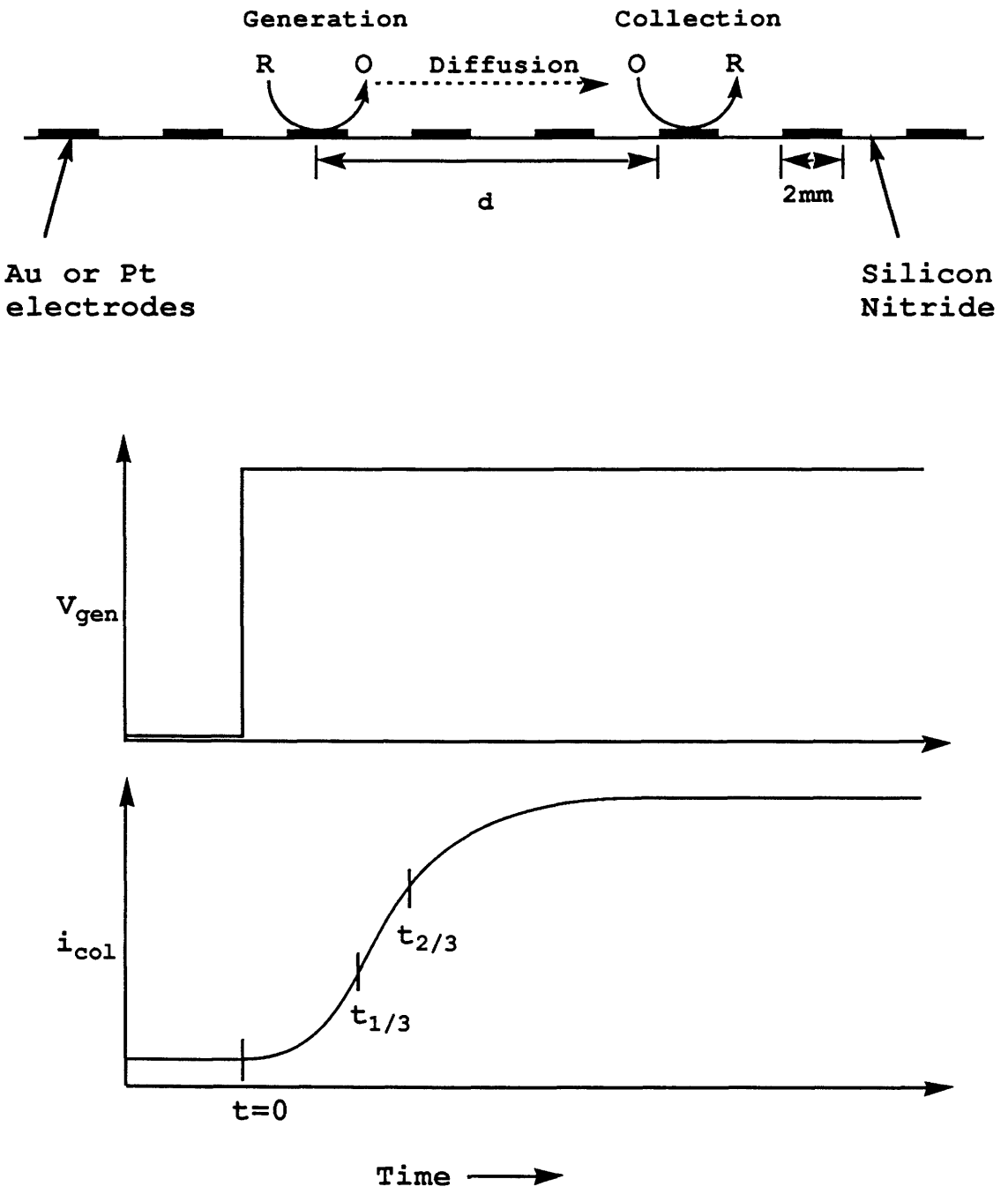

Scheme I. Step Generation-Collection Experiment

Pt evaporated onto an insulating Si_3N_4 substrate and patterned using photolithography. The electrodes are nominally 2 μm wide x 100 μm long x 0.1 μm thick in an array with 4 μm center to center spacings. Their fabrication has been described.[18] In step generation-collection experiments one electrode, termed the generator, is stepped to a potential that will oxidize (or reduce) a species in solution while another electrode, the collector, is held at a potential that will re-reduce (or re-oxidize) the reagent created at the generator. The onset of current at the collector electrode, following the beginning of generation, is dependent on D of the generated species. The D was calculated from equation (2), which is based on the Einstein

$$t_f = \frac{k_f d^2}{D} \qquad (2)$$

equation, and where the transit time, t_f, is proportional to the mean squared distance traveled, d^2, and $1/D$.[19] The t_f is the time required to reach a fraction, f, of the steady-state collector current and d is the distance from the center of the generator electrode to the nearest edge of the collector electrode as shown in Scheme I. The constant of proportionality, k_f, is empirically determined by measuring transit times for a species of known D.

Generation-collection at microelectrodes is analogous to rotating ring-disk experiments[20] with the exception that forced flow conditions are not necessary, because radial

diffusion and small distances between collector and generator maintain high flux to the microelectrodes. This allows measurement of diffusion coefficients in unusual media, *e.g.* solids, gels and supercritical fluids. Note that measurement of D by the generation-collection method does not require knowledge of the concentration of the diffusing species. A similar generation-collection technique using potential pulses at the generator electrode has been used to measure diffusion coefficients of Ag^+ in solid electrolyte systems based on poly(2-methoxyethoxyethoxyphosphazene) and poly(ethyleneoxide).[21] Potential steps[1b] were used in this chapter instead, because the collector currents, which are about two orders of magnitude higher, are easier to detect.

Since the calculation of D from potential step generation-collection experiments requires knowledge of the magnitude of the collector current in both transient and steady-state regimes, time dependent factors that affect the current magnitude at either the generator or collector electrodes must be considered. This is especially important when comparing different electrochemical systems, as we do in this chapter. Influences from convection, intervening electrodes, unequal diffusion coefficients of the oxidized and reduced forms of the probe molecule, and passivation of the electrodes are addressed. Random walk digital simulations aid in the evaluation of some of these phenomena.

Experimental

Chemicals. The preparation of 1,1'-*bis*(hydroxymethyl)-ferrocene[22] and *N,N'-bis*[*p*-(trimethoxysilyl)benzyl]-4,4'-bipyridinum[23] have been described. Poly(acrylic acid) was obtained as Carbopol® 940 (B. F. Goodrich Co.); $Ru(NH_3)_6Cl_3$ (Strem), K_2RuO_4 (Alfa), and all other reagents (Aldrich) were used as received. Aqueous solutions of $NaCH_3CO_2$ and $LiCH_3CO_2$ were prepared by neutralizing 0.1 M acetic acid with 0.1 M NaOH or LiOH to pH 7.

Gel Preparation. Polyacrylate gels were prepared by neutralization of a 0.5% (w/v) aqueous stock solution with 20% NaOH or LiOH to pH 7.[8] Upon neutralization, the cloudy, colorless, somewhat viscous stock solution became a highly viscous, clear gel. To prepare gels for electrochemical experiments, the poly(acrylic acid) stock solution was purged with Ar, and $Fc(CH_2OH)_2$ was added prior to neutralization.

Viscosity Measurements. Viscosities of sucrose solutions were measured using a Cannon-Fenske routine viscometer (size 75). Values used were the average of five trials.

Electrochemistry. Electrochemical transistor experiments, long distance diffusion measurements and microelectrode cleaning and characterization were carried out using a Pine Instrument Co. RDE-4X1 bipotentiostat. Data were recorded on a Kipp & Zonen BD 90 or BD 91 XY recorder. All solutions used for electrochemistry were first deoxygenated by purging with Ar.

Microelectrode Arrays. Fabrication and mounting of microelectrode arrays have been described.[18] After mounting, arrays were cleaned with an oxygen plasma at 100 mtorr and 300 W for 5 min. Immediately prior to diffusion measurements, microelectrode arrays were electrochemically cleaned by scanning individual electrodes between -0.8 V and -1.3 V vs. SCE several times in aqueous 0.1 M K_2HPO_4. Electrodes were characterized by cycling individual electrodes and adjacent pairs between 0 V and -0.6 V in 2 mM $Ru(NH_3)_6Cl_3$ in pH 7 Na_3PO_4 buffer. Individual electrodes gave sigmoidal cyclic voltammograms with current maxima of 10 to 20 nA. Adjacent pairs of electrodes were considered to be electrically isolated from each other when cycling both electrodes together gave current maxima ~30% higher than individual electrodes. Electrodes were cleaned again in 0.1 M K_2HPO_4 following characterization.

Microelectrode Generation-Collection Diffusion Measurements. Generation and collection were accomplished using two different electrode configurations within the same cell. The generator circuit of the cell consisted of one of the working microelectrodes of the array and a Ag wire counter/quasi-reference electrode. Potential control was provided by a PAR 175 universal programmer. The collector circuit was a three-electrode configuration, controlled by a BAS100 low current module with an SCE reference or a Ag wire quasi-reference. Current output was recorded on a Nicolet 4094B or Hi-Techniques IQ300 digital oscilloscope. For

experiments monitoring generator current, generator and collector configurations were reversed so that the three-electrode setup contained the generator (controlled by the BAS100) and the two-electrode setup contained the collector (controlled by the PAR 175).

Microelectrode Removal. For experiments testing the effect of intervening microelectrodes, selective removal of Au microelectrodes was accomplished by cycling electrodes to be removed from 0.0 to +1.2 V vs. SCE while holding the remaining electrodes at -1.0 V. This was followed by rinsing with concentrated HNO_3 which removed traces of Au and formed a passivating oxide layer on the underlying Cr (used as an adhesion layer for Au on Si_3N_4). XPS of macroscopic samples treated similarly showed that little or no Au remained and Cr which had stayed behind was mostly oxidized.

Selective removal of Pt electrodes was accomplished by cycling electrodes in K_2HPO_4 to a potential sufficiently negative that cavitation from gas evolution caused the electrodes to delaminate from the Si_3N_4 substrate.

Long Distance Diffusion Measurements. Diffusion over long distances (up to 1 mm) was measured using two Au macroelectrodes as generator and collector in a closed face sandwich configuration. The electrodes were rectangular pieces of Si wafer coated with 5000 Å SiO_2 and 1500 Å Si_3N_4 onto which 50 Å of Cr and then 1000 Å of Au had been evaporated. Electrodes were mounted on the jaws of a Vernier

caliper using double-sided tape so that the distance between them could be adjusted.[20]

Data Treatment. Collector currents at microelectrodes have undergone a 7-point smooth. Values shown in t_f vs. d^2 plots are the average of 2-15 trials. Error estimates given for numbers reported are one standard deviation.

Transistor Preparation. RuO_x transistors were prepared from solutions of 5 mM K_2RuO_4 in 1 M NaOH using a two-compartment cell to isolate the counter electrode. Adjacent pairs of microelectrodes were cycled between -0.2 V and -0.8 V vs. SCE one to three times at 100 mV/s to deposit RuO_x. Electrodes not involved in the deposition were held at +0.1 V.[6]

Transistors were characterized by applying an oscillating gate voltage, V_G, that spanned the potential window of the transition between conduction and nonconduction of the transistor material. Gate current, I_G, was determined by measuring current response with V_D = 0 and drain current, I_D, was measured with V_D = 50 mV. Transistor speed was characterized by measuring the frequency at which current gain, I_D/I_G, reached unity.

Electrochromic Devices. Electrochromic devices were prepared and characterized using a PAR 363 poteniostat driven by a PAR 175 universal programmer. Pt flag electrodes (area = ~1 cm^2) were pretreated by first cycling between -0.3 V and +1.2 V vs. SCE in 0.5 M H_2SO_4 for several minutes and then holding at the +1.2 V for 5 min. Electrodes were derivatized

from a ~3 mM aqueous solution of **III** with 0.2 M KCl and 0.1 M K_2HPO_4. Electrodes were cycled between 0 V and -0.6 V vs. SCE several times in the derivatizing solution to verify growth of the surface-confined polymer and then held at -0.6 V for 5 min to give a coverage of ~10^{-8} moles/cm^2. The electrode was then soaked in 1 M KCl for at least 1 h and characterized by cyclic voltammetry in 0.1 M KCl. Chronoamperometric and time-dependent absorbance data were recorded on a Hi-Techniques IQ300 digital oscilloscope. Absorbance changes were measured using a Aerotech 25 mW He-Ne laser and a Thorlabs DET2-SI silicon photodiode as described previously.[7]

Digital Simulations. Our simulations were based on the simple Einstein-Smoluchowski random walk in two dimensions.[1] We modified an early version of the method, where only a finite number of species were created at the generator electrode at a given moment. Here, we report simulations that better represent the real experiments because diffusion from the bulk solution to generator electrode is taken into consideration. Consequently, our simulations require larger amounts of computation time. We addressed the need for additional computation in two ways. First, we moved the simulations from an IBM AT Personal Computer to a Silicon Graphics IRIS computer. Second, we simplified the random walk algorithm. The diffusive process was originally modeled by allowing *every* molecule in the discretized space to be randomly displaced into adjacent

spatial elements during each time iteration. The large number of calls to the random number generator was very time-consuming, however, and increased with increasing concentrations. Instead of randomly displacing each molecule, we evenly distributed the molecules of each spatial element among adjacent elements, and then randomly distributed only the remainder. The simulation results from this partially randomizing algorithm were unchanged from those of the fully randomizing algorithm, except that the signal-to-noise ratio was about six times better. In addition, the run-time of the simulations became independent of the concentration of redox molecules in the system.

Even with these improvements, the time required to simulate a step generation-collection experiment until it reached quasi-steady-state was unacceptably long, especially at larger generator-collector separations. Consequently, we used a parameter, $\theta_{gap} = 4Dt/d^2$,[25] to consistently select pre-steady-state end times, t, for simulations at different generator-collector distances. The θ_{gap} used was 98, which corresponds to t = 0.38 s, 2.07 s, and 5.11 s for d = 3 μm, 7 μm, and 11 μm, respectively

We simulated both pulse and step generation-collection experiments. Several assumptions are made in the simulations:

(a) The initial concentration of the starting species, A, is uniform in all boxes.

(b) After each iteration, all A molecules in boxes adjacent to an active generator electrode are converted to B, and all B molecules adjacent to an active collector electrode are converted to A.

(c) Redox species only diffuse up, down, left or right into adjacent boxes or remain in the same box with each time iteration.

(d) Diffusion along the length of each band in the electrode array is assumed to be uniform and the length is great enough that end effects are negligible. Thus, only two-dimensional simulations were performed.

(e) Since the height of each band in the array is very small (1/20) compared to its width, the electrodes in the simulations were simplified by making them flush with the substrate.

Graphical representations of simulated data use normalized currents in the form $i/(nFDCl)$, where n is the number of equivalents of electrons transferred, F is the Faraday constant, C is the bulk concentration of the starting species and l is the electrode length.

Results and Discussion

a. Step Generation-Collection Measurement of Diffusion at Short Distances. The value of k_f used to determine D for $Fc(CH_2OH)_2^+$ from equation (2) was determined empirically by measuring transit times of $Ru(NH_3)_6^{2+}$ (for which $D = 7.8 \times 10^{-6}$ cm^2/s)[1a] and then solving equation (2) ($k_{1/3} = 0.65$, $k_{2/3} = 1.92$). Diffusion coefficients were determined from the slopes of plots of $t_{1/3}$ and $t_{2/3}$ vs. d^2.

The diffusion coefficients of $Fc(CH_2OH)_2^+$ in polyacrylate gel and aqueous sodium acetate, listed in Table I, were determined by potential step generation-collection experiments, Figures 1 and 2. The fact that diffusion in polyacrylate gel is nearly as fast as it is in H_2O indicates that polyacrylate gel could serve as a useful electrolyte medium for a variety of electrochemical devices.

The diffusion coefficient of $Fc(CH_2OH)_2^+$ in polyacrylate is much larger than D predicted by the Stokes-Einstein equation, equation (1), for an ideal solution of comparable viscosity.[16] In order to verify that solutions of $Fc(CH_2OH)_2^+$ behaved ideally, we measured its transit times in aqueous solutions with varying concentrations of sucrose (added to change viscosity). As predicted by equation (1), the transit time of $Fc(CH_2OH)_2^+$ increases linearly with solution viscosity, Figure 3.

The rapid diffusion we observed in the polyacrylate gel supports the description of the gel as a two-phase system.[10] This is further illustrated by diffusion in polyacrylate gel

Figure 1. Time dependence of collector current following step generation of $Fc(CH_2OH)_2^+$, conducted in 2 mM $Fc(CH_2OH)_2$ in polyacrylate gel at a microelectrode array distances of 3 μm to 27 μm that increase from topmost to lowest curves in 4 μm increments. Inset: a plot of average $t_{1/3}$ and $t_{2/3}$ values vs. d^2 obtained from ten repetitions.

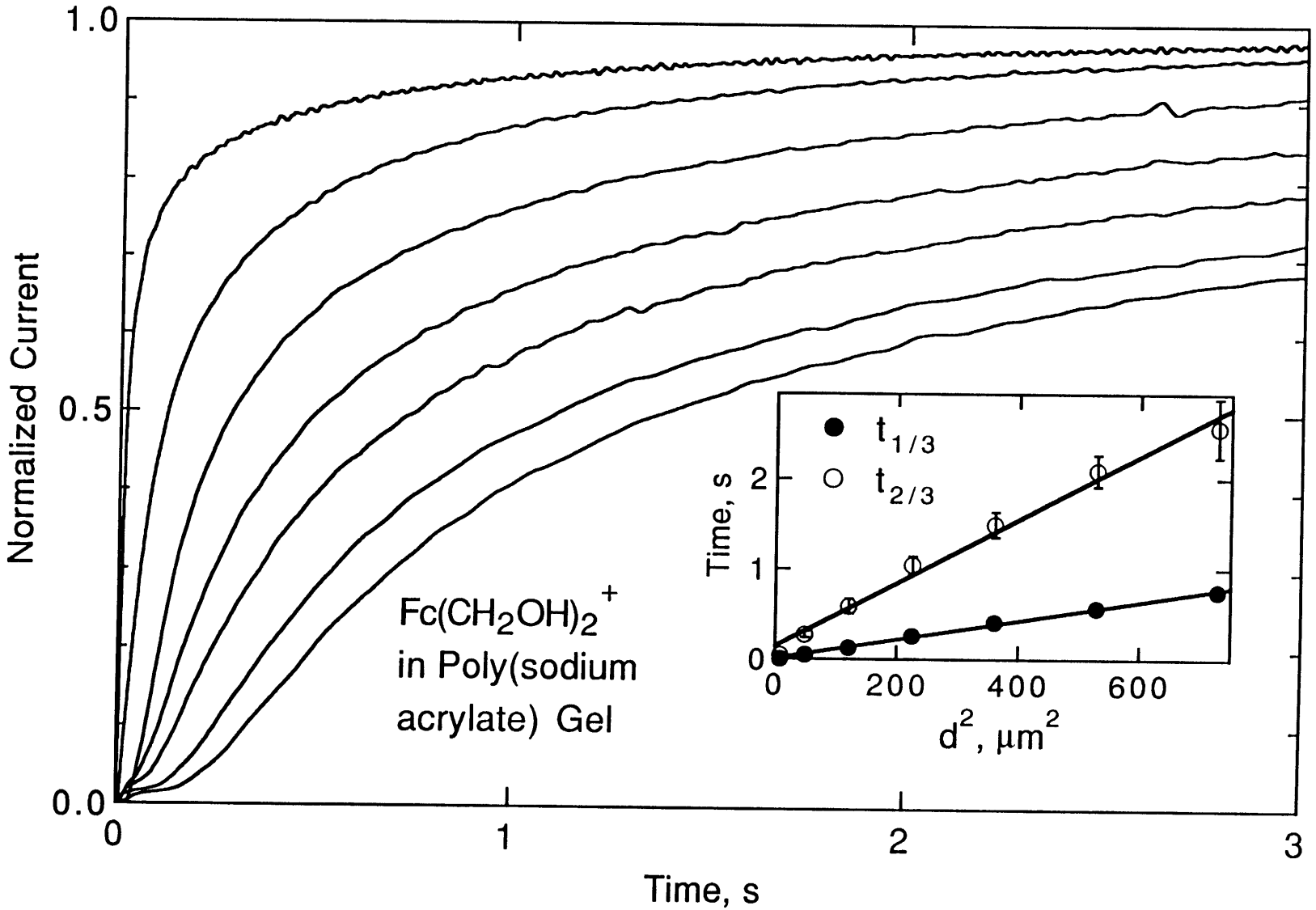
1.0
0.5
0.0
Normalized Current
0
1
2
3
Time, s
Fc(CH2OH)2+
in Poly(sodium
acrylate) Gel
t1/3
t2/3
Time, s
0
1
2
0
200
400
600
d2, μm2

Figure 2. Time dependence of collector current following step generation of $Fc(CH_2OH)_2^+$, conducted in 2 mM $Fc(CH_2OH)_2$ in 0.1 M aqueous sodium acetate at a microelectrode array with distances of 3 μm to 27 μm that increase from topmost to lowest curves in 4 μm increments. Inset: a plot of average $t_{1/3}$ and $t_{2/3}$ values vs. d^2 obtained from ten repetitions.

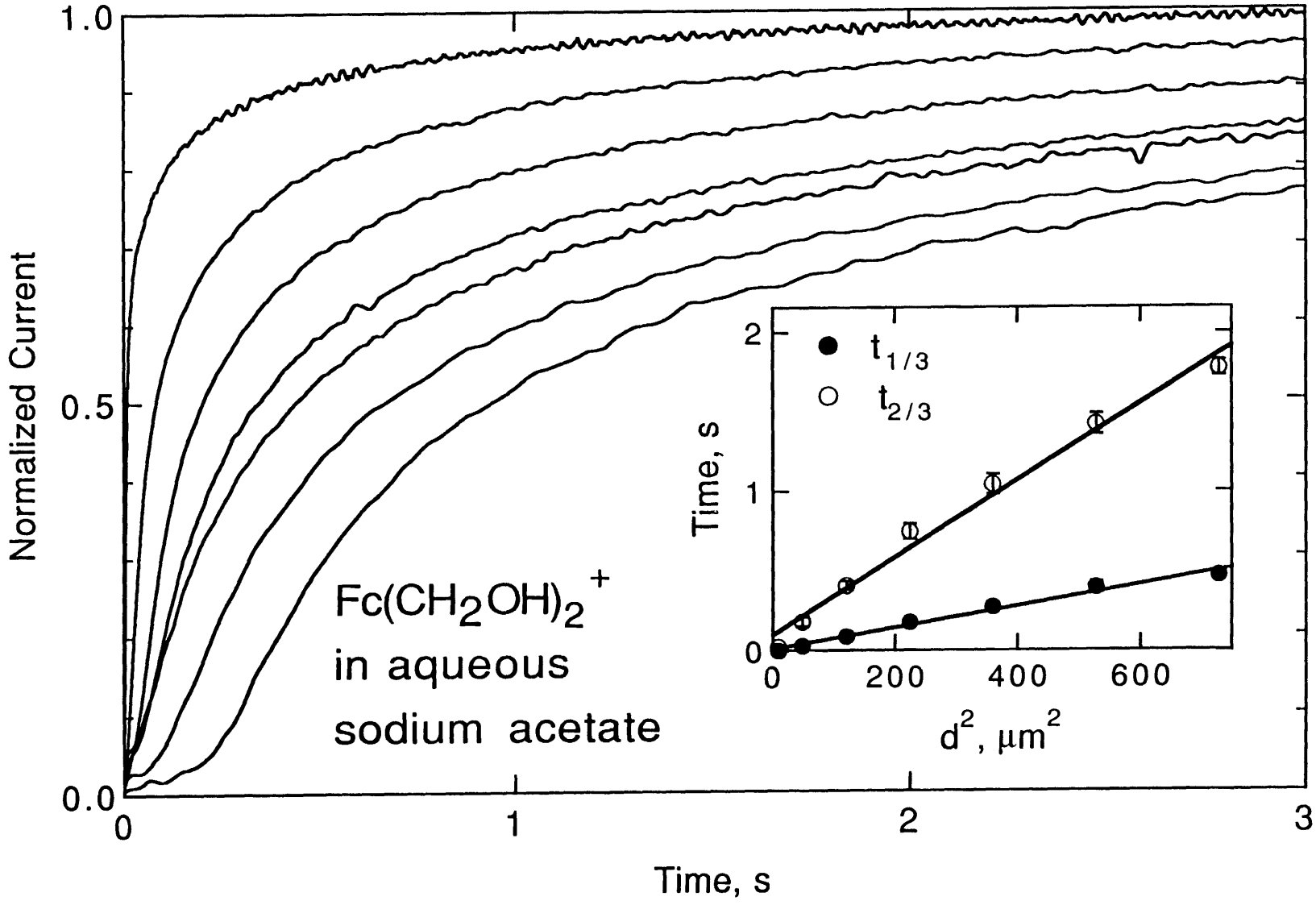
1.0
0.5
0.0
Normalized Current
0
1
2
3
Time, s
Fc(CH2OH)2+
in aqueous
sodium acetate
t1/3
t2/3
Time, s
2
1
0
0
200
400
600
d2, μm2

Figure 3. Time dependence of collector current following step generation of $Fc(CH_2OH)_2^+$, conducted in 2 mM $Fc(CH_2OH)_2$ in 0.1 M aqueous sodium acetate with 0%, 10%, 20%, 30%, 40% (w/w) sucrose for a distance of 11 μm between generator and collector at a microelectrode array; viscosity increases from upper to lower curves. Inset: a plot of average $t_{1/3}$ and $t_{2/3}$ values vs. viscosity obtained from three repetitions.

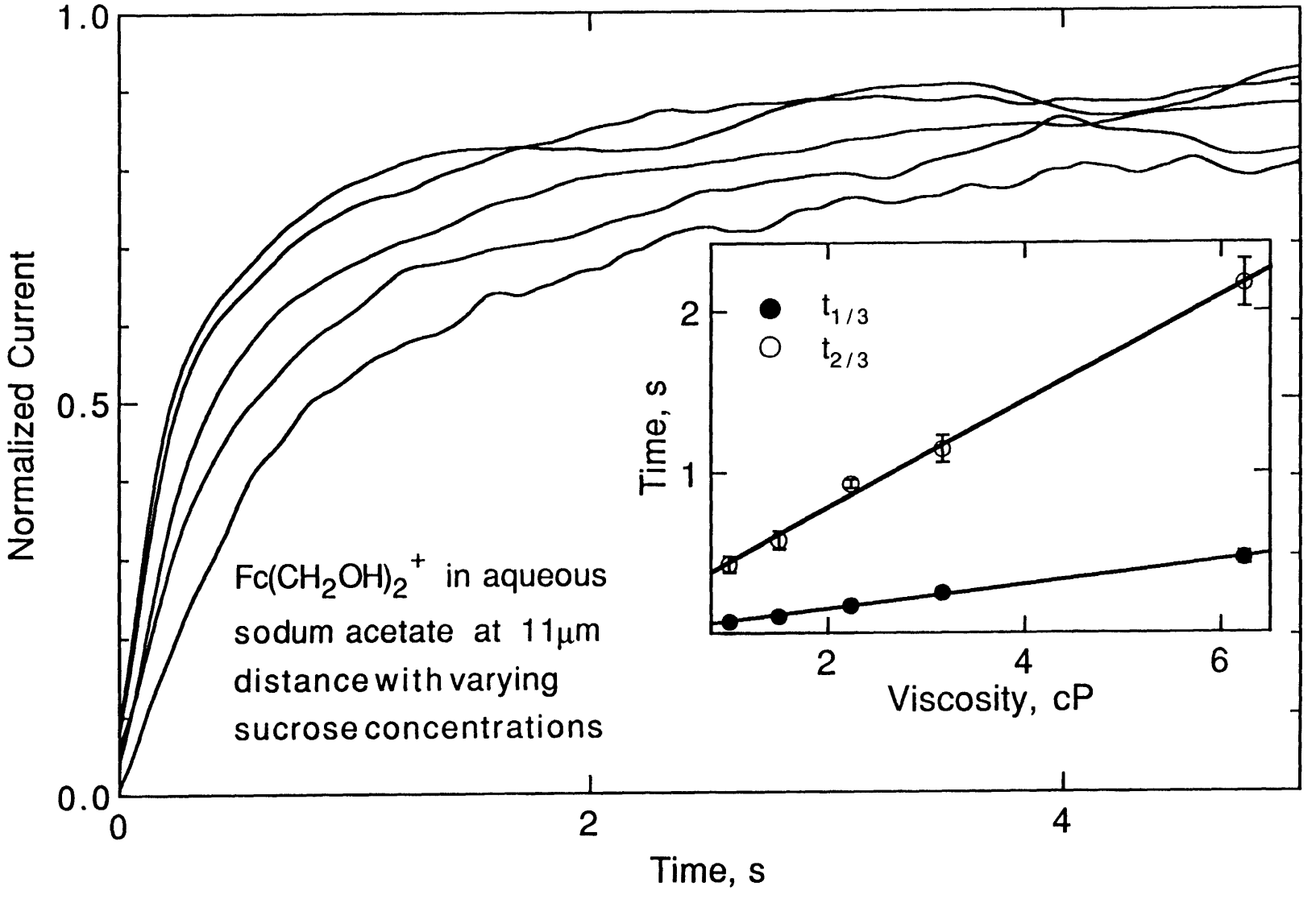
1.0
0.5
0.0
Normalized Current
0
2
4
Time, s
$Fc(CH_2OH)_2^+$ in aqueous
sodum acetate at 11μm
distance with varying
sucrose concentrations
$t_{1/3}$
$t_{2/3}$
Time, s
2
1
2
4
6
Viscosity, cP

containing sucrose. The diffusion coefficient of $Fc(CH_2OH)_2^+$ in polyacrylate containing 40% sucrose was found to be $1.0(\pm 0.1) \times 10^{-6}$ cm^2/s, Figure 4. The sucrose and diffusing molecules are solvated in the continuous phase, where they interact as they would in an ideal solution, while the global viscosity is controlled by the discontinuous phase.

b. Diffusion at Long Distances. We have used a closed face sandwich configuration of generator and collector macroelectrodes to study diffusion over distances up to 1 mm.[20] A k_f for the closed face sandwich electrode geometry was determined from transit times of $Fc(CH_2OH)_2^+$ in H_2O containing 0.1 M sodium acetate at pH 7 using the D determined from microelectrode transit times. For this geometry $k_{1/3} = 0.10$ and $k_{2/3} = 0.17$. The diffusion coefficient of $Fc(CH_2OH)_2^+$ in polyacrylate at long distances was found to be $3.9(\pm 0.5) \times 10^{-6}$ cm^2/s, Figure 5. Diffusion in gel at long distances was slightly slower than diffusion over short distances. This small difference is most likely due to a calibration error resulting from convection in the aqueous sodium acetate, and not the result of the gel forming barriers that inhibit diffusion. Convection becomes an important factor when the diffusion layer reaches larger distances in media of low viscosity, like aqueous sodium acetate. Convection would cause a decrease in transit times and lead to an artificially low value for k_f in the macroelectrode system. Since the viscous gel is essentially

Figure 4. Time dependence of collector current following step generation of $Fc(CH_2OH)_2^+$, conducted in 2 mM $Fc(CH_2OH)_2$ in polyacrylate with 40% sucrose at a microelectrode array with distances of 3 μm to 27 μm distances that increase from topmost to lowest curves in 4 μm increments. Inset: a plot of average $t_{1/3}$ and $t_{2/3}$ values vs. d^2 obtained from ten repetitions.

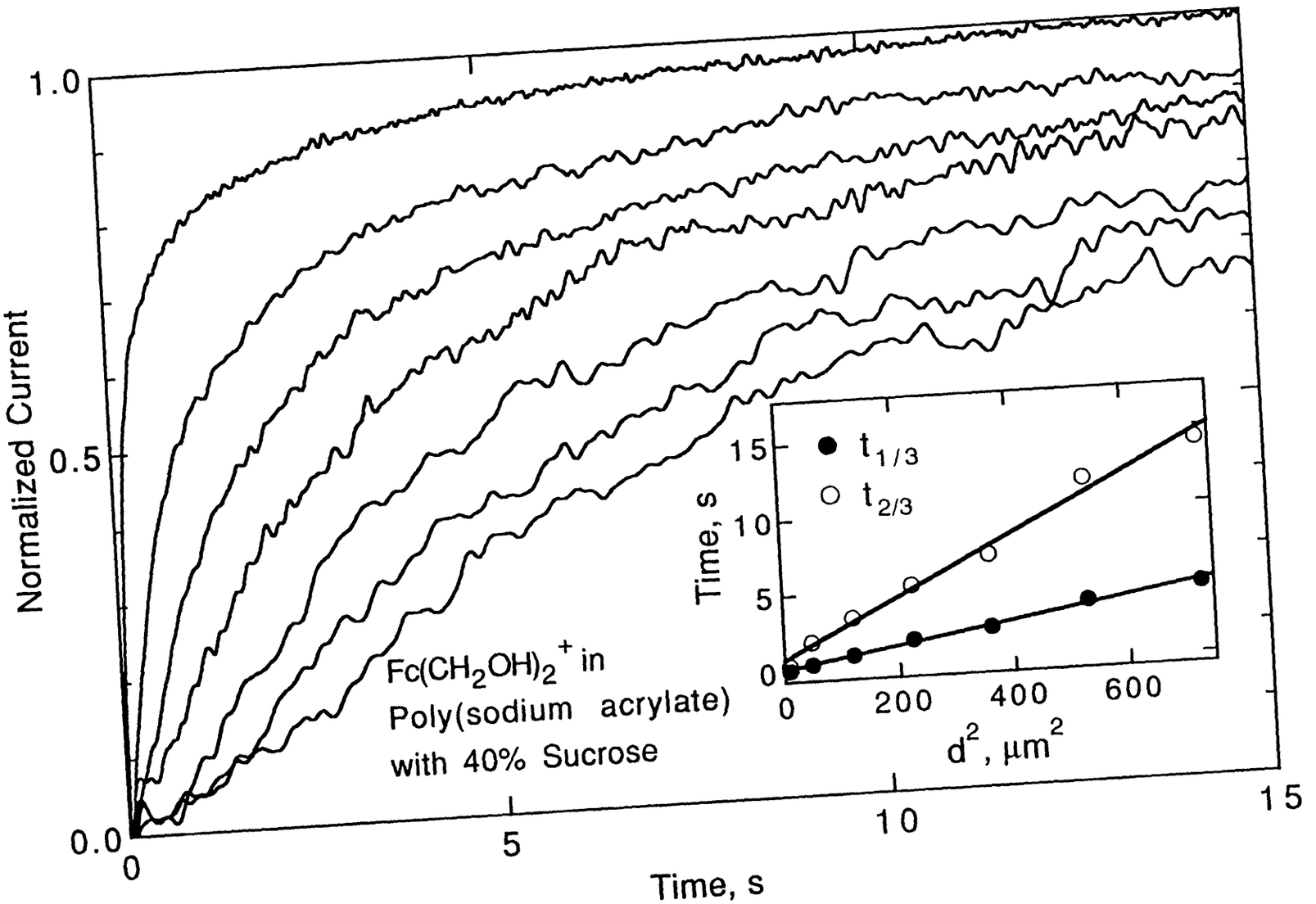
1.0
0.5
0.0
Normalized Current
0
5
10
15
Time, s
Fc(CH2OH)2+ in
Poly(sodium acrylate)
with 40% Sucrose
t1/3
t2/3
Time, s
d2, μm2
0
200
400
600

Figure 5. Plots of average $t_{1/3}$ and $t_{2/3}$ vs. d^2 at closed-face sandwich electrodes conducted for (a) 2 mM $Fc(CH_2OH)_2$ in 0.1 M aqueous sodium acetate, and (b) 2 mM $Fc(CH_2OH)_2$ in polyacrylate gel.

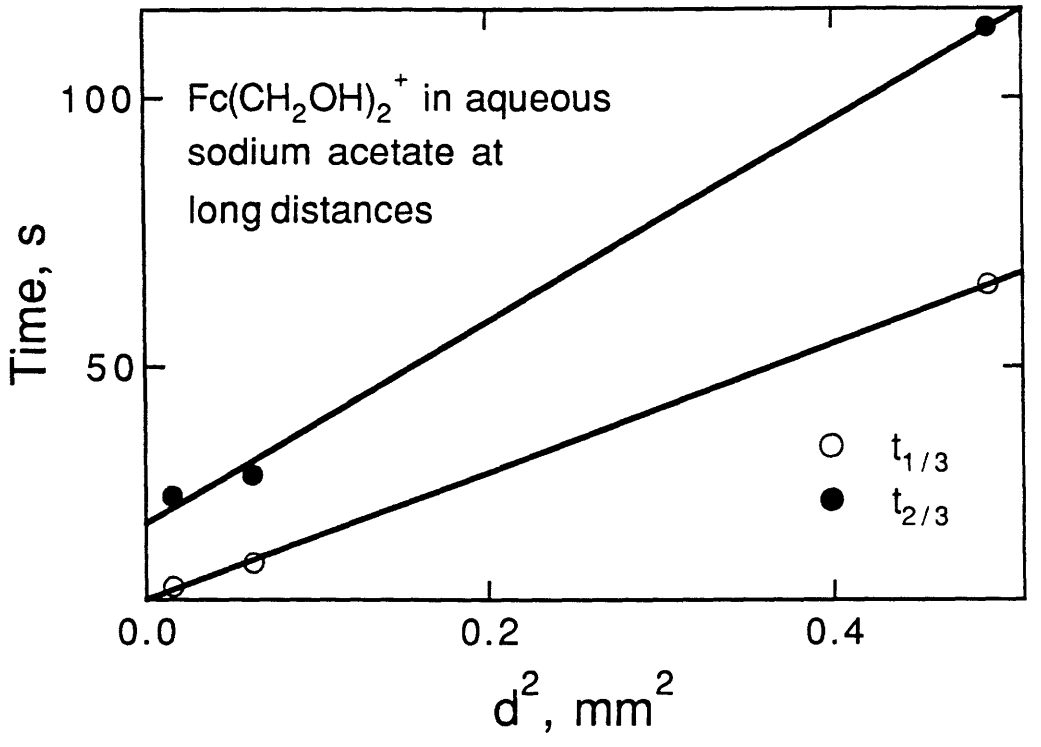
100
50
Time, s
$Fc(CH_2OH)_2^+$ in aqueous
sodium acetate at
long distances
$t_{1/3}$
$t_{2/3}$
0.0
0.2
0.4
d^2, mm^2

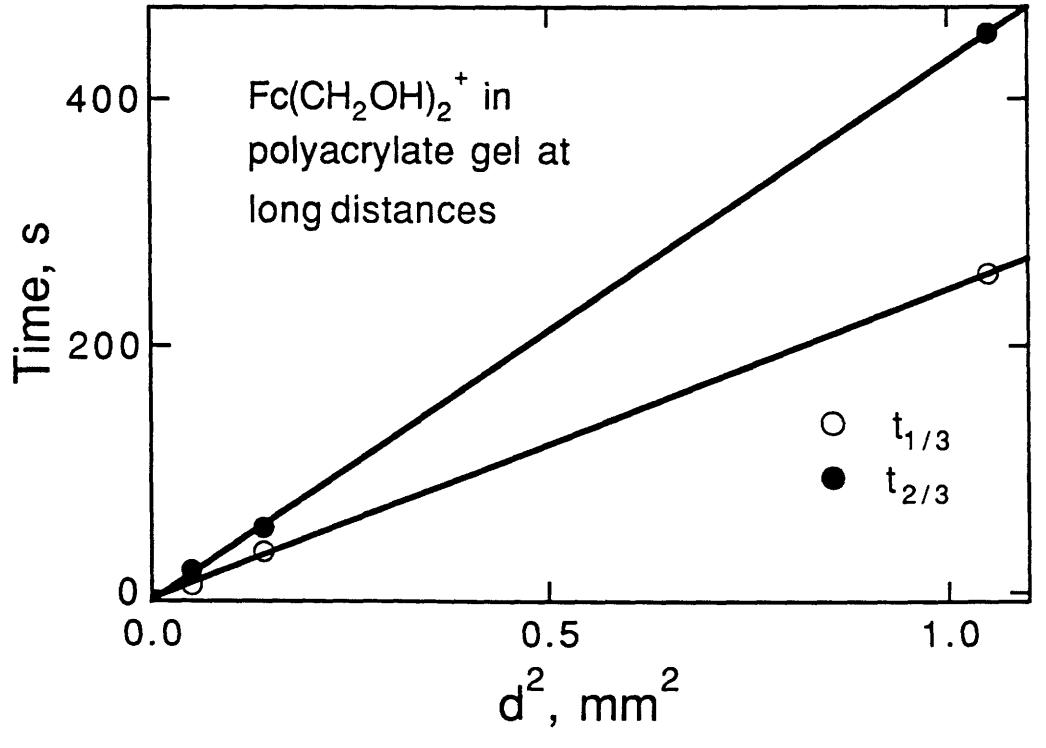
400
200
0
Time, s
$Fc(CH_2OH)_2^+$ in
polyacrylate gel at
long distances
$t_{1/3}$
$t_{2/3}$
0.0
0.5
1.0
d^2, mm^2

unaffected by convection, the low k_f results in a calculated D for the gel that is also artificially low.

The benefit of the closed face sandwich electrode experiment was actually twofold. The first purpose was to observe whether diffusion varied with distance moving from the micron distances on the microelectrode arrays to the millimeter distances of the macroelectrode configuration. Second, it allowed measurement of diffusion in gel between two electrodes that did not share a common substrate. We could thus be assured that the rapid diffusion observed in polyacrylate at microelectrodes was not an artifact resulting from diffusion in a thin layer of water separating the gel from the electrodes, but represented diffusion through the gel itself.

c. Curvature in t_f vs. d^2 Plots. Our t_f vs. d^2 plots obtained from microelectrode experiments exhibit a slight downward curvature, Figures 1 and 2. This nonlinearity indicates that k_f of these data is actually dependent on the distance between generator and collector. Similarly curved t_f vs. d^2 plots for step generation-collection at a pairs of band microelectrodes were also observed previously,[1b] but not addressed. The curvature could limit the extent to which we can accurately compare diffusivity in different systems.

The phenomenon that causes curvature in the t_f vs. d^2 plots apparently does not affect data from pulse experiments, where generation is accomplished by a potential pulse with a

length that is short compared to the transit time. The collector current in a pulse experiment exhibits a peak and the time of that peak is the transit time.[1,21] We verified the lack of curvature with pulse experiments on $Fc(CH_2OH)_2^+$ in polyacrylate gel and $Ru(NH_3)_6^{2+}$ in phosphate buffer. In order to calculate D from the step experiments, the relative magnitudes of the collector current must be known in the transient and quasi-steady-state regimes. In pulse experiments, only the time of the collector current peak is important and not its magnitude. Pulse experiments also involve a much shorter total time than step experiments. Since experiments at larger d require longer experiment times, factors that influence the collector current's magnitude as a function of distance and/or time should cause t_f vs. d^2 plots to curve.

We eliminated several possible causes for the curvature: convection, different diffusivity for starting and generated species, and electron transport facilitated by electrodes lying at open circuit between generator and collector. Convection can influence the flux of species to an electrode, especially at long time scales. Although polyacrylate gel dampens natural convection, t_f vs. d^2 plots from step experiments in that medium are also slightly curved. The transient behavior of the collector current in a step experiment is dependent on the diffusion coefficients of both forms of the redox couple, especially when the starting species is the slower one.[24] However, assuming the diffusion

coefficients remain constant, as we would expect for a dilute solution, this effect is independent of distance and cannot contribute to curvature in the t vs. d^2 plots. Electrodes that lie between the active generator and collector may equilibrate the generated species with the starting species from the surrounding solution, and shuttle electrons faster across the array. In order to test this, we measured transit times from one side to the other of microelectrode arrays from which the intervening electrodes had been removed. The transit times obtained using these arrays did not differ significantly from those obtained using an array with all electrodes present.

d. Simulations to Investigate Factors Affecting t_f vs. d^2 Plots. Aoki and Tanaka[3] have computed currents for step generation-collection experiments at IDA's using a time-dependent finite element method. Their representation of the dependence of transit time, $t_{1/2}$, on the separation between generator and collector electrodes of the IDA is somewhat analogous to our t_f vs. d^2 plots for pairs of band microelectrodes. However, because each generator-collector unit in an IDA experiences strong shielding and feedback effects from neighboring units, we cannot quantitatively compare the simulated or experimental IDA results with ours.

We made use of digital simulations to further investigate the effects of time-dependent factors on step and pulse measurements at a pairs of band microelectrodes. Methods that have been used to simulate step generation-collection

experiments include (1) a two-dimensional finite difference method in real space,[25] which is favorable for the transient regime of the collector currents, and (2) conformal mapping,[26] which provides a simpler way to arrive at currents at long time (steady-state). We chose the random walk technique that uses the Einstein-Smoluchowski equation and was previously reported by our laboratory.[1] We modified the algorithm to include diffusion of species from the bulk (see the Experimental section). The random walk methodology closely estimates experimental collection efficiencies,[1b] which must be obtained at long times, and at short times, it demonstrates acceptable transient behavior. Other advantages of the random walk method include its easy application to multiple electrode geometries and dimensions, and to systems that approach discrete particle behavior. We first evaluate the modified algorithm, then use the simulations to investigate possible causes of curvature in the t_f vs. d^2 plots.

i. Comparison of simulated and experimental generator current. Figure 6a shows simulated and experimental generator current for a solution of $Ru(NH_3)_6^{3+}$ with and without active collectors. There is some variability in the experimental currents which is probably caused by differences in the electrode areas. The charging and background current (which the simulations do not take into consideration) were removed from the experimental data by subtracting generator current in blank electrolyte from the current in electrolyte

Figure 6. Comparison of data from experiment, theory and random walk simulations. Two sets of experimental data are overlaid to demonstrate variability; the experimental curves were scaled by the same factor. Electrodes are 2 μm wide and separated by 2 μm. (a) Generator response with no collectors (lower curve), one collector (middle curve), and two collectors (upper curve). (b) Collector response to a single generator; one collector (lower set of curves), and two collectors (upper set of curves).

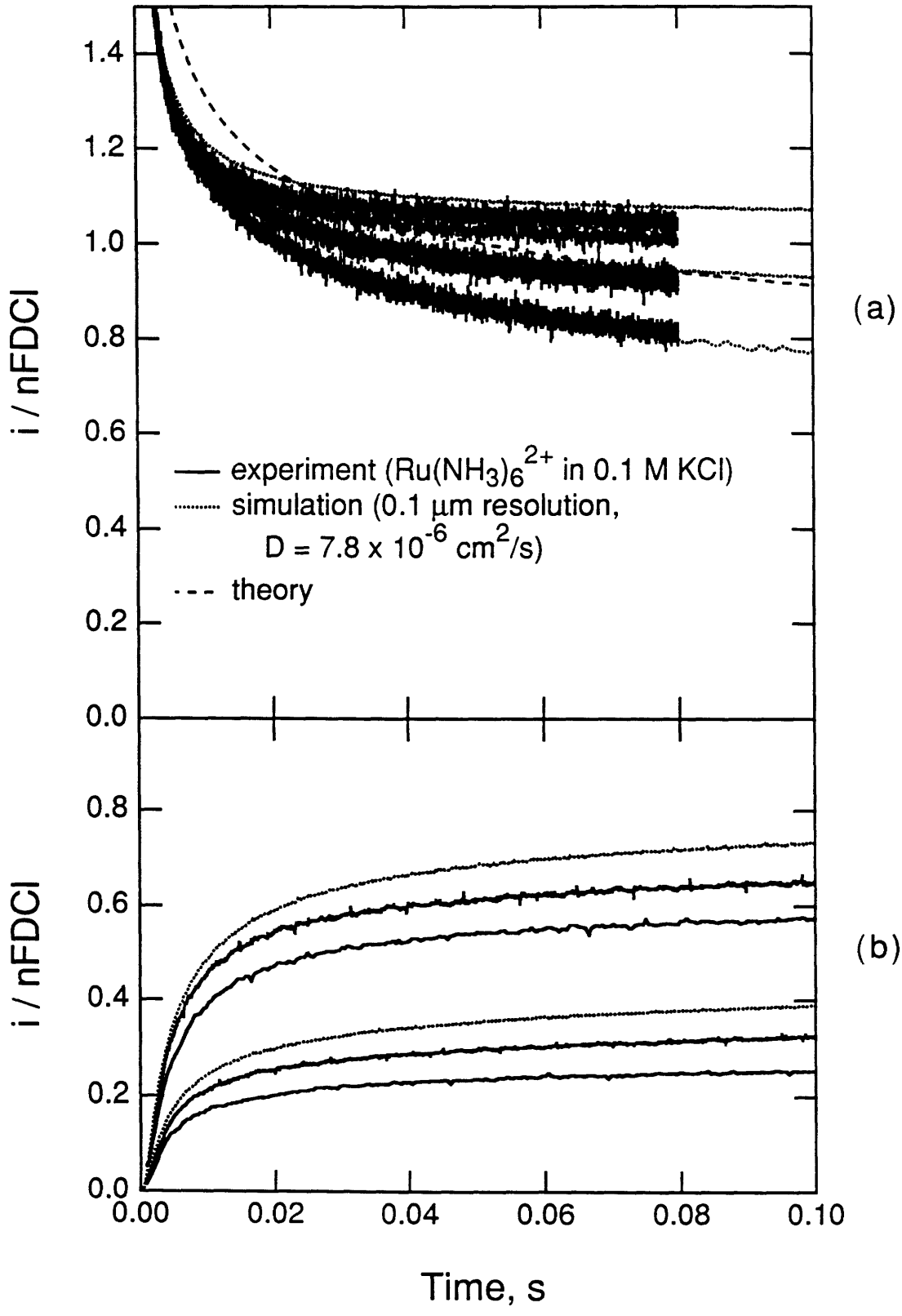
i / nFDCl
1.4
1.2
1.0
0.8
0.6
0.4
0.2
0.0
experiment ($Ru(NH_3)_6^{2+}$ in 0.1 M KCl)
simulation (0.1 μm resolution,
D = 7.8 x 10^{-6} cm^2/s)
theory
(a)
i / nFDCl
0.8
0.6
0.4
0.2
0.0
(b)
0.00
0.02
0.04
0.06
0.08
0.10
Time, s

containing redox species. The experimental data were then scaled by the factor required to match the simulated and experimental curves for the case without collectors. In addition, the feedback current from the collectors is lower than in the simulations. One factor contributing to this difference is that the diffusion coefficients of the oxidized, D_O, and reduced, D_R, forms of the molecule are equal in the simulation ($D_O = D_R = 7.8 \times 10^{-6}$ cm^2/s), but in the experiment they are not equal ($D_O = 7.1 \times 10^{-6}$ cm^2/s, and $D_R = 7.8 \times 10^{-6}$ cm^2/s).[1,25] Since feedback current is proportional to $D_O D_R/(D_O+D_R)$,[27] the simulation should over estimate the experimental feedback current by about 5%. Although current magnitudes from the simulations and experiments cannot be directly compared, they are internally consistent in that the feedback current for one active collector is half the feedback current for two active collectors.

The "theoretical" curve in Figure 6a is the graphical representation of the numerical solution, equation (9) in reference 28, for the time dependence of current at a single microband generator electrode; an exact equation does not exist. The magnitude of the theoretical and simulation curves differ by about 13%. The numerical solution can lie within 1.3% of the experimental data, but will especially overestimate the magnitude in the transient regime.[28] In addition, the shape of the transient portion of the

experimental curve more closely matches the simulated than the theoretical curve.

ii. Comparison of simulated and experimental collector current. An internal comparison of the collector current from simulations is consistent with that from experiments, Figure 6b. In both cases, because of shielding effects, the shape of the two-collector current is flatter and the magnitude is less than two times the one-collector current.

iii. Grid Size. The size and shape of grid elements can influence the outcome of a digital simulation, and control the computation time.[26] Previous work with the random walk algorithm involved only one grid size of low resolution, equal to the separation (1.37 μm) between two microband electrodes.[1] Figure 7 compares collector currents at 0.5 μm, 0.2 μm, and 0.1 μm resolutions for step generation-collection simulations.

The simulations attempt to approximate a non-Cartesian coordinate system with Cartesian coordinates.[26] Thus, smaller grid dimensions better approximate the radial diffusion of the molecules. The t_f vs. d^2 plots of simulated data actually curve slightly upward, Figure 8, the opposite of experimental t_f vs. d^2 plots. This is because the gap-to-grid-size ratio increases with d. This means that for a constant grid size, the diffusion pathway between generator and collector is always more direct across the smallest gaps, yielding higher feedback currents and shorter transit times. Therefore, at higher resolutions, more linear t_f vs. d^2 plots

Figure 7. Comparison of step simulations with different resolutions; (a) Generator response with no collectors (lower curve), one collector (middle curve), and two collectors (upper curve). (b) Collector response to a single generator; one collector (lower set of curves), and two collectors (upper set of curves). Electrodes are 2 μm wide and separated by 2 μm, D = 7.8×10^{-6} cm^2/s.

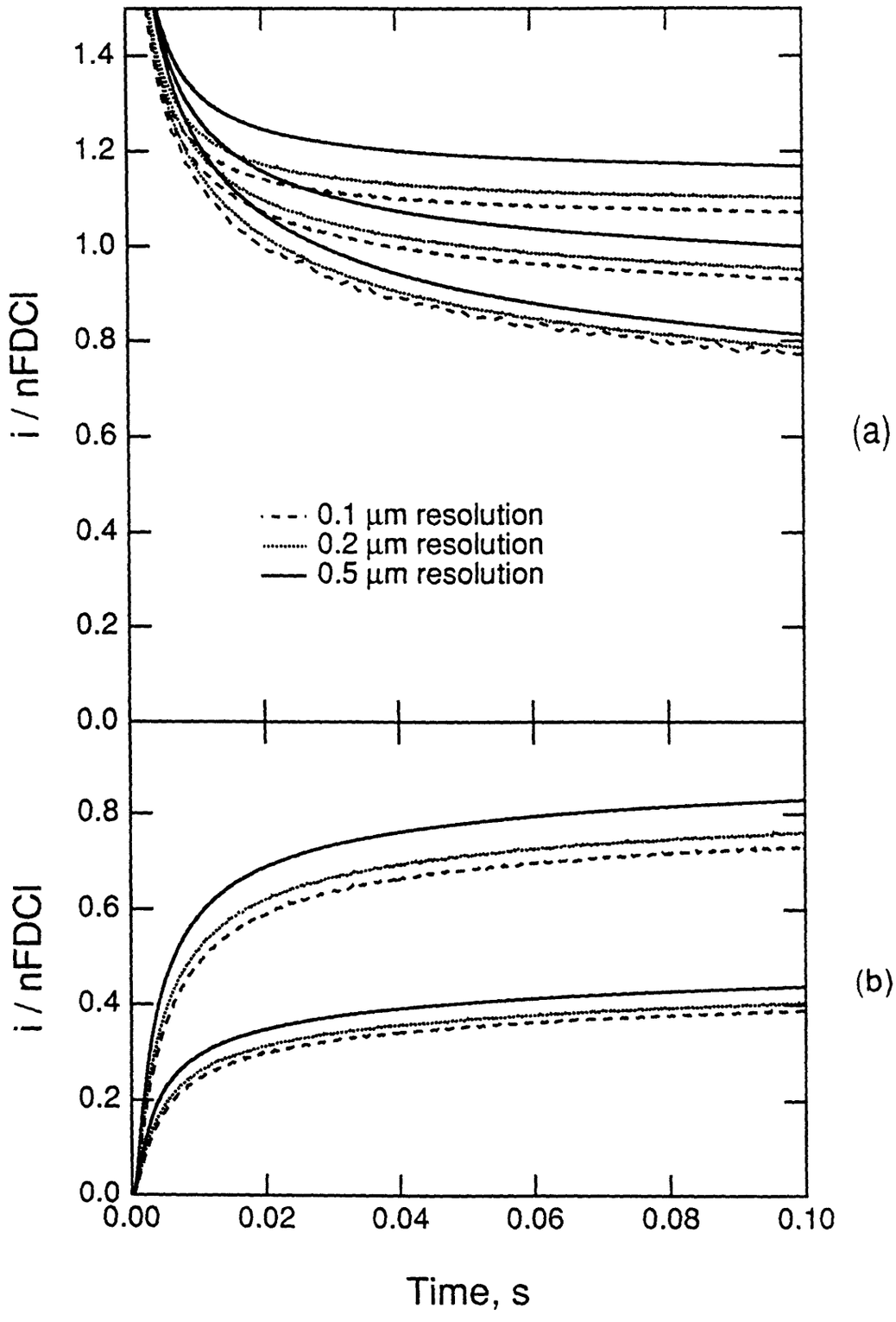
i / nFDCI
1.4
1.2
1.0
0.8
0.6
0.4
0.2
0.0
0.1 μm resolution
0.2 μm resolution
0.5 μm resolution
(a)
i / nFDCI
0.8
0.6
0.4
0.2
0.0
(b)
0.00
0.02
0.04
0.06
0.08
0.10
Time, s

can be achieved. The t_{peak} vs. d^2 plots of data from pulse simulations also curve upward more at lower resolution. The proportionality constant we calculated from pulse simulations, where the resolution was 0.5 μm and d ranged from 3 μm to 27 μm, was 0.21(±0.008) which is within error of previously reported experimental results (0.22).[1] Thus, the sections that follow refer to simulations that were performed at 0.5 μm resolution to demonstrate trends, rather than absolute magnitudes, and to expend minimal computation time.

iv. Quasi-Steady-State Generator Current. The flux to the generator consists of a contribution from species in the bulk solution and from collector feedback. The contribution from the bulk decays slowly with time.[28] This time-dependent phenomenon may contribute to downward curvature in the t_f vs. d^2 plots. Since our simulations are limited by resolution, we have not been able to conclusively determine whether this decaying generator current contributes to the downward-curvature in the k_f vs. d^2 plots. Determination of k_f (equation (2)) by calibrating with a redox system having diffusivities similar to the system under investigation on an array with the same geometry minimizes this concern.

v. Passivation. Microelectrodes passivate quickly due to high current density. Passivation decreases the effective electrode area.

In our simulations we focused on the passivation of the generator electrode, equation (3), where A is the

$$A + M \rightarrow AM \quad (3)$$

starting species electrolyzed at the generator, M is the number of free sites, and AM is an irreversibly, passivated product. The following rate expression was used to calculate the change in available area:

$$\text{Rate} = \Delta\theta/\Delta t = k(1-\theta)[A] \quad (4)$$

The rate is expressed as a change in the fraction of passivated sites $\Delta\theta$ (or area), in a given amount of time, Δt.

The influence of passivation on both pulse and step experiments was simulated for $k = 1 \times 10^4$ M^{-1}. In pulse simulations, which involve very short time scales, the collector response under passivating conditions remained unchanged. Figure 9 illustrates the passivating effect on the collector current for step simulations at d = 3 μm, 7 μm, and 11 μm. As in the pulse simulations, the behavior at short time scales is unaffected.

At longer times, however, the current flattens faster for $k = 1 \times 10^4$ M^{-1} than for $k = 0$ M^{-1}. This time-dependent effect is subtle, but if k is large, and the time scale of the experiment is long enough, the current will peak and then begin to drop. Figure 8 shows that the t_f vs. d^2 plot of data under passivating conditions bends downward from the nonpassivating case. Thus, the simulations indicate that passivation can significantly contribute to curvature in the

Figure 8. The $t_{1/3}$ and $t_{2/3}$ vs. d^2 plots for step generation-collection simulations with and without passivation. D = 5.8 x 10^{-6} cm^2/s, resolution = 0.5 μm.

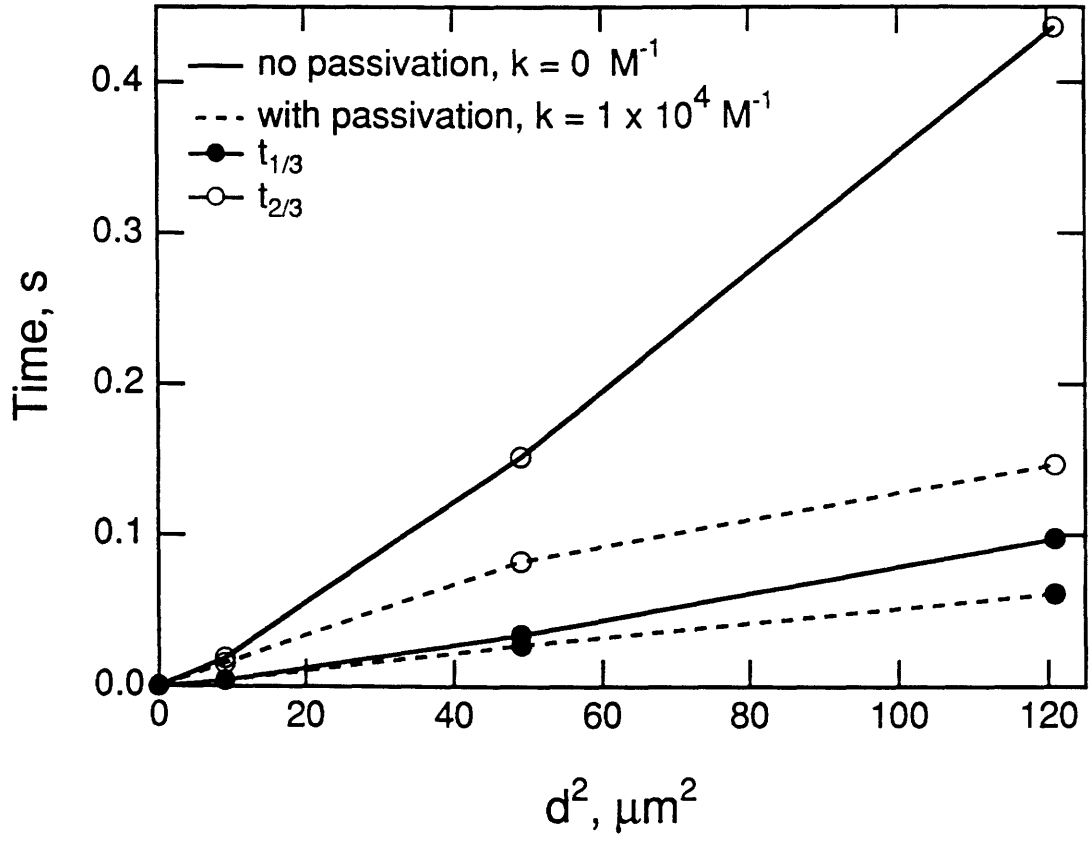
no passivation, k = 0 M-1
with passivation, k = 1 x 10^4 M-1
t1/3
t2/3
Time, s
0.0
0.1
0.2
0.3
0.4
0
20
40
60
80
100
120
d2, µm2

Figure 9. Passivation effects on collector currents for step generation-collection simulations with d of 3 μm (upper curves), 7 μm (middle curves), and 11 μm (lower curves); $D = 5.8 \times 10^{-6}$ cm^2/s, resolution = 0.5 μm.

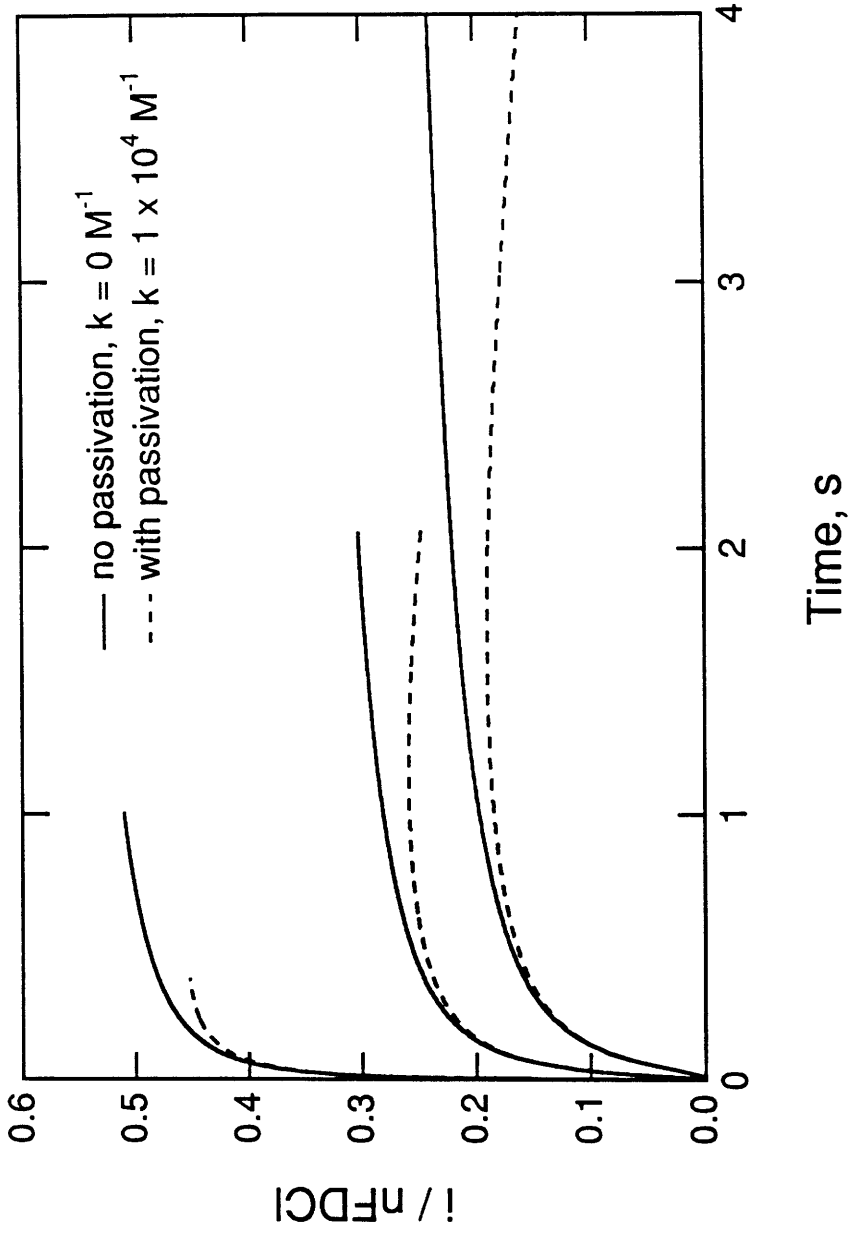
i / nFDCI
Time, s
— no passivation, k = 0 M-1
- - - with passivation, k = 1 x 10^4 M-1
0.0
0.1
0.2
0.3
0.4
0.5
0.6
0
1
2
3
4

t_f vs. d^2 plots. Although collector currents from our step generation-collection experiments did not peak, we believe that some degree of passivation did occur, because over the course of several cyclic voltammograms a decrease in current was observed.

Caution must be taken when comparing D's that are determined by the step generation-collection method. It is not clear to what extent passivation effects the calibration system and the other systems that are under investigation here. It is also possible that the collector current never achieves true steady-state because the contribution of diffusion from the bulk to the generator current is always time dependent. Since the values of maximum collector current are taken at different times for each distance, a time dependence of generator current could affect the values of t_f for different distances in such a way as to cause a systematic deviation from linearity in t_f vs. d^2 plots. However, the D calculated for $Fc(CH_2OH)_2^+$ in aqueous acetate solution, based on k_f from the $Ru(NH_3)_6^{2+/3+}$ calibration system, lies within the range expected for this species. The D for $Fc(CH_2OH)_2^+$ in polyacrylate was found to be similar to that in acetate with two different electrode configurations: microelectrode array and close-faced macroelectrodes. Thus, in spite of the errors introduced in D by slight curvature in t_f vs. d^2 plots, our conclusions remain unchanged.

e. Electrochemical Transistor Based on RuO_x. Because diffusion in polyacrylate gel is rapid, and its

viscosity high, it shows promise as a convenient electrolyte medium for various electrochemical devices. The high diffusivities of species through polyacrylate gel indicate that the gel should also exhibit ion mobilities higher than those of conventional solids,[29] and the gel would allow rapid diffusion of analyte molecules to an electrochemical sensing device.

One kind of microelectrode device that can serve as a sensor is an electrochemical transistor.[14b,12] The switching speed of such a device is often slower in solid than in liquid electrolytes, however.[14c] This is probably due to slow movement of charge-compensating ions. We compared the switching speed of an electrochemical transistor in polyacrylate and aqueous acetate to determine the viability of the gel as an electrolyte medium for the device.

A typical electrochemical transistor consists of two adjacent microelectrodes that are joined by an electroactive material whose conductivity varies with its extent of oxidation, Scheme II. The oxidation state, and thus the conductivity of the material, is modulated by controlling the potential (gate voltage, V_G) of the microelectrodes with respect to a reference electrode. A small drain voltage, V_D, applied between the two electrodes results in a drain current, I_D, that varies with V_G. Current gain of the transistor is defined as I_D/I_G where I_G, gate current, is the Faradaic current required to oxidize or reduce the conducting material.

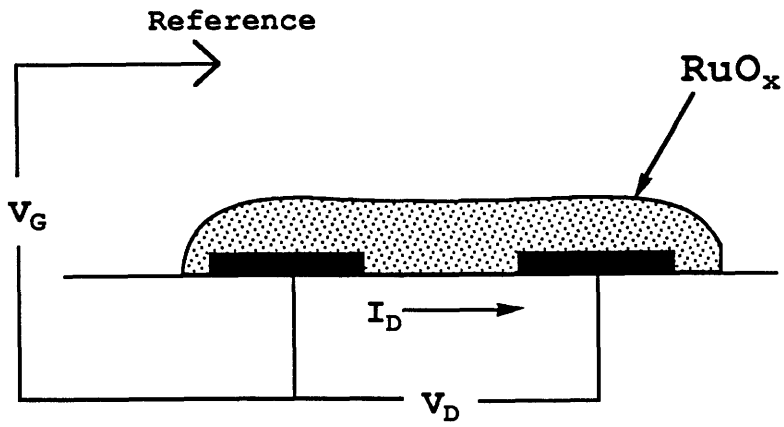

Scheme II. Electrochemical Transistor

Electrochemical transistors based on RuO_x were made. The current-voltage characteristic of a typical device has been shown previously.[6,30] We chose RuO_x because it is stable in aqueous media at pH 7. The speed of a transistor was assessed by measuring current gain over a range of frequencies, Figure 10. Frequency response of a transistor in polyacrylate gel was the same as that in aqueous sodium acetate. The speed of the electrochemical transistor is not reduced by using polyacrylate gel as the electrolyte medium. Unity gain occurs at approximately 1.5 Hz in both electrolytes; this value is typical of RuO_x based transistors.

f. Electrochromic Device. We investigated polyacrylate gel, which is optically transparent, as an electrolyte for electrochromic devices. The response of an electrochromic material deposited on a platinum flag electrode was measured by monitoring the time dependence of the change in absorbance of the material when it was oxidized

Figure 10. Current gain vs. frequency for RuO_x transistor in 0.1 M aqueous sodium acetate and polyacrylate gel electrolytes.

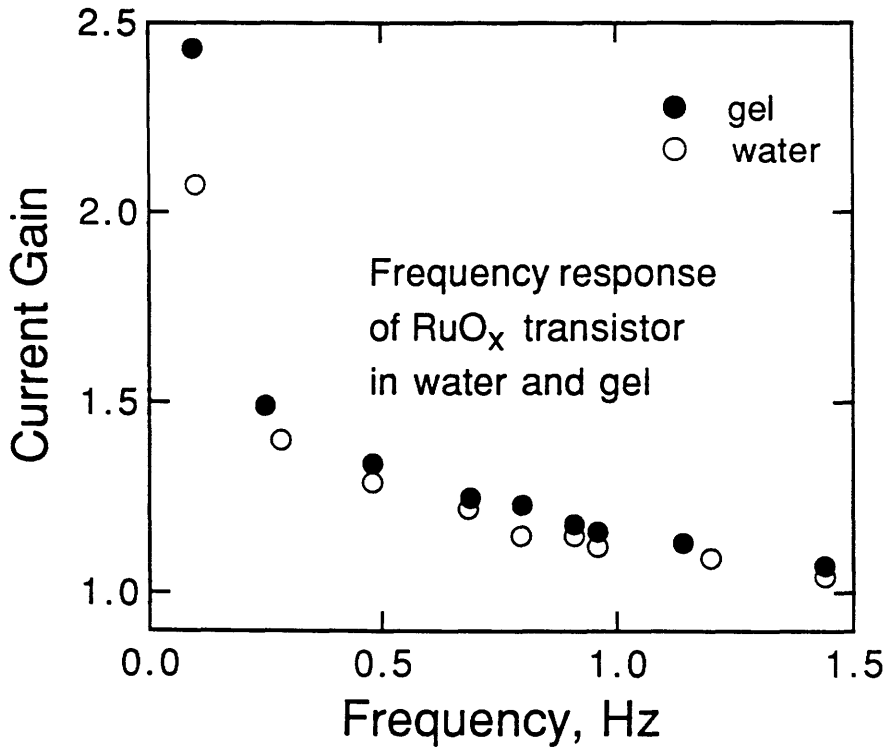
2.5
2.0
1.5
1.0
Current Gain
gel
water
Frequency response
of RuO_x transistor
in water and gel
0.0
0.5
1.0
1.5
Frequency, Hz

and reduced. The current response and absorbance change resulting from oxidation and reduction of a film of viologen polymer in polyacrylate and liquid electrolytes is shown in Figure 11. The device was characterized by the time required for the absorbance change of the film to reach half of its maximum value. The results are summarized in Table II, where t_{ox} is the response to oxidation and t_{red} is the response to reduction.

The electrochromic device showed a slower response in polyacrylate than in aqueous media. This is probably due to the fact that the redox chemistry of viologen requires charge compensation by anions. Incorporation of the large, multi-anionic polymer chains of polyacrylate into the film may impede redox processes. The response time of the RuO_x based microelectrochemical transistor, however, is not limited in the same way because its charge is compensated by cations.[30]

Figure 11. Absorbance and current responses for an electrochromic device based on **III** in aqueous acetate and polyacrylate gel electrolytes. Coverage = 1 x 10^{-8} mol/cm^2.

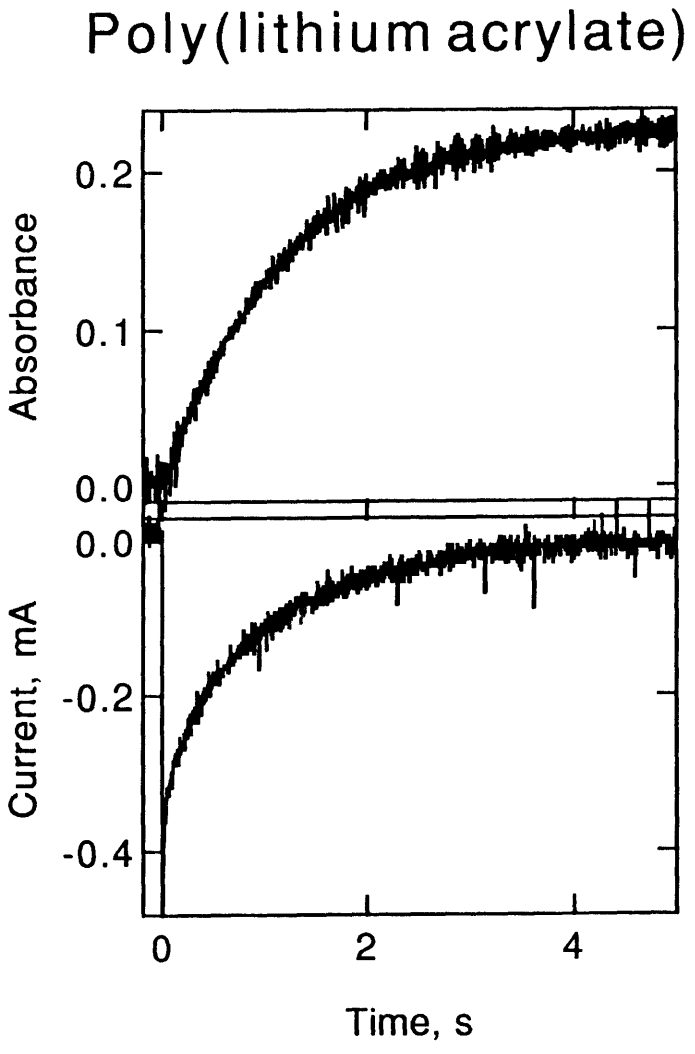
Poly(lithium acrylate)
Absorbance
0.2
0.1
0.0
Current, mA
0.0
-0.2
-0.4
0
2
4
Time, s

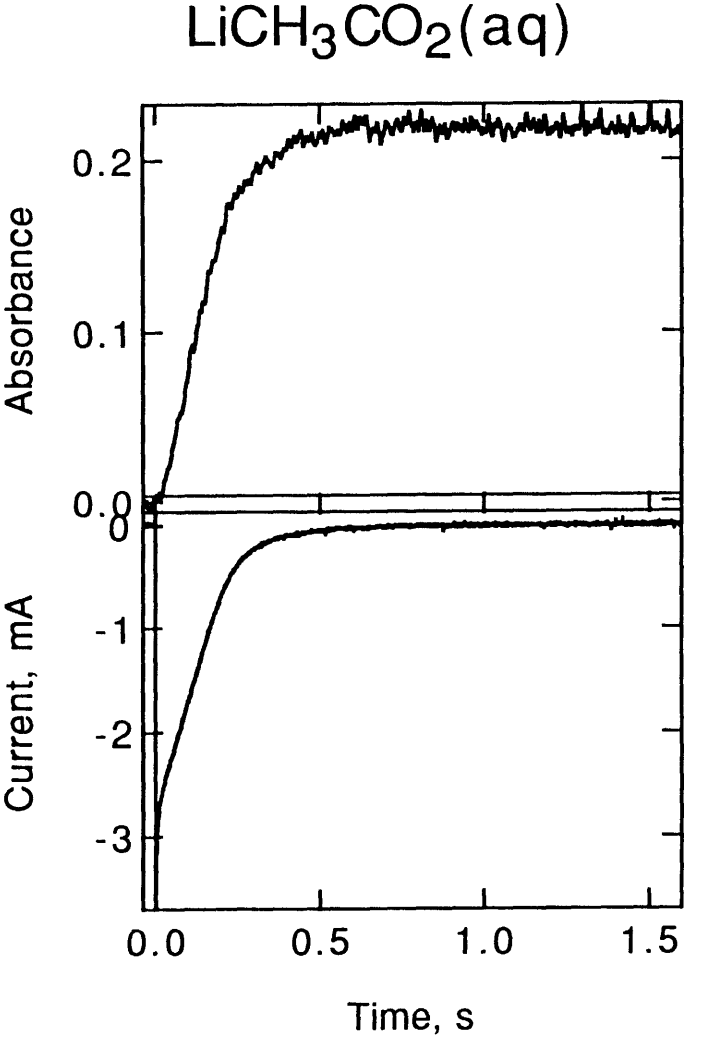
LiCH3CO2(aq)
Absorbance
0.2
0.1
0.0
Current, mA
0
-1
-2
-3
0.0
0.5
1.0
1.5
Time, s

Conclusions

We have presented electrochemical measurement of the diffusion coefficient of $Fc(CH_2OH)_2^+$ in polyacrylate, a polymer gel electrolyte. It was found that diffusion in polyacrylate gel is nearly as fast as in aqueous electrolytes, in spite of the non-fluid behavior of polyacrylate. We did not find a significant difference in diffusivities across long (up to 1 mm) and short (3 μm - 27 μm) distances in polyacrylate. This indicates that diffusion is not limited to small-scale liquid domains that are trapped near the surface of a microelectrode array used to study the diffusion of small species in the gel electrolyte.[9] In addition, the experimental diffusion results presented here are consistent with the proposed structure of polyacrylate.

There are limitations to the accuracy of diffusion coefficients determined by step generation-collection, as exemplified by the small curvature in the t_f vs. d^2 plots. However, our conclusions, which are based on comparison of chemically similar systems, are unaffected. Because the transit times from step experiments require knowledge of the ratio of the collector current in two different time regimes, time-dependent phenomena, such as passivation or failure of generator currents to reach true steady state, can yield non-linear t_f vs. d^2 plots for step experiments. The most accurate D's will be determined for systems that best mimic the calibration system that was used to determine k_f. The

advantage of the step technique over the pulse technique is that the collector current is larger, and thus, easier to measure. Pulse[1] or time-of-flight[4] experiments are preferred transient techniques if their small currents are measurable.[25]

Rapid diffusion makes polyacrylate a promising medium for electrochemical devices, as long as device materials are compatible with the pH range over which polyacrylate maintains its high viscosity and clarity. We have demonstrated that a microelectrochemical device based on RuO_x and an electrochromic device based on a surface-confined viologen polymer can operate with polyacrylate gel as their electrolyte medium. Since it is possible to make polyacrylate gels in nonaqueous solvents it should also be possible to employ a wide variety of device-active materials.

Acknowledgments. We thank the Office of Naval Research and the Department of Energy for partial support of this research. We thank Dr. G. Tayhas Palmore for preparing **III**, and Dr. Suchi Chao for preparing $Fc(CH_2OH)_2$. We thank B. F. Goodrich Co. for supplying the Carbopol® 940 used in this study. The work described chapter is the result of a collaborative effort with Dr. Ingrid Fritsch-Faules and has been published in the *Journal of Physical Chemistry* [*J. Phys. Chem.* **1990**, *94*, 2680].

Tables

Table I. Diffusion coefficients of $Fc(CH_2OH)_2^+$.

Medium	D ($\times 10^{-6}$ cm^2/s)	Distance
polyacrylate	5.8(±0.4)	short
polyacrylate	3.9(±0.5)	long
$NaCH_3CO_2$(aq)	8.8(±0.8)	short
polyacrylate, 40% sucrose	1.0(±0.1)	short
*$NaCH_3CO_2$(aq), 40% sucrose	1.3	short

*Estimated from two data points.

Table II. Electrochromic response times to oxidative and reductive potential steps.*

Electrolyte	t_{ox} (ms)	t_{red} (ms)
$NaCH_3CO_2$(aq)	80	138
LiCl(aq)	55	100
Polyacrylate Gel	470	1220

*Values listed are the times required to reach half of the maximum absorbance change for oxidation, t_{ox}, and reduction, t_{red}, of a film of **III**.

References

1. (a) Licht, S.; Cammarata, V.; Wrighton, M. S. *Science* **1989**, *243*, 1176 (b) Licht, S.; Cammarata, V.; Wrighton, M. S. J. Phys. Chem., **1990**, *94*, 6133.

2. Niwa, O.; Morita, M. Tabei, H. *Anal. Chem.* **1990**, *62*, 447.

3. Aoki, K.; Tanaka, M. *J. Electroanal. Chem.* **1989**, *266*, 11.

4. Feldman, B. J.; Feldberg, S. W.; Murray, R. W. *J. Phys. Chem.*, **1987**, *91*, 6558.

5. White, H. S.; Kittleson, G. P.; Wrighton, M. S. *J. Am. Chem. Soc.* **1984**, *106*, 5375.

6. Lyons, D. F. Ph.D. Thesis, Massachusetts Institute of Technology, Jan. 1988.

7. Bookbinder, D. C.; Wrighton, M. S. *J. Electrochem. Soc.*, **1983**, *130*, 1080.

8. "Carbopol® Water Soluble Resins," Document No. GC-67, B. F. Goodrich Co., Specialty Polymers and Chemicals Div., Cleveland.

9. Taylor, N. W.; Bagley, E. B. *J. Applied Polymer Science*, **1974**, *18*, 2747.

10. Davison, J. A.; Collins, E. A. *J. Colloid and Interface Science*, **1976**, *55(1)*, 163.

11. Deasy, P. B.; O'Neill, C. T. *Pharm. Acta. Helv.*, **1989** *64(8)*, 231.

12. Schloh, M. O. Ph.D. Thesis, Massachusetts Institute of Technology, Jan. 1990.

13. Chao, S.; Wrighton, M. S. *J. Am. Chem. Soc.* **1987**, *109*, 6627.

14. (a) Talham, D. R.; Crooks, R. M.; Cammarata, V.; Leventis, N.; Schloh, M. O.; and Wrighton, M. S. *NATO ASI "Lower-Dimensional Systems and Molecular Electronics"* Spetses, Greece, 1989, Metzger, R. M.; Day, P; Papavassiliou, G. Eds. Plenum Press. (b) Chao, S.; Wrighton, M. S. *J. Am. Chem. Soc.*, **1987**, *109*, 6627. (c) Chao, S.; Wrighton, M. S. *J. Am. Chem. Soc.* **1987**, *109*, 2197.

15. Stinson, S. *Chem. Eng. News* **1992**, 70(16), 20.

16. Levine, I. N. *Physical Chemistry* McGraw-Hill Book Co., New York, 1983, p. 471.

17. Yam, K. L.; Anderson, D. K.; Buxbaum, R. E. *Science* **1988**, *241*, 330.

18. Kittleson, G. P.; White, H. S.; Wrighton, M. S. *J. Am. Chem. Soc.* **1984**, *106*, 7389.

19. Einstein, A. *Investigations on the Theory of Brownian Movement*; Dover: U.S.A., 1965.

20. Bard, Allen J., and Faulkner, Larry R. *Electrochemical Methods* John Wiley & Sons, Inc., New York, 1980, p. 406.

21. Cammarata, V.; Talham, D. R.; Crooks, R. M.; Wrighton, M. S. *J. Phys. Chem.* **1990**, *94*, 2680.

22. Nesmeyanov, A. N.; Perevalova, E. G.; Beinoravichute, Z. A. *Doklady Akad. Nauk S.S.S.R.* **1957**, *112*, 439.

23. Dominey, R. N.; Lewis, N. S.; Wrighton, M. S. *J. Phys. Chem.* **1983**, *87*, 5345.

24. Fritsch-Faules, I.; Faulkner, L. R. *J. Electroanal. Chem*, in press.

25. Bard, A. J.; Crayston, J. A.; Kittlesen, G. P.; Shea, T. V.; Wrighton, M. S. *Anal. Chem.* **1986**, *58*, 2321.

26. Fosset, B.; Amatore, C. A.; Bartlett, J. E.; Michael, A. C.; Wightman, R. M. *Anal. Chem.* **1991**, *63*, 306.

27. Anderson, L. B.; Reilly, C. N. *J. Electroanal. Chem.*, **1965**, *10*, 295.

28. Szabo, A.; Cope, D. K.; Tallman, D. E..; Kovach, P. M.; Wightman, R. M. *J. Electroanal. Chem.* **1987**, *217*, 417.

29. (a) Wooster, T. T.; Longmire, M. L.; Zhang, H.; Watanabe, M.; Murray, R. W. *Anal. Chem.* **1992**, *64*, 1132. (b) Grecki, W.; Andreni, R.; Berthier, c.; Armand, M.; Mali, M.; Roos, J.; Brinkman, D. *Solid State Ionics* **1986**, *18 & 19*, 295.

30. "Chemically Modified Microelectrode Arrays," Natan, M. J.; Wrighton, M. S. In *Progress in Inorganic Chemistry* vol. 37, S. J. Lippard, Ed., John Wiley & Sons, Inc., New York, 1989, p 440.

Chapter Three

Pulse Generation-Collection Measurement of Diffusion of Silver Ions in Frozen Perchloric Acid Hydrate: Evidence for Two-Phase Behavior

Introduction

We report measurement of diffusion of Ag^+ in frozen $HClO_4 \cdot 5.5H_2O$ in the temperature range of -45°C to -85°C. Diffusion was measured using a pulse generation-collection technique[1] at arrays of band microelectrodes on a device whose design provides for placement of a quasi-reference electrode in close proximity to the working electrodes. The microelectrode array design facilitates electrochemistry in resistive media such as solid polymer electrolytes and frozen solvent electrolytes. The pulse generation-collection technique was developed in this laboratory,[2] and is similar to "time-of-flight" experiments which have been described elsewhere.[3]

While the study of electrochemical processes is frequently limited to temperatures where solvents are liquid, electrochemistry at low temperatures where many electrolyte media are rigid is interesting for a number of reasons.[4] Low temperatures allow more complete experimental investigation of theories of electron transfer reactions,[5] tunneling processes[6,7] and double-layer capacitance.[8] At low temperatures it is possible to study the behavior of species that are thermally labile,[9] and to kinetically separate electrode processes of interest from interfering processes.[10] There have also been recent examples of electrochemistry using superconducting electrodes above and below their critical temperatures.[11] Electrochemistry has been done at low temperatures in liquid SO_2 and NH_3 electrolytes (primarily

because of their unusual potential windows and/or solvation properties)[12,13] and in eutectic solvent mixtures that freeze as low as -185°C.[14]

Electrochemistry in $HClO_4 \cdot 5.5H_2O$ and other acid hydrates has been demonstrated, but studies have focused primarily on conductivity,[7] electrode reaction kinetics[15,16] and double layer capacitance[8] with little attention to diffusion of dissolved species.[4] Electrochemical diffusion studies of redox active solutes in $HClO_4 \cdot 5.5H_2O$ to date have not been able to distinguish physical diffusion from electron hopping between redox centers. Pulse generation-collection of Ag^+ provides for measurement of physical diffusion in the absence of any contribution from electron hopping. Electron hopping is excluded because the diffusing species is present in solution in only one oxidation state. Because "collected" Ag precipitates onto the collector electrode, its movement can be unambiguously established following generation-collection using electrochemical or surface analysis.

The $HClO_4 \cdot 5.5H_2O$ system is convenient for electrochemical studies because it freezes congruently at approximately -45°C to give a plastic crystalline,[17,18] ionic solid.[19] NMR and X-ray diffraction studies indicate that $HClO_4 \cdot 5.5H_2O$ crystallizes in a clathrate structure that allows high proton mobilities at temperatures as low as -93°C.[18,20] Studies show that the same electrode processes that occur in liquid electrolytes also occur when the electrolytes is frozen.[7,15] Use of $HClO_4 \cdot 5.5H_2O$ avoids complications arising from

incongruent freezing of other aqueous acid systems[7,21] and precipitation of supporting electrolytes as organic solvent systems are cooled.[22]

Complications caused by precipitation of the analyte molecule and the large iR drop in resistive electrolyte media are avoided in pulse generation-collection of Ag. Our experiments utilize arrays of band microelectrodes in the device configuration shown in Figure 1. The working electrodes are ~2 μm x ~100 μm and are separated by spaces of ~2 μm. The six working electrodes are located ~400 μm from a larger rectangular electrode that serves as both counter and quasi-reference electrode.

A representation of the pulse generation-collection experiment is shown in Scheme I. A typical experiment involves one generator from which Ag^+ is generated in a pulse and one collector electrode upon which the diffusing Ag^+ is collected as plated Ag. The generator is pulsed to a potential where the Ag will be oxidized to Ag^+. The Ag^+ dissolves in the electrolyte and diffuses away. Upon reaching the collector electrode, which is held at a potential that will reduce Ag^+, the dissolved Ag^+ is plated. The collector current associated with Ag^+ to Ag reduction is time dependent and exhibits a peak time, t_{mt}, related to the diffusion coefficient, D, of Ag^+, according to equation (1) where d is the distance from the center of the generator electrode to the

$$t_{mt} = 0.22 \frac{d^2}{D} \qquad (1)$$

Figure 1. Optical micrograph of a microelectrode array showing (a) band working electrodes only, (b) working and counter/quasi-reference electrodes, and (c) the entire device including leads and bonding pads that provide electrical contact for each of the eight electrodes on the device.

A)

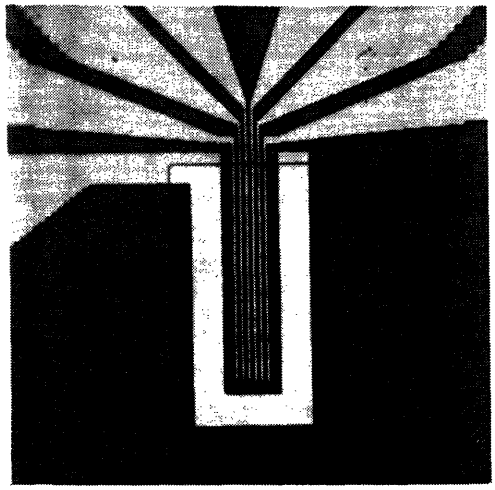

50μm

B)

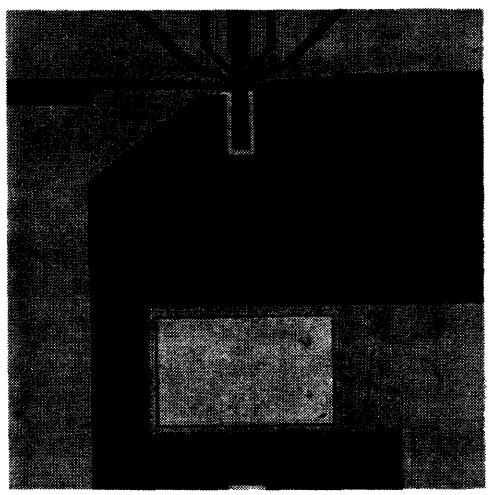

200μm

C)

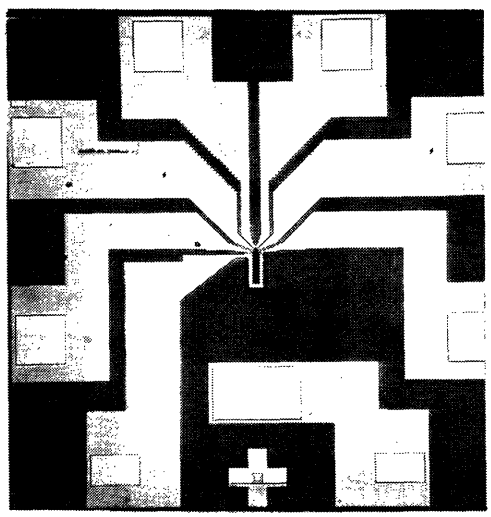

500μm

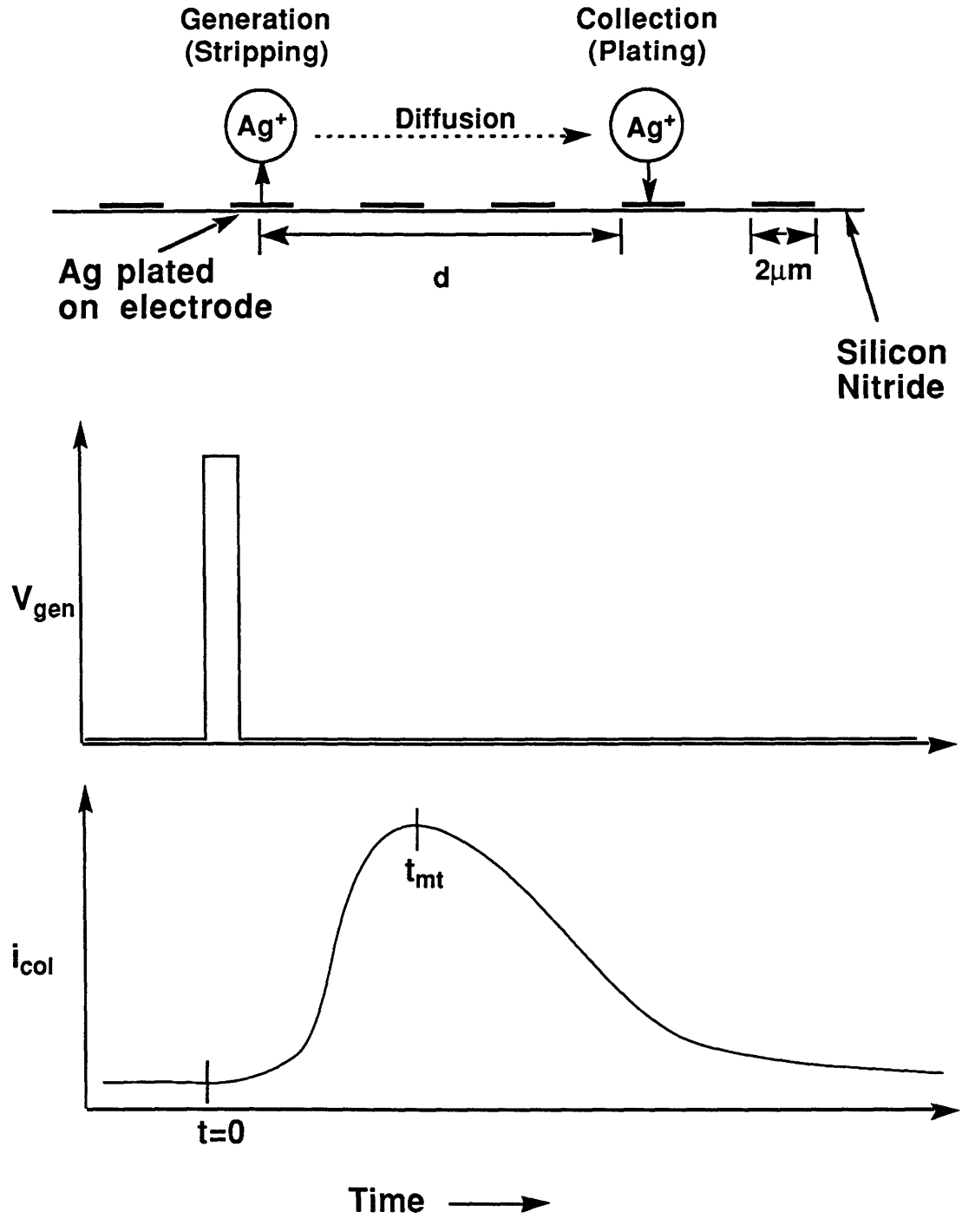

Scheme I. Pulse Generation-Collection Experiment.

nearest edge of the collector electrode. The constant of proportionality, 0.22, in equation (1) is an empirically determined value and is characteristic of the band microelectrode array.[1,2] Note that the measurement of t_{mt}, and knowing the microelectrode array geometry (including d) allows determination of D without knowing the solubility or concentration of the diffusing species. Thus, in principle, the technique represented in Scheme I allows measurement of the diffusion constant of Ag^+ in the frozen $HClO_4 \cdot 5.5H_2O$ medium.[2]

Experimental

Electrochemistry. All electrochemical measurements were carried out using a Pine Instrument Co. RDE-4X1 bipotentiostat. Data were recorded on a High Techniques IQ300 digital oscilloscope or a Kipp & Zonen BD90 XY chart recorder. All solutions used for electrochemistry were first deoxygenated by purging with Ar. For pulse generation-collection experiments and Ag plating the RDE-4X1 was driven by a PAR 174 Universal programmer. Since the value of t_{mt} can be distorted if the length of the pulse is too great, we compared the pulse length to t_{mt} after each measurement, and if the pulse was longer than $t_{mt}/3$ the data were thrown out and the pulse length was reduced in proceeding experiments.

Microelectrode Arrays. Fabrication techniques and mounting of microelectrode arrays have been described,[23] and slight modification of these were involved in the preparation of Au arrays used in this work (Figure 1). After mounting, arrays were etched three times with 3:1 mixture of concentrated H_2SO_4 and 30% H_2O_2 for 5-15 s. Immediately prior to diffusion measurements, microelectrode arrays were electrochemically cleaned by scanning individual electrodes between -0.8 V and -1.3 V vs. SCE several times in aqueous 0.1 M K_2HPO_4. Electrodes were then characterized by cycling individual electrodes and adjacent pairs between 0 V and -0.6 V in 2 mM $Ru(NH_3)_6Cl_3$ in pH 7 Na_3PO_4 buffer. Well-behaved individual electrodes give sigmoidal cyclic voltammograms with current maxima of 10 to 20 nA. Adjacent pairs of electrodes were

considered to be electrically isolated from each other when cycling both electrodes together gave current maxima ~30% higher than individual electrodes. Although the microelectrode array design includes an electrode ~10 μm from the working electrodes which could serve as quasi-reference (the "shield" around the six microelectrodes in Figure 1), we discovered that this distance was actually too close. Stray current passing through the reference circuit was found to interfere with measurements at the working electrodes. Therefor the counter and quasi-reference are the same and are the rectangular (~300 μm x ~400 μm) electrode located 400 μm away from the generator-collector pairs.

Generator Electrode Preparation. Silver was plated onto every other electrode of the six band array and on the quasi-reference electrode by stepping the electrode from 0 to -0.5 V vs. an Ag wire that served as both quasi-reference and counter electrode for 0.5 s. The resulting layer of Ag was optically smooth (bright plated) and did not measurably affect the dimensions of the electrodes. Thus, the three Ag plated Au microelectrodes serve as three independent generator electrodes and any one of the remaining three Au electrodes cold serve as a collector.

Low Temperature Cell. The temperature controlled electrochemical cell consisted of a glass tube with a ground glass stopper, and two septum-covered inlets at the top. An o-ring joint at the bottom was sealed around the microelectrode array (mounted on the end of an 11 mm glass

tube), so that the array faced upward. A glass jacket surrounding the cell held the cold probe from an FTS Systems Flexi-Cool refrigeration unit, the thermocouple probe from an FTS Systems TC10 temperature controller and an isopropanol bath. The cell was cooled from room temperature to its set point over 15 to 30 min. Each time the cell was cooled or the temperature was changed it was allowed to equilibrate for at least 30 min.

Auger Electron Spectroscopy. Auger electron spectroscopy line scans (~0.1 μm lateral resolution) were obtained using a PHI 660 scanning Auger microprobe operating at 8 kV, 10 nA. Prior to analysis, each sample was sputtered using a 2 kV, 20 $\mu A/cm^2$ Ar^+ beam. To minimize charging from the insulating regions, the samples were tilted at 30° with respect to the e^- beam. To each sample, a thin layer of Ag paint was applied to areas surrounding the microelectrode arrays. The samples were grounded with Ag paint to a piece of Al foil which was grounded to the spectrometer stage.

Chemicals. High purity 60% $HClO_4$ (G. Frederick Smith); $Ru(NH_3)_6Cl_3$ (Strem) and all other chemicals (Aldrich) were used as received.

Electrolyte Preparation. The $HClO_4 \cdot 5.5H_2O$ was prepared by dilution of 60% $HClO_4$ with Omnisolve glass distilled water to the appropriate concentration.

Results

We have measured physical diffusion of Ag^+ through frozen $HClO_4 \cdot 5.5H_2O$ using pulse generation-collection. The peak collection currents measured ranged between 0.1 and 1 nA. Figure 2 shows a typical collection current trace before and after smoothing. Traces shown in Figure 2 were subjected to a 55 point smooth 5 times to allow for a clearer presentation, but t_{mt} values were extracted from collection current prior to smoothing.

Normalized collection current for diffusion of Ag^+ across distances ranging from 3 μm to 19 μm at -60°C is shown in Figure 3. The peak time of the collector current (t_{mt}) is linear with d^2. These data indicate that physical diffusion of Ag^+ through $HClO_4 \cdot 5.5H_2O$ does, in fact, occur by what appears to be a random diffusion process since D is proportional to d^2. Direct experimental evidence that Ag^+ physically diffuses through frozen $HClO_4 \cdot 5.5H_2O$ is provided in Figure 4. First, in Part b the location of Ag plated on a microelectrode array prior to generation-collection measurements is shown. The location of the Ag following generation-collection is shown in Part c of Figure 4; Ag has moved from the generator electrodes to the collector electrodes.

After several repetitions of diffusion measurements at -60°C (using different microelectrode arrays on different days) an unusually large day to day variation in the data was observed, and we noted that t_{mt} seemed to cluster around two

Figure 2. Overlay of smoothed and unsmoothed collection current traces for a distance of 3 μm at -60°C. Smoothed data has been subjected to a 55 point smooth 5 times.

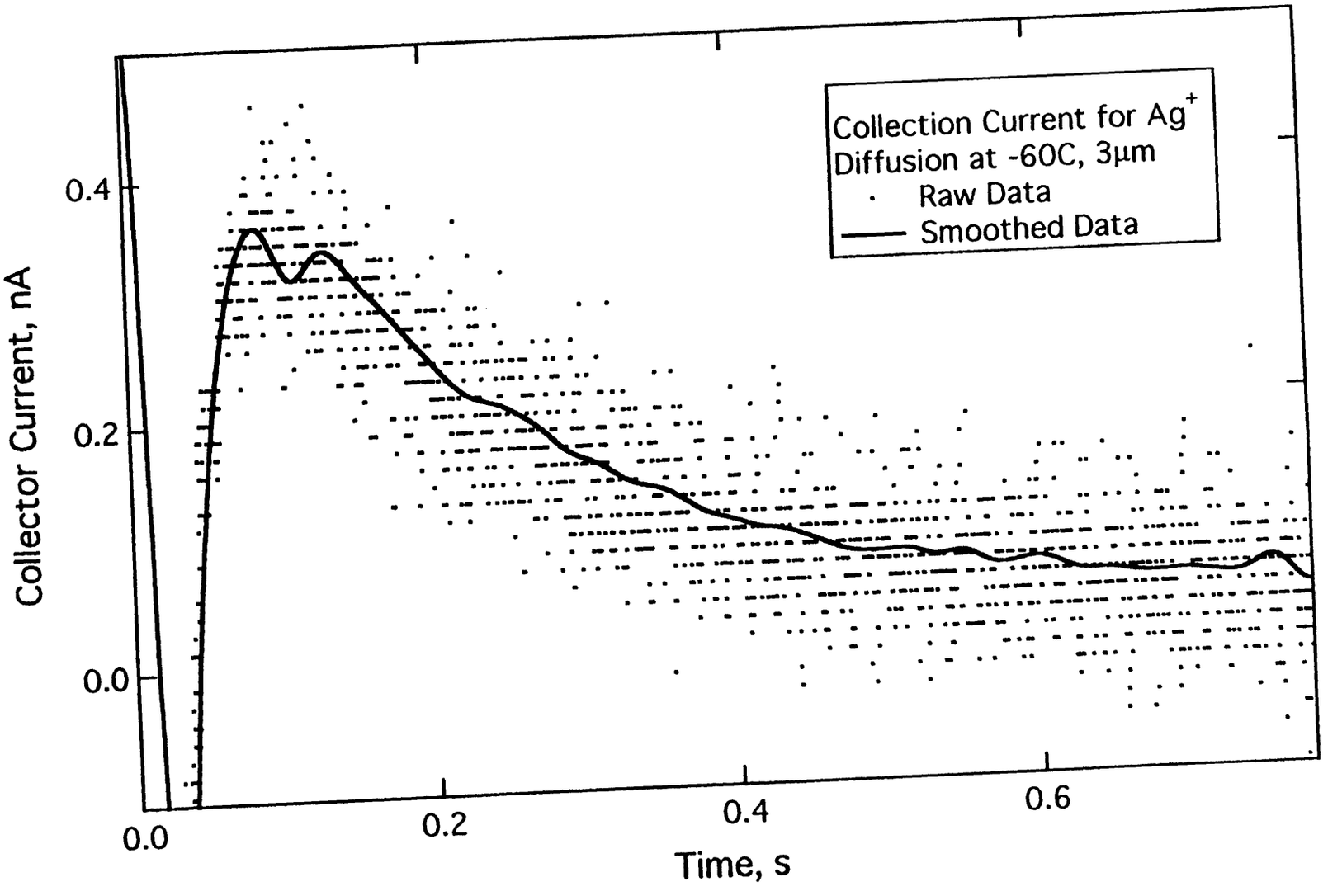
Collection Current for Ag+
Diffusion at -60C, 3µm
Raw Data
Smoothed Data
Collector Current, nA
0.4
0.2
0.0
0.0
0.2
0.4
0.6
Time, s

Figure 3. Time dependence of normalized collector current following pulse generation of Ag^+ in $HClO_4 \cdot 5.5H_2O$ at -60°C across distances of 3, 7, 11, 15 and 19 μm. Inset: a plot of t_{mt} vs. d^2. Values are the average of 2 to 3 repetitions.

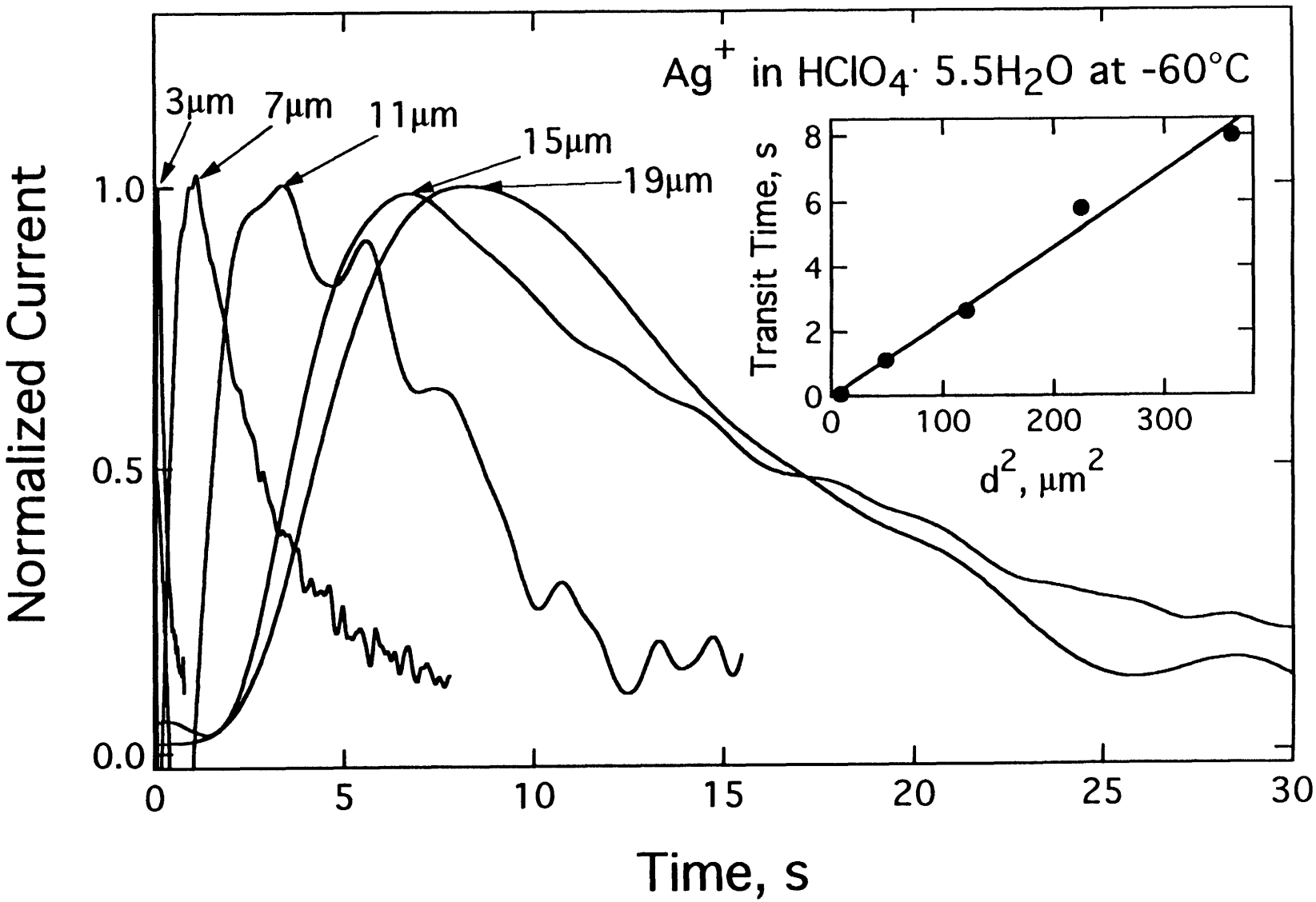
Ag+ in HClO4· 5.5H2O at -60°C
3μm
7μm
11μm
15μm
19μm
Normalized Current
1.0
0.5
0.0
0
5
10
15
20
25
30
Time, s
Transit Time, s
0
2
4
6
8
0
100
200
300
d2, μm2

Figure 4. Auger microprobe line scans of Au microelectrode arrays plated with Ag before and after generation-collection of Ag^+ in $HClO_4 \cdot 5.5H_2O$ at -60°C: a) Au scan of array before generation-collection; b) Ag scan before generation-collection; c) Ag scan after generation-collection.

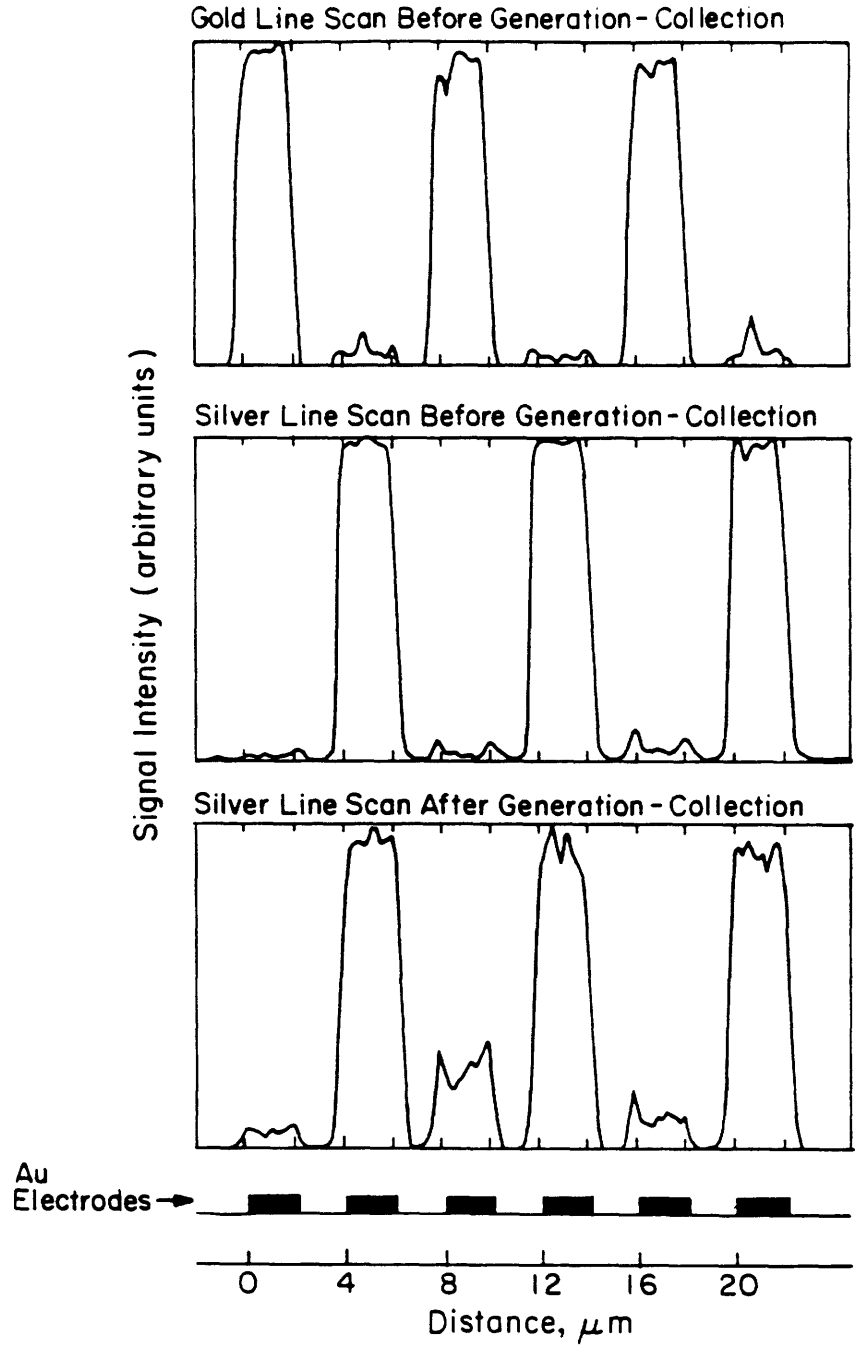
Gold Line Scan Before Generation - Collection
Silver Line Scan Before Generation - Collection
Silver Line Scan After Generation - Collection
Signal Intensity (arbitrary units)
Au
Electrodes
0
4
8
12
16
20
Distance, μm

values. Figure 5 shows a histogram of data collected at -60°C. The histogram is clearly bimodal indicating that we have actually measured two different diffusion coefficients. At -60°C the diffusion coefficients measured were $7.3(\pm1.6) \times 10^{-7}$ and $1.9(\pm0.6) \times 10^{-7}$ cm^2/s. Initially we suspected that the observed variation in diffusion behavior was due to intermittent supercooling of the acid. That is, sometimes the acid would fail to crystallize as it cooled, resulting in measurements of the crystalline acid or a supercooled, disordered phase. We attempted to control this behavior by changing the rate at which the cell was cooled, approaching the target temperature from different direction (above or below), annealing, and cycling the temperature of the cell between measurements. Although studies of the phase behavior of $HClO_4 \cdot 5.5H_2O$ make no mention of a tendency to supercool, others who have done electrochemistry in frozen $HClO_4 \cdot 5.5H_2O$ have used various cooling protocols that approach the target temperature by warming from the temperature of liquid nitrogen,[7] by cooling very slowly,[15a,16] or by cycling the temperature around the target temperature after cooling.[21]

Figure 6 shows t_{mt} values for two series of measurements where cycling the temperature of the cell in between measurements seemed to induce a change in diffusion behavior. There were, however, numerous experiments where similar treatment did not induce a change in t_{mt} values. The data shown in Figure 6 represent two experiments out of nine, the

Figure 5. Histogram of data from pulse generation collection of Ag^+ in $HClO_4 \cdot 5.5H_2O$ showing bimodal distribution of values. The data set is composed of 5 points from each of 24 experiments.

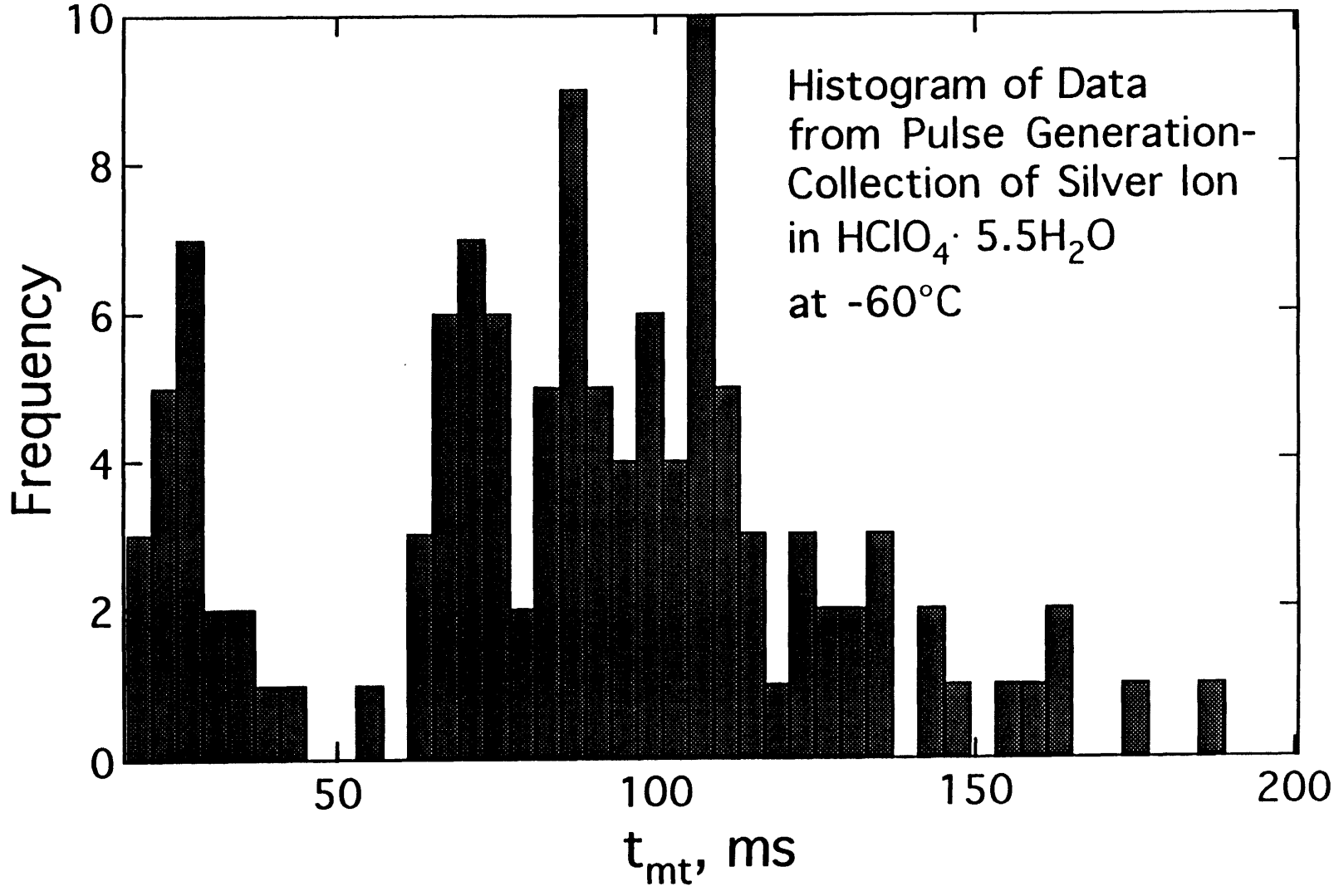
Histogram of Data
from Pulse Generation-
Collection of Silver Ion
in $HClO_4 \cdot 5.5H_2O$
at -60°C
Frequency
0
2
4
6
8
10
50
100
150
200
t_{mt}, ms

Figure 6. Changes in t_{mt} that occur after cycling the cell temperature. All data was collected at -60°C before and after cycling cell temperature as indicated.

Variation in Transit Time with Temperature Cycling (data collected at -60°C)

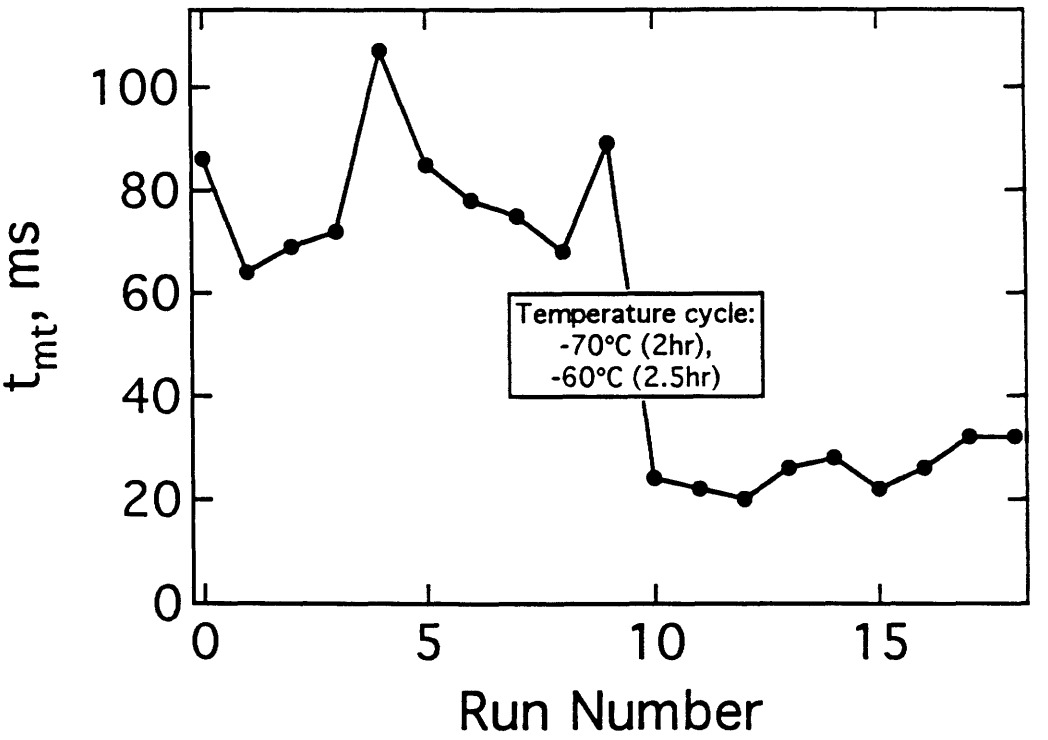

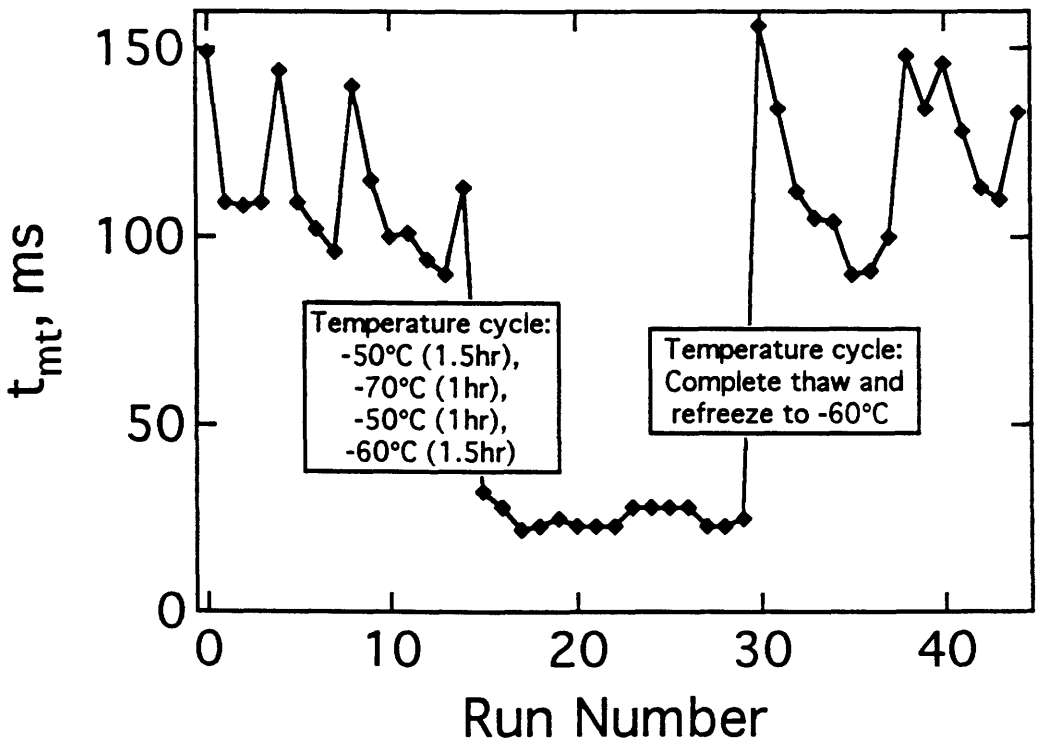

remainder of which showed no change in t_{mt} upon temperature cycling. Since both fast and slow t_{mt} values have been measured on the same microelectrode array and in the same sample of acid, the variation cannot be attributed to irregularities in device or sample preparation.

Figure 7 is an Arrhenius plot for diffusion of Ag^+ in $HClO_4 \cdot 5.5H_2O$. The two data sets are from two different experiments that appear to have been collected in each of the two different regimes. Diffusion in the slow regime shows an activation energy of 0.33(±0.03) eV, which is close to the activation energy reported for proton mobility in $HClO_4 \cdot 5.5H_2O$.[18] Diffusion in the fast regime, however, has an activation energy of only 0.19(±0.02) eV.

Figure 7. Arrhenius plot of t_{mt} for temperatures ranging from -45°C to -80°C. Each data point is the average of 5-7 measurements. Error bars represent the value of one standard deviation for each data set.

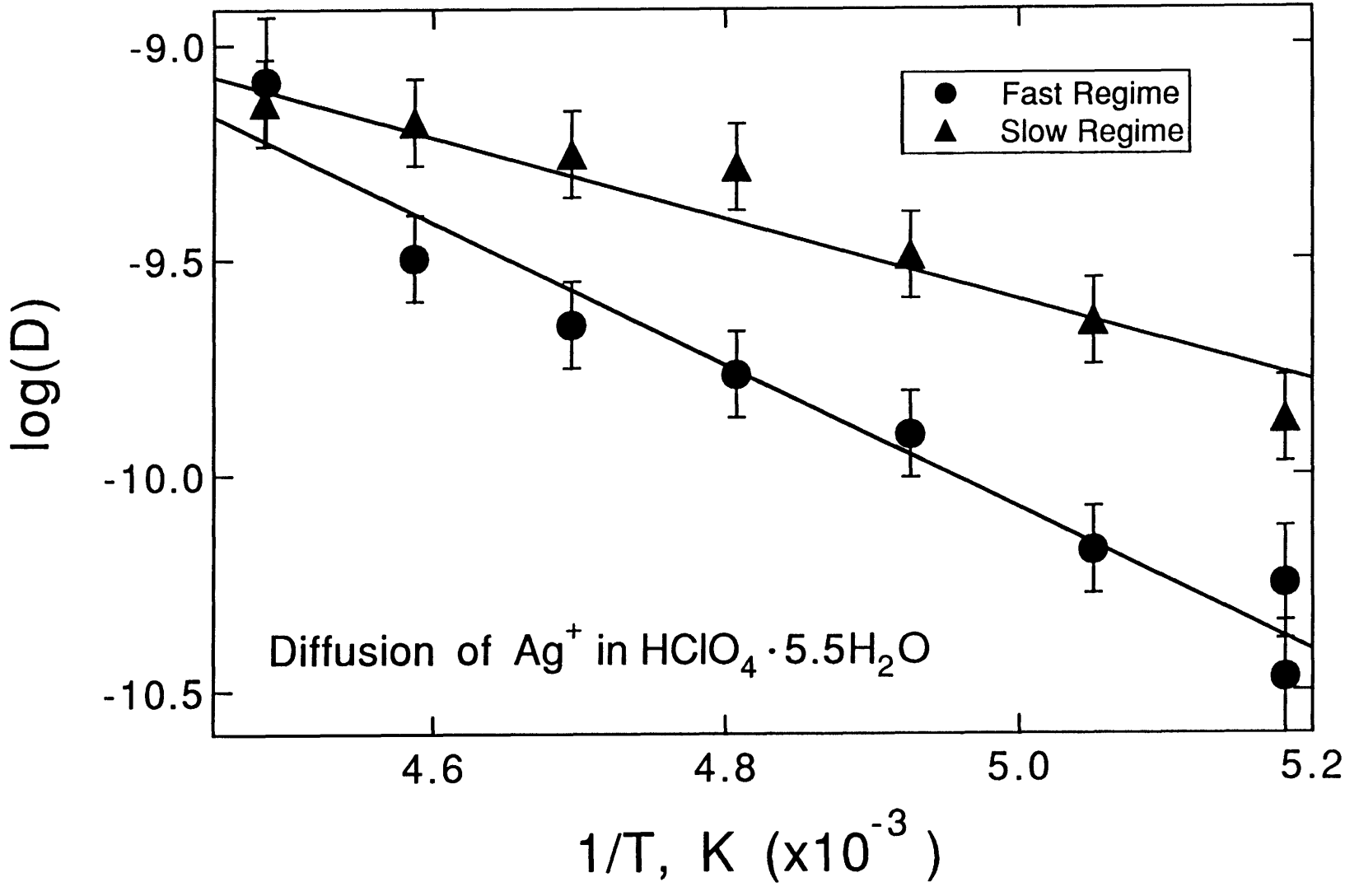
-9.0
-9.5
-10.0
-10.5
log(D)
Fast Regime
Slow Regime
Diffusion of Ag^+ in $HClO_4 \cdot 5.5H_2O$
4.6
4.8
5.0
5.2
1/T, K (x10^{-3})

Discussion

The phase behavior of $HClO_4 \cdot 5.5H_2O$ and other hydrates of perchloric acid have been studied.[17,19] The 5.5 hydrate is known to exist in a plastic crystalline phase over the temperature range examined that is sufficiently disordered that an X-ray crystal structure could not be obtained.[18] The lower hydrates of perchloric acid have been found to exist in α and ß crystal forms, and the 5.5 hydrate is dimorphic below -105°C. It was noted that annealing extended the range over which the two forms coexist.[17] A study of the proton NMR of $HClO_4 \cdot 5.5H_2O$ showed one type of signal as the sample was cooled and two signals as the sample was warmed through the range of -45°C to -60°C.[18] This behavior was attributed to a "supercooling" effect.

The bimodal variation in t_{mt} and the sudden changes which have been observed must result from diffusion through two different phases of the acid. The nature of the phases, however, is not clear; they could be either α and ß crystalline forms, or crystalline and amorphous forms of the acid. The variation in D could be the result of supercooling where D is first measured in a disordered state and then in the crystalline state. In this case the change in D is caused by a thermodynamically favored, but kinetically slow phase change. Another possible explanation for the changes in D is that the acid exists simultaneously in two crystal phases. If there are two phases present simultaneously, they must exist in separate spatial domains, and we have not been able to

control which phase is in contact with the microelectrode array. The observed changes in D would, in this case, result from motion in the solid which cause the form of the acid present in the vicinity of the array to vary with time. Given the dynamic and disordered nature of plastic crystalline phases, this degree of motion in the solid is not unexpected.[24]

Even within each of the two modes of the histogram in Figure 5 the deviation (20-30%) is greater than what is ordinarily[25] observed in pulse generation-collection measurements. This unusually large scatter may be due to inhomogeneity in the acid medium. If $HClO_4 \cdot 5.5H_2O$ does, in fact, consist of small domains of two different crystalline forms, it is possible that instead of simply one phase or the other, there is a mixture of the two phases in contact with the microelectrode array (Scheme II). The collection current, then would be the sum of currents from the two different phases and would vary slightly depending on the fraction the electrode gap covered by each phase. In addition, the empirically derived constant in equation (1) is specific to the type of device geometry shown in Figure 1. Geometric considerations would become important if, for example, there was a small region spanning the gap between two electrodes where diffusion was very fast. The signal observed for that region would represent diffusion between two electrodes of a different geometry than that described accurately by equation (1).

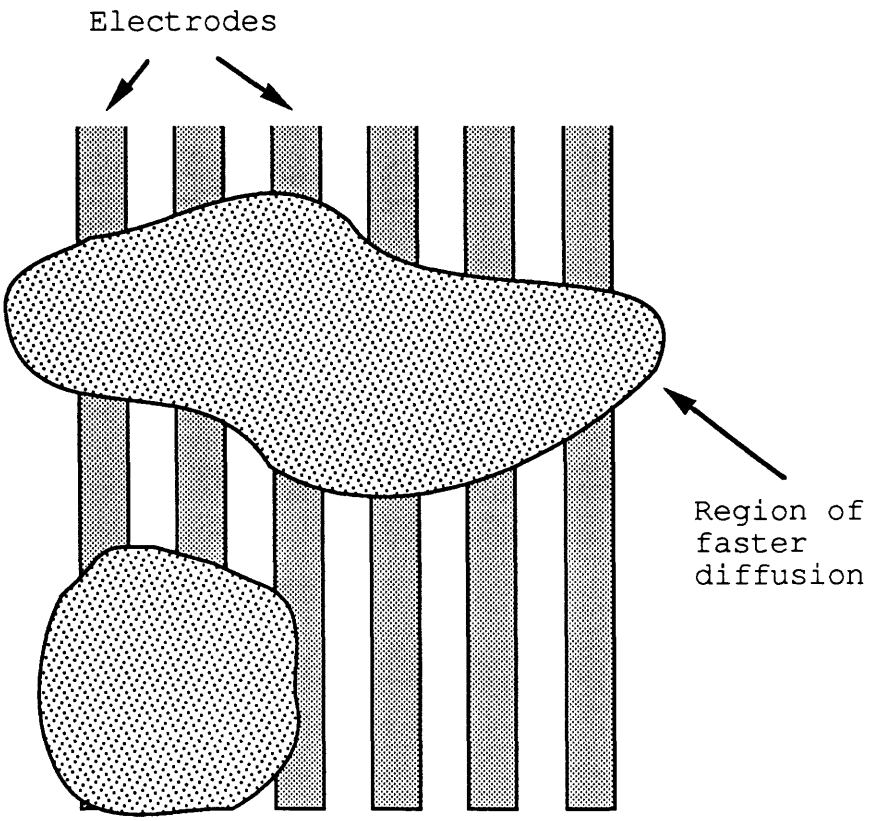

Scheme II. Microelectrode array covered by inhomogeneous electrolyte.

The data in Figure 6 show changes in D, brought about by temperature cycling without a complete thaw of the sample, in only one direction (slow to fast). This would point to supercooling as an explanation for the two values of D, the value measured at earlier times representing the supercooled state, and the value at later times representing diffusion through the frozen state. However, the total number of changes we have observed is not sufficiently large to be certain that changes from the fast to the slow regime cannot occur.

The direction of change shown in Figure 6 is from the slow regime to the fast regime. Ordinarily one would predict that diffusion would be slower through a more crystalline phase, and it would appear that Figure 6 shows a transition from a crystalline state to a more amorphous state. However, $HClO_4 \cdot 5.5H_2O$ is known to be a mobile, disordered plastic crystal, so it is not inconceivable that diffusion through the crystalline state is faster than through an amorphous phase. The fact that temperature cycling only brought about a change of D in two out of nine cases suggests that the changes are not dependent on the procedure used for cooling the acid. Others who have studied the electrochemistry and phase behavior of $HClO_4 \cdot 5.5H_2O$ make no mention of glass formation or unusually slow crystallization over this temperature range, so it is unlikely that supercooling is responsible for our observations.

Diffusion in the fast regime constitutes the smaller fraction of the total measurements. At -60°C approximately 15% of the diffusion data collected fell in the fast regime. If the observed variation in D does result from the simultaneous presence of two phases, the phase in which D is faster probably constitutes a small fraction of the total bulk. While we can establish an approximate lower limit of the size of the domains in the acid (100 μm), by virtue of the microelectrode array dimensions, we have no indication of what the upper size limit is except to note that perhaps this behavior has not been observed previously because the

techniques used to study electrochemistry in $HClO_4 \cdot 5.5H_2O$ employed electrodes whose dimensions were on the order of 1 cm^2. The pulse generation technique probes a relatively small, well-defined region of the electrolyte. This may make it able to distinguish microstructure that would not be observable using other methods.

Conclusions

We have demonstrated that pulse generation collection can be used to measure physical diffusion of Ag^+ in $HClO_4 \cdot 5.5H_2O$ at temperatures as low as -85°C. This measurement has made use of a microelectrode array with a quasi-reference electrode placed in close proximity to the working electrodes, making iR compensation unnecessary. The configuration of the band microelectrodes allows the probing of a small, well-defined region of electrolyte.

Diffusion of Ag^+ in $HClO_4 \cdot 5.5H_2O$ shows a linear dependence on d^2 indicating that Ag^+ transport is in accord with the standard "random walk" model for diffusion. Variations in diffusion measurements, however, indicate that the $HClO_4 \cdot 5.5H_2O$ is not homogeneous, but exists in two phases. We have measured two different D's at each temperature over the range studied, and calculated two different values for the activation energy of diffusion. Changes in D over time suggest that the two phases are two different crystalline forms of the acid which exist in small spatial domains. By probing a very small region of the electrolyte, generation-collection techniques utilizing microelectrodes can detect spatial inhomogeneities in the electrolyte that would not be observed by techniques using larger electrodes. Although it cannot be unequivocally eliminated, supercooling seems an unlikely explanation for the measurement of two different values of D.

Acknowledgments. This work was supported in part by the United States Department of Energy, Office of Basic Energy Science, Division of Chemical Sciences. We thank Lawrence F. Rozsnyai for scanning Auger microprobe experiments. We thank Christopher H. McCoy, Dr. Michael O. Wolf and Tu Nguyen for helpful discussions. The work described chapter has been the result of a collaborative effort with Dr. Timothy J. Gardner and Dr. Richard M. Crooks and will be submitted for publication in the *Journal of Physical Chemistry*.

References

1. Cammarata, V.; Talham, D. R.; Crooks, R. M.; Wrighton, M. S. *J. Phys. Chem.* **1990**, *94*, 2680.

2. (a) Licht, S.; Cammarata, V.; Wrighton, M. S. *Science* **1989**, *243*, 1176. (b) Licht, S.; Cammarata, V.; Wrighton, M. S. *J. Phys. Chem.* **1990**, *94*, 6133.

3. Feldman, B. J.; Feldberg, S. W.; Murray, R. W. *J. Phys. Chem.* **1987**, *91*, 6558.

4. Stimming, U. in "ACS Symposium Series 378: Electrochemical Surface Science: Molecular Phenomena at Electrode Surfaces"; M. P. Soriaga, Ed.; American Chemical Society: Washington, 1988; p 275.

5. Kestner, N. R.; Logan, J.; Jortner, J. *J. Phys. Chem.* **1974**, *78*, 2148.

6. (a) Matsunaga, A.; Itoh, K.; Fujishima, A; Honda, K. *J. Electroanal. Chem.* **1986**, *205*, 343. (b) Conway, B. E.; Salmon, M. *J. Chem. Phys.* **1964**, *41*, 3169. (c) Bockris, J. O'M.; Wass, J. *J. Electroanal. Chem.* **1989**, *267*, 325.

7. Stimming, U.; Schmickler, W. *J. Electroanal. Chem.* **1983**, *150*, 125.

8. (a) Borkowska, Z.; Stimming, U. *J. Electroanal. Chem.* **1991**, *312*, 237. (b) Dinan, T.; Stimming, U. *J. Electrochem. Soc.* **1986**, *133*, 2662.

9. (a) Van Duyne, R. P.; Reilley, C. N. *Anal. Chem.* **1972**, *44*, 142. (b) Van Duyne, R. P.; Reilley, C. N. *Anal. Chem.*

1972, *44*, 153. (c) Van Duyne, R. P.; Reilley, C. N. *Anal. Chem.* **1972**, *44*, 158.

10. Dalton, E. F.; Ching, Stanton; Murray, Royce W. *Inorg. Chem.* **1991**, *30*, 2642.

11. (a) Green, S. J.; Rosseinsky, D. R.; Toohey, M. J. *J. Am. Chem. Soc.* **1992**, *114*, 9702. (b) Peck, S. R.; Curtin, L. S.; McDevitt, J. T.; Murray, R. W.; Collman, J. P.; Little, W. A.; Zetterer, T.; Duan, H. M.; Dong, C.; Hermann, A. M. *J. Am. Chem. Soc.* **1992**, *114*, 9702. (c) McDevitt, J. T.; Longmire, M.; Gollmar, R.; Jernigan, J. C.; Dalton E. F.; McCarley, R.; Murray, R. W.; Little, W. A.; Yee, G. T.; Holcomb, M. J.; Hutchinson, J. E.; Collman, J. P. *J. Electroanal. Chem.* **1988**, *234*, 465. (d) Pinkowski, A.; Juttner, K.; Lorenz, W. J. *J. Electroanal. Chem.* **1990**, *287*, 203.

12. For examples of electrochemistry in SO_2 see (a) Garcia, E.; Kwak, J.; Bard, A. J. *Inorg. Chem.* **1988**, *27*, 4377. (b) Miller, L. L.; Mayeda, E. A. *J. Am. Chem. Soc.* **1970**, *92*, 5218. (c) Tinker, L. A.; Bard, A. J. *J. Am. Chem. Soc.* **1979**, *101*, 2316.

13. For examples of electrochemistry in NH_3 see: (a) Teherani, T. H.; Peer, W. J.; Lagowski, J. J.; Bard, A. J. *J. Am. Chem. Soc.* **1978**, *100*, 7768. (b) Teherani, T.; Itaya, K.; Bard, A. J. *Nov. J. Chim.* **1978**, *2*, 481. (c) Harima, Y.; Aoyagui, S. *J. Electroanal. Chem.* **1982**, *137*, 171. (d) Gordon, R. P.; Sundheim B. R. *J. Phys. Chem.* **1964**, *68*, 3347. (e) Harmima, Y.; Aoyagui, S. *J. Electroanal. Chem.* **1980**,

109, 167. (f) Schindewolf, U. *J. Phys. Chem.* **1984**, *88*, 3820.

14. McDevitt, J. T.; Ching, S.; Sullivan, M.; Murray, R. W. *J. Am. Chem. Soc.* **1989**, *111*, 4528.

15. (a) Frese, U.; Iwasita, T.; Schmickler, W.; Stimming, U. *J. Phys. Chem.* **1985**, *89*, 1059. (b) Frese, U.; Stimming, U. *J. Electroanal. Chem* **1986**, *198*, 409.

16. Borgerding, A.; Brost, E.; Schmickler, W.; Dinan, T.; Stimming, U. *Ber. Bunsenges. Phys. Chem.* **1990**, *94*, 607.

17. Karelin, I. A. *Bull. Acad. of Sci. USSR, Div. Chem. Sci.* **1988**, *37*, 6.

18. Mootz, D.; Oellers, E.-J.; Wiebcke, M. *J. Am. Chem. Soc.* **1987**, *109*, 1200.

19. Mascherpa, G. *Rev. Chim. Min.* **1965**, *2*, 379.

20. Huang, T.-H.; Davis, R. A.; Frese, U.; Stimming, U. *J. Phys. Chem.* **1988**, *92*, 6874.

21. Bond, A. M.; Svestka, M. *J. Electroanal. Chem.* **1991**, *301*, 139.

22. (a) Bond, A. M.; Fleischman, M.; Robinson, J. *J. Electroanal. Chem.* **1984**, *180*, 257. (b) Bowyer, W. J.; Engelman, E. E.; Evans, D. H. *J. Electroanal. Chem.* **1989**, *262*, 67.

23. Kittleson, G. P.; White, H., S.; Wrighton, M. S. *J. Am. Chem. Soc.* **1985**, *107*, 7373.

24. *The Plastically Crystalline State;* Sherwood, John N., Ed.; Wiley & Sons, New York, 1979.

25. Tatistcheff, H. B.; Fritsch-Faules, I.; Wrighton, M. S. unpublished results.

Chapter Four

Charge Transfer to Solvent Photochemistry of Electrode-Confined, Ferrocene- and Cobaltocene-Based Polymers: Photoelectrochemical Reduction of Halocarbons

Introduction

We report sustained photoreduction of halocarbons via charge transfer to solvent (CTTS) excitation of electrode-confined ferrocene-based polymers made by polymerization of monomers **I** (FcEMA), **II** (Me_8FcPMA), and **III** (CcSiO). Ferrocene, cobaltocene and their derivatives are known to form charge transfer complexes with halocarbons and these have characteristic electronic spectra.[1,2] Upon irradiation resulting in the excitation the metallocene-halocarbon charge transfer complexes undergo a photoreaction which begins with charge transfer to yield oxidized metallocene and reduced

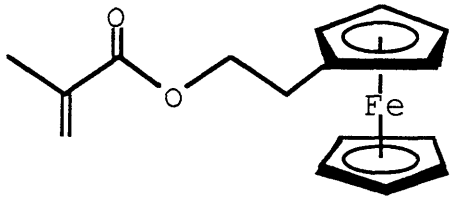

I

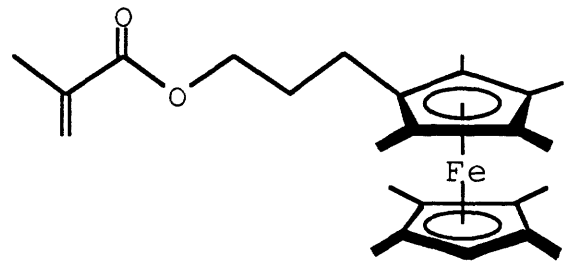

II

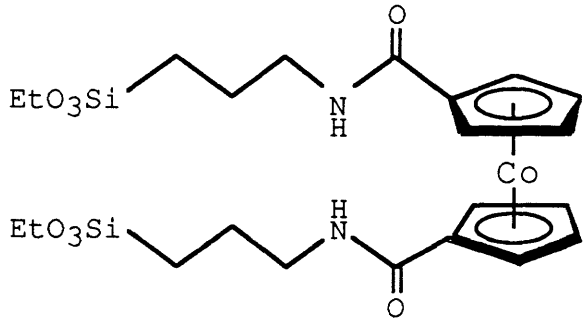

III

halocarbon. The photoelectrochemistry of charge transfer complexes of FcEMA with CCl_4, $CHCl_3$, $CHBr_3$ and CBr_4 was characterized in this study, as well as Me_8FcPMA-CCl_4 and CcSiO-CH_2Cl_2 complexes. Our study elaborates earlier findings that irradiation of electrode-confined polyvinylferrocene in the presence of CCl_4 and $CHCl_3$ yields cathodic photocurrent due to the CTTS photochemistry.[3]

Electronic spectra of CT complexes of ferrocene with numerous halocarbon acceptors have been reported,[4] as have a few similar complexes of cobaltocene and nickelocene.[2] Complexes of ferrocene and its derivatives with CCl_4 have received the most attention.[5,6] Reactions that occur following charge transfer from ferrocene to CCl_4 have been studied,[7] and quantum yields as high as 1.9 for oxidation of ferrocene have been measured. Because CCl_4^- decomposes rapidly upon reduction, there is little chance for back electron transfer to occur, so the quantum yield for the initial photoprocess is high. The quantum yield for ferrocene oxidation is further increased by reactions of CCl_4^- decomposition products (Cl^- and $\cdot CCl_3$). The $\cdot CCl_3$ or some other radical species is probably responsible for oxidation of a second ferrocene. Addition of acrylamide as a radical trap reduces the quantum yield for ferrocene oxidation to ~1 and yields polyacrylamide.[4a] Similarly, polypyrrole can be made by irradiation of ferrocene-CCl_4 solutions containing pyrrole.[8]

If radicals generated by the photoprocess are not otherwise trapped, they can attack ferrocenium. Ferrocenium may react with $\cdot CCl_3$ and/or solvent to give cyclopentadienyl ring substitution products or $FeCl_3$.[7] Electrochemical reduction of ferrocenium could reduce the extent of decomposition reactions because ferrocene is more robust than ferrocenium, and could also make the ferrocene center available for repeated photooxidation. Thus, if ferrocenium is electrochemically reduced, the process of halocarbon reduction becomes catalytic in ferrocene.[3]

Our work was undertaken with the objective of using the CTTS absorption to effect photoreduction of CCl_4 and other halocarbons in a system that is catalytic in ferrocene, octamethylferrocene or cobaltocene. Rapid reduction, facilitated by confinement of the metallocene to an electrode surface should minimize the extent of side reactions which result in irreversible decomposition of the metallocene centers. Regeneration of the reduced metallocene makes it available for subsequent CTTS reactions.

A cathodic photocurrent results from irradiation of electrode-confined metallocenes when the electrode is held at a potential where the metallocene is reduced. Thus, a metallocene with a more negative formal potential will exhibit an onset of photocurrent at more negative potentials. For different derivatives of a given metallocene a shift to lower reduction potential is accompanied by a shift in CTTS absorbance to longer wavelength. The wavelength of the CTTS

absorbance can also be manipulated by selection of the halocarbon acceptor, with more potent acceptors having lower energy CTTS absorbances. The photocurrent is characterized by its variation with excitation wavelength, the identities of the metallocene and the halocarbon in solution, the concentration of halocarbon, and the electrode potential.

Experimental

*2-Ferrocenylethanol, **VII***. (Dimethylaminomethyl)ferrocene (25 ml) was added dropwise to 10 ml chilled Me_3I in methanol. The mixture was refluxed for 1 hr. (Trimethylammonium methyl)ferrocene iodide, **IV** was precipitated by dropwise addition of ethyl ether and collected by filtration. **IV** was then added to a chilled aqueous solution containing 6 equiv KCN and refluxed for 1.5 hr to give ferrocene acetonitrile, **V**. **V** was extracted into ether which was extracted with H_2O and percollated through Na_2SO_4. A slurry of **V** in ethanol was added to 10% aqueous KOH and refluxed for 5 hr. The solid dissolved slowly followed by evolution of NH_3. Most of the ethanol was removed by rotary evaporation and the mixture was diluted with water and extracted with ether, filtered, cooled in an ice bath and acidified with 85% H_3PO_4. The product, 2-ferrocenylacetic acid, **VI**, was collected by filtration and dried under vacuum at 100°C. Dry ether (500 ml) was placed in a flask with 4.3g $LiAlH_4$, and 25g **VI** was placed in a soxhlet extractor. The ether was refluxed under Ar for 20 hr, and then extracted with 200 ml 20% HCl, washed with water and dried over Na_2SO_4. Solvent was removed and the product 2-(ferrocenyl)ethanol, **VII** was recrystallized from petroleum ether. mp 41.0-41.5°C ^1H NMR 4.09(m), 3.71(q) 2.57(t), 1.6(t)

*Ferrocenylethyl methacrylate, **I***. One equiv. **VII** was dissolved in 50 ml CH_2Cl_2 with 1 equiv dimethylphenylamine and 1.5 equiv methacryloyl chloride and refluxed until TLC

indicated consumption of **VII**. The reaction mixture was washed two times each with H_2O, Na_2CO_3(aq), H_2O, dried over $MgSO_4$ and filtered. The product was further purified by silica gel chromatography to afford an 83% yield of bright gold crystals.

*ß-octamethylferrocenyl ethylacrylate, **VIII***, was prepared according to the method of Zou and Wrighton.[9]

*3-octamethylferrocenylpropen-1-ol, **IX***. In a round bottomed flask 1.9 g $LiAlH_4$ and 150 ml ether were combined and purged with Ar. A deaerated solution of 9.0 g **VIII** in 100 ml ether was then added dropwise via an addition funnel. The mixture was stirred for 1 hr at room temperature. After quenching unreacted $LiAlH_4$ with H_2O, a solution containing 10 g NH_4Cl and 100 ml H_2O was added. The organic layer was extracted with H_2O and saturated aqueous NaCl, and dried over Na_2SO_4. Rotary evaporation of the solvent resulted in the collection of an orange solid in quantitative yield. mp 59-62°C.

*3-Octamethylferrocenyl-1-propanol, **X***. To a three necked 500 ml round bottomed flask was added 8.0 g **IX** (0.023 moles) and 1.0 g 10% Pd on activated carbon catalyst (0.94 mmoles Pd). After purging the flask with Ar, 250 ml of deaerated ethyl acetate were transferred via cannula. The solution was bubbled with H_2 for 1 hr, and an H_2 atmosphere was maintained for an additional 2 hr. The reaction mixture was then filtered through Celite to reveal a yellow colored solution. Upon rotary evaporation a yellow oil was observed which solidified upon pumping *in vacuo*. mp 64-66 °C

*Octamethylferrocenylpropyl methacrylate, **II***. **X** was treated directly with distilled, degassed methacryloyl chloride and stirred overnight. Product was isolated in the same manner as **I**.

Polymerization. Polymers based on **I** and **II** were prepared by heating the monomers in with 2,2'-azobis(2-methylpropionitrile) in benzene to 80 °C for 12 hr.

Ferrocene Polymer Deposition. Electrodes were prepared by oxidative precipitation of polymer onto a platinum flag electrode from solutions in CH_2Cl_2 (in the case of **I**) or THF (in the case of **II**) containing 0.1 M [*n*-Bu_4N]ClO_4. Coverages, which were determined by integration of the cyclic voltammogram taken in CH_3CN/[*n*-Bu_4N]ClO_4 or CH_3OH/[*n*-Bu_4N]ClO_4, were usually 10^{-9} to 10^{-8} moles/cm^2.

Cobaltocene Polymer Deposition. Generation of **III** *in situ* and its electrochemical deposition has been reported.[10]

Equipment and Procedures. All electrochemical experiments utilized one channel of a Pine Inst. Co. RDE4-X1 bipotentiostat. Monochromatic illumination for wavelength dependence measurements was provided by placing the quartz electrochemical cell in a Perkin-Elmer MF-44 fluorescence spectrometer equipped with a 150 W Xe lamp while the electrode was held at a potential negative of the formal potential of the metallocene, but positive of the onset of halocarbon reduction in the dark. Extended irradiation and potential dependence experiments utilized a Bausch & Lomb 250 W high pressure Hg lamp.

UV-vis spectra were recorded on a Hewlett-Packard model 8452A spectrophotometer. In order to distinguish CT absorbances a two compartment mixing cell was used in which each compartment had a path length of 4 mm (Wilmad Corp.). One compartment contained the metallocene, either in solution, or as a film of the metallocene polymer electrodeposited or cast onto an indium-tin oxide/quartz electrode in an electrolyte solution with no halocarbon. Charge transfer absorbance was taken to be the difference between the sum of the absorbances of the unmixed donor and acceptor solutions and the absorbance of the mixed solution. Pt flag electrodes were made from Si wafers coated with 5000 Å SiO_2 and 1500 Å Si_3N_4 onto which 50 Å Ti and then 1000 Å Pt were deposited by e^- beam evaporation.

Results and Discussion

We have characterized the photoresponse of metallocene polymers confined to the surfaces of Pt electrodes in the presence of halocarbon acceptors. When the electrode is held at a potential that is negative of the redox potential of the metallocene, irradiation at the appropriate wavelength causes charge transfer from the metallocene center to the halocarbon in solution. Very small background photocurrents were observed in the absence of either the surface-confined metallocene or the halocarbon acceptor.

Figures 1-6 show absorption spectra of the metallocene polymers in the presence and absence of halocarbons as well as the wavelength dependence of photocurrent (action spectra) resulting from irradiation of electrode-confined metallocenes in electrolyte solutions containing halocarbons. The action spectra correspond to the difference spectra, indicating that it is the CTTS absorbance that is responsible for the photocurrent. Maxima of the difference and action spectra are given in Table I. For the series of FcEMA complexes studied, the CTTS absorption shifts to longer wavelengths with stronger electron acceptors. Also, changing from FcEMA to Me_8FcPMA shifts the CTTS absorbance with CCl_4 to longer wavelength, and the photocurrent onset is at a more negative potential. Figure 7 shows the dependence of photocurrent from an FcEMA derivatized electrode on CCl_4 concentration.

Figure 1. (a) Electronic spectra of 6 mM ferrocene and 0.5 M $CHCl_3$ both in CH_3CN/0.1 M [*n*-Bu_4N]PF_6 mixed and unmixed. (b) The difference between spectra in Part a showing absorbance due to formation of the CT complex. (c) Wavelength dependence of photocurrent resulting from irradiation of a Pt electrode derivatized with FcEMA in CH_3CN/0.5 M $CHCl_3$/0.1 M [*n*-Bu_4N]PF_6.

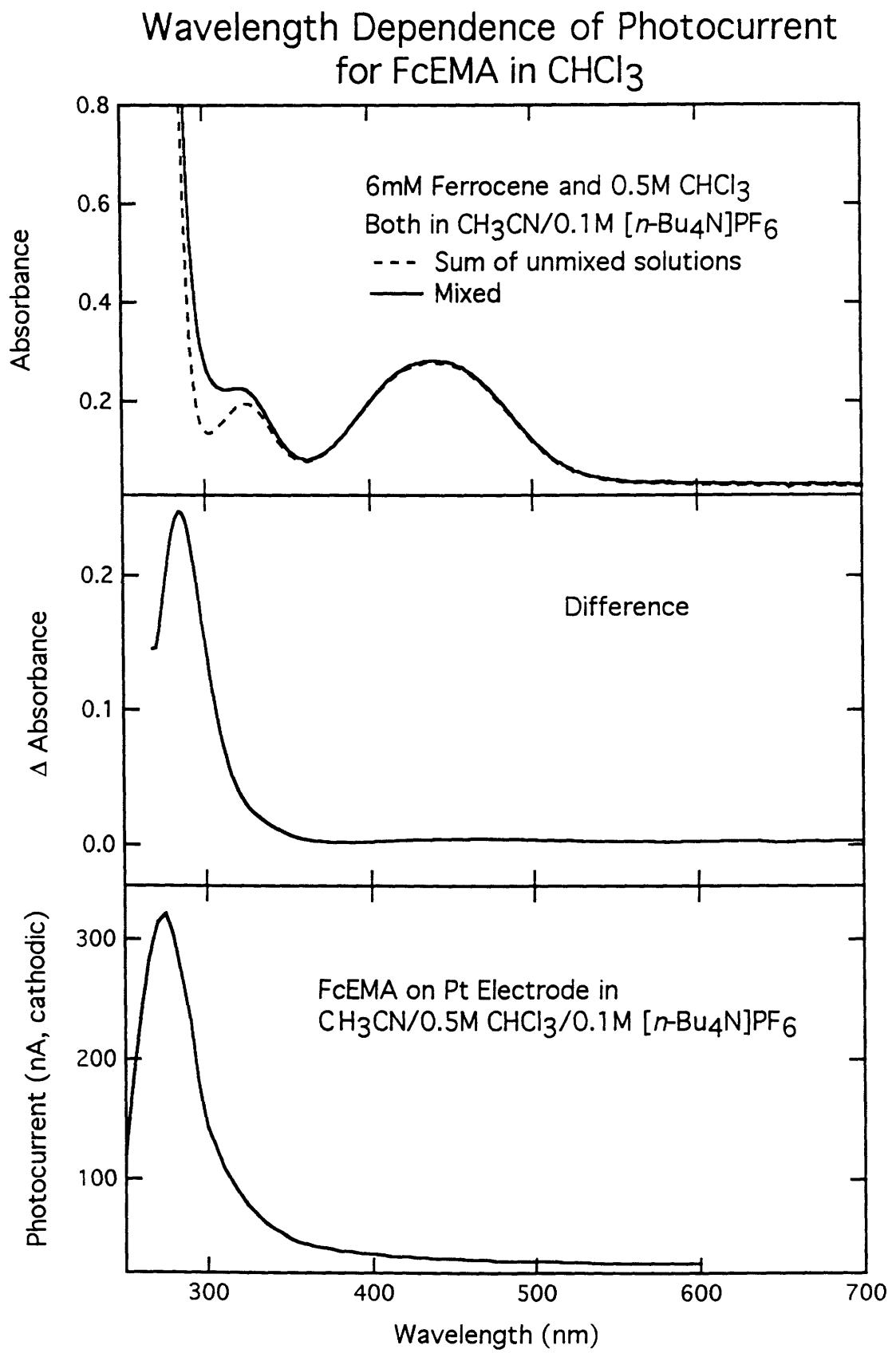
Wavelength Dependence of Photocurrent for FcEMA in CHCl3
Absorbance
0.8
0.6
0.4
0.2
6mM Ferrocene and 0.5M CHCl3
Both in CH3CN/0.1M [n-Bu4N]PF6
--- Sum of unmixed solutions
—— Mixed
Δ Absorbance
0.2
0.1
0.0
Difference
Photocurrent (nA, cathodic)
300
200
100
FcEMA on Pt Electrode in
CH3CN/0.5M CHCl3/0.1M [n-Bu4N]PF6
300
400
500
600
700
Wavelength (nm)

Figure 2. (a) Electronic spectra of a film of FcEMA electrodeposited on an indium-tin oxide/quartz electrode in the presence and absence of CCl_4. (b) The difference between spectra in Part a showing absorbance due to formation of the CT complex. (c) Wavelength dependence of photocurrent resulting from irradiation of a Pt electrode derivatized with FcEMA in CH_3CN/50% CCl_4/0.1 M [*n*-Bu_4N]ClO_4.

Wavelength Dependence of Photocurrent for FcEMA

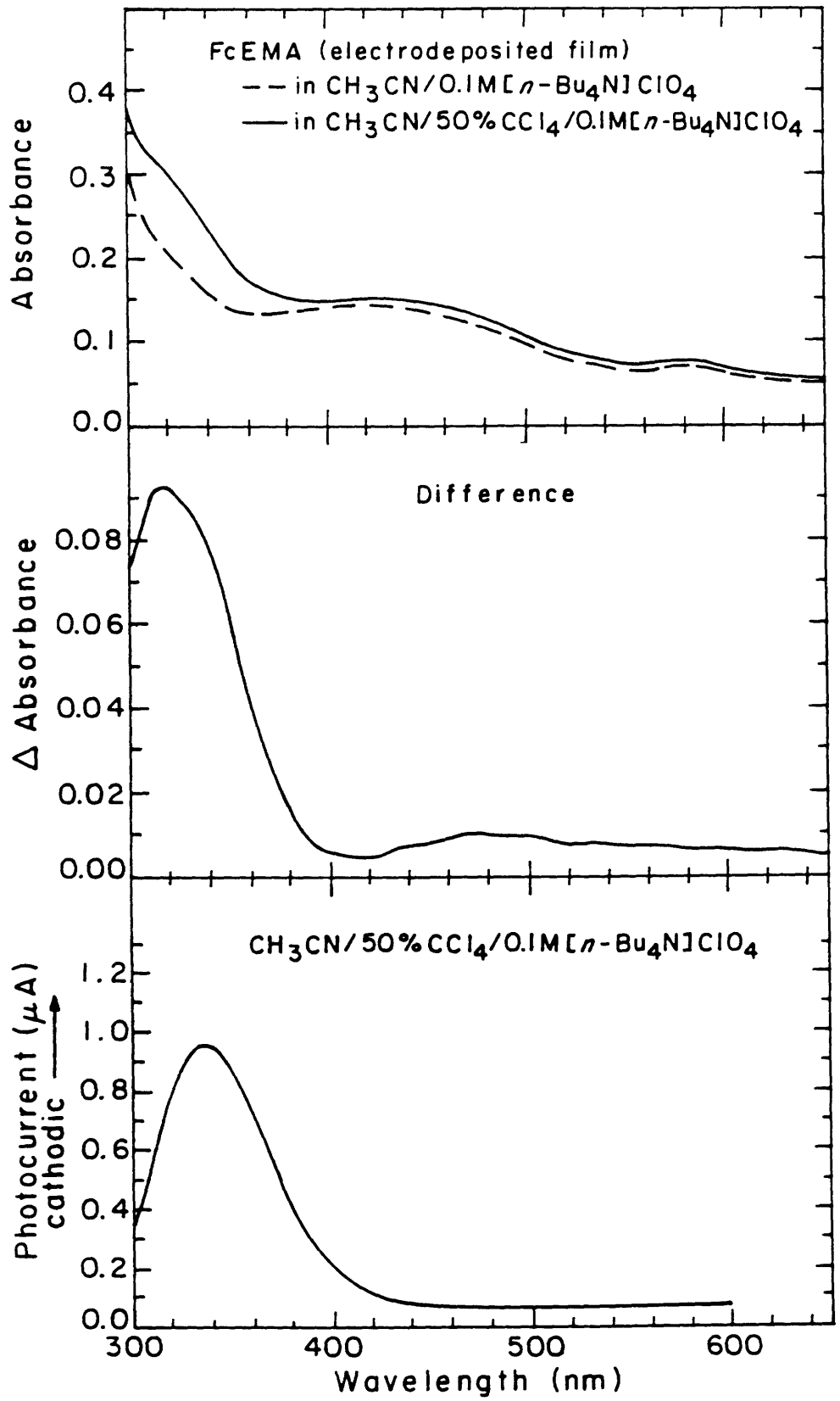

Figure 3. (a) Electronic spectra of 6 mM ferrocene and 0.5 M $CHBr_3$ both in CH_3CN/0.1 M [*n*-Bu_4N]PF_6 mixed and unmixed. (b) The difference between spectra in Part a showing absorbance due to formation of the CT complex. (c) Wavelength dependence of photocurrent resulting from irradiation of a Pt electrode with and without and electrodeposited film of FcEMA in CH_3CN/0.5 M $CHBr_3$/0.1 M [*n*-Bu_4N]PF_6.

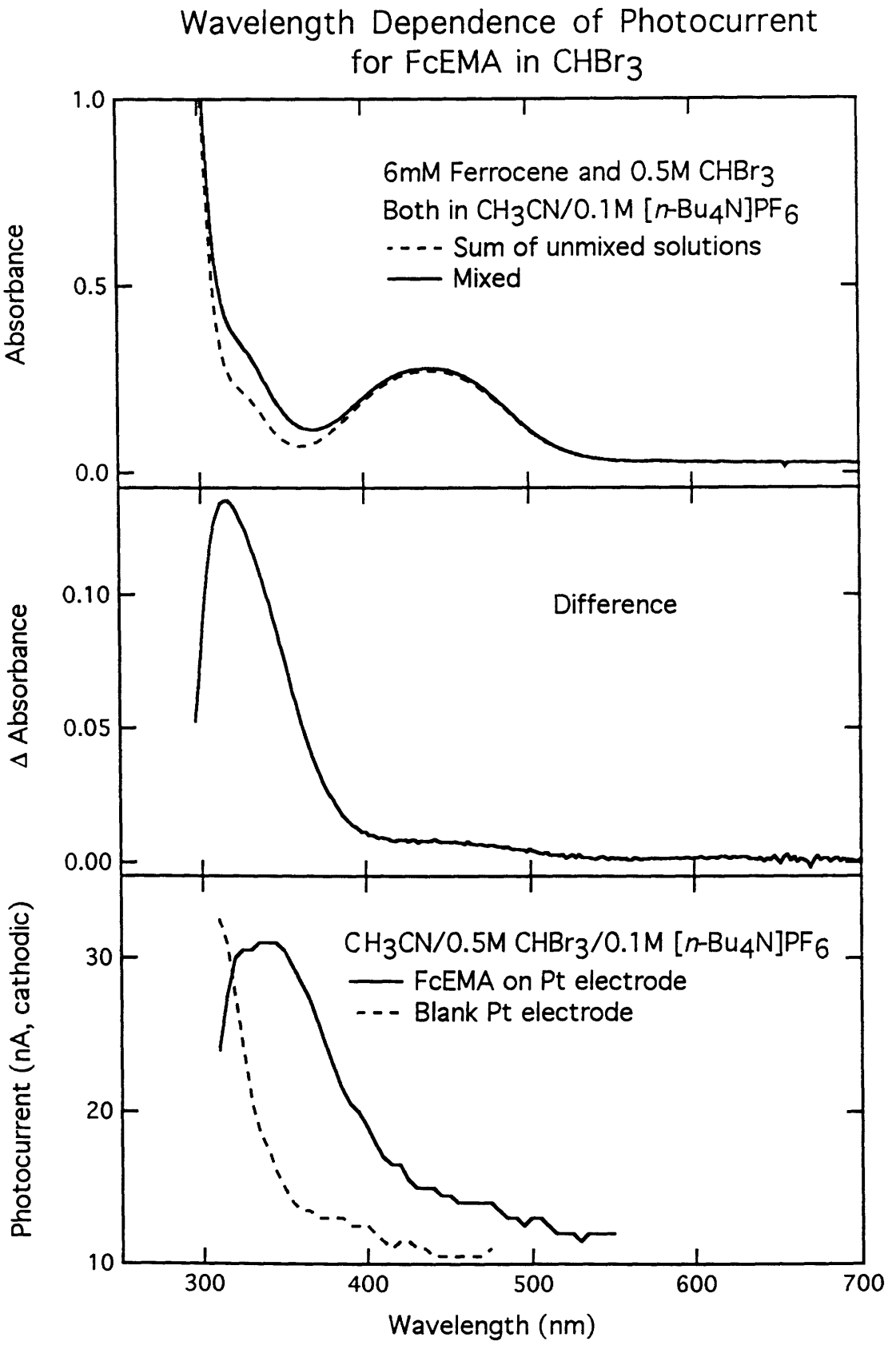
Wavelength Dependence of Photocurrent
for FcEMA in CHBr3
Absorbance
1.0
0.5
0.0
6mM Ferrocene and 0.5M CHBr3
Both in CH3CN/0.1M [n-Bu4N]PF6
Sum of unmixed solutions
Mixed
Δ Absorbance
0.10
0.05
0.00
Difference
Photocurrent (nA, cathodic)
30
20
10
CH3CN/0.5M CHBr3/0.1M [n-Bu4N]PF6
FcEMA on Pt electrode
Blank Pt electrode
300
400
500
600
700
Wavelength (nm)

Figure 4. (a) Electronic spectra of 6 mM ferrocene and 0.5 M CBr_4 both in CH_3CN/0.1 M [*n*-Bu_4N]PF_6 mixed and unmixed. (b) The difference between spectra in Part a showing absorbance due to formation of the CT complex. (c) Wavelength dependence of photocurrent resulting from irradiation of a Pt electrode derivatized with FcEMA in CH_3CN/0.5 M CBr_4/0.1 M [*n*-Bu_4N]PF_6.

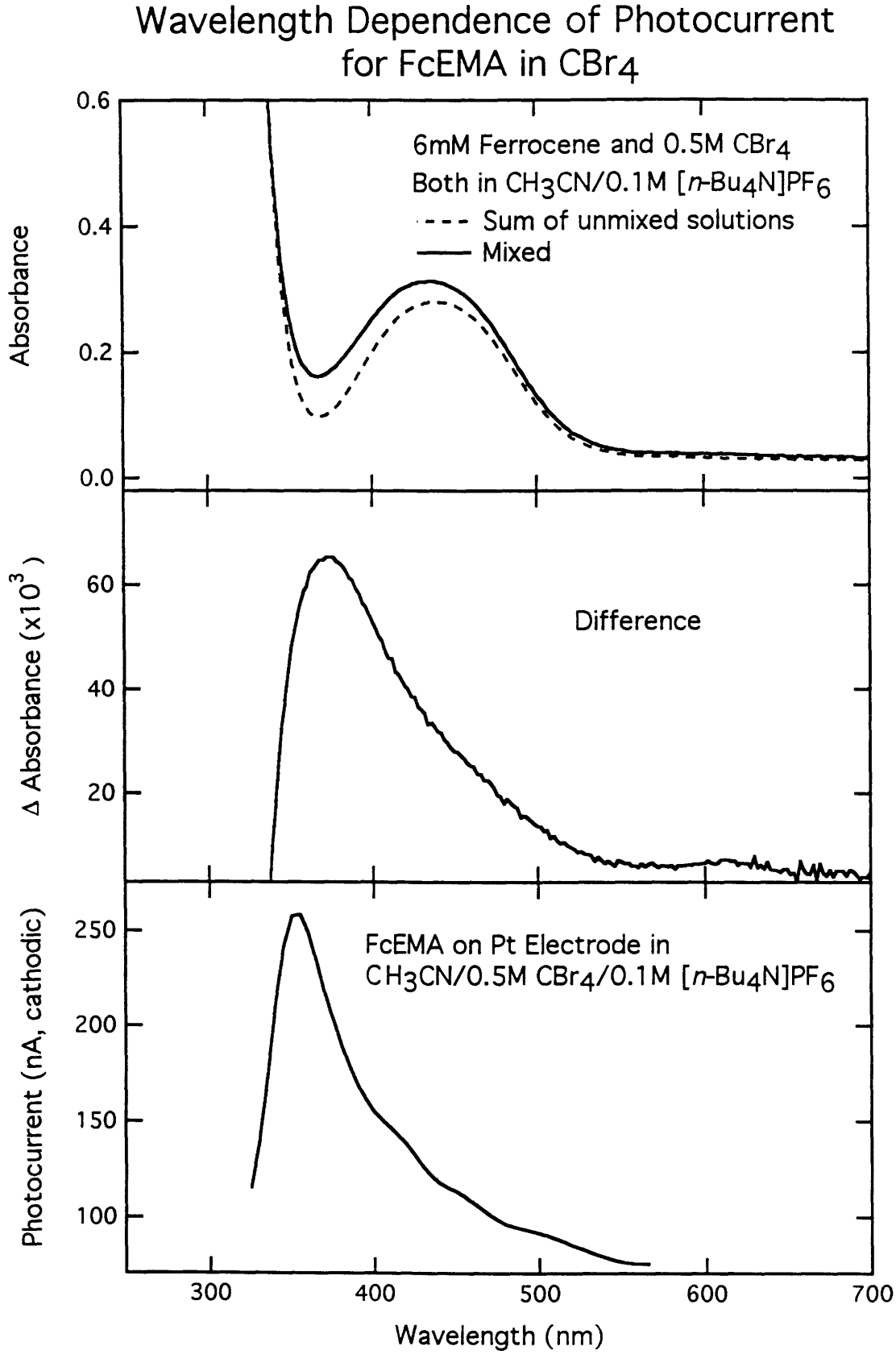
Wavelength Dependence of Photocurrent for FcEMA in CBr4
6mM Ferrocene and 0.5M CBr4
Both in CH3CN/0.1M [n-Bu4N]PF6
Sum of unmixed solutions
Mixed
Absorbance
0.6
0.4
0.2
0.0
Difference
Δ Absorbance (x10^3)
60
40
20
FcEMA on Pt Electrode in
CH3CN/0.5M CBr4/0.1M [n-Bu4N]PF6
Photocurrent (nA, cathodic)
250
200
150
100
300
400
500
600
700
Wavelength (nm)

Figure 5. (a) Electronic spectra of a film of Me8FcPMA cast onto a quartz plate in the presence and absence of CCl_4. (b) The difference between spectra in Part a showing absorbance due to formation of the CT complex. (c) Wavelength dependence of photocurrent resulting from irradiation of a Pt electrode derivatized with Me8FcPMA in CH_3OH/50% CCl_4/0.1 M [*n*-Bu_4N]ClO_4.

Wavelength Dependence of Photocurrent for Me_8FcPMA

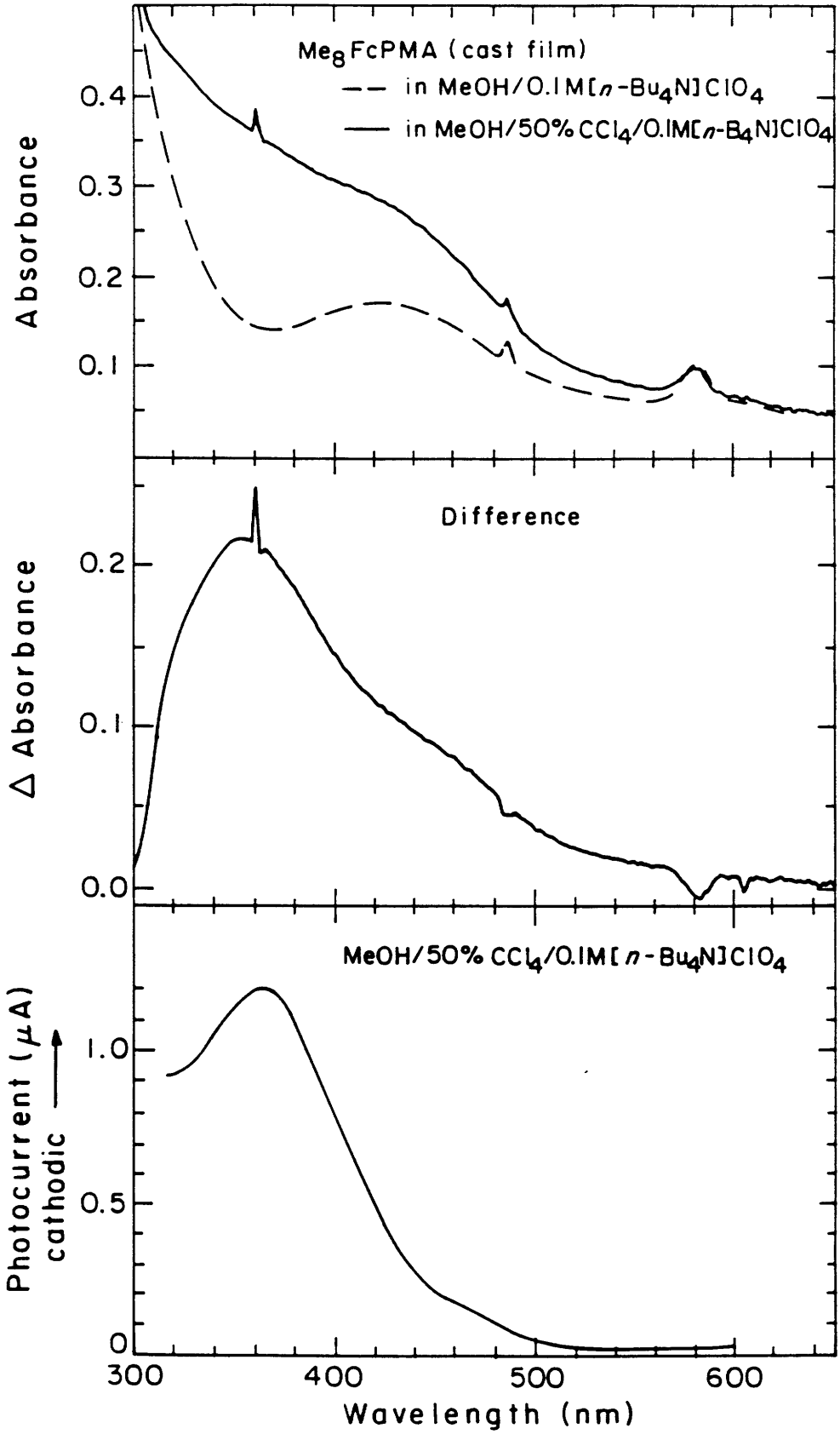

Figure 6. (a) Electronic spectra of a film of CcSiO electrodeposited on an indium-tin oxide/quartz electrode in the presence and absence of CH_2Cl_2. (b) The difference between spectra in Part a showing absorbance due to formation of the CT complex. (c) Wavelength dependence of photocurrent resulting from irradiation of a Pt electrode derivatized with FcEMA in CH_3OH/50% CH_2Cl_2/0.1 M [*n*-Bu_4N]ClO_4.

Wavelength Dependence of Photocurrent for CcSiO in CH_2Cl_2

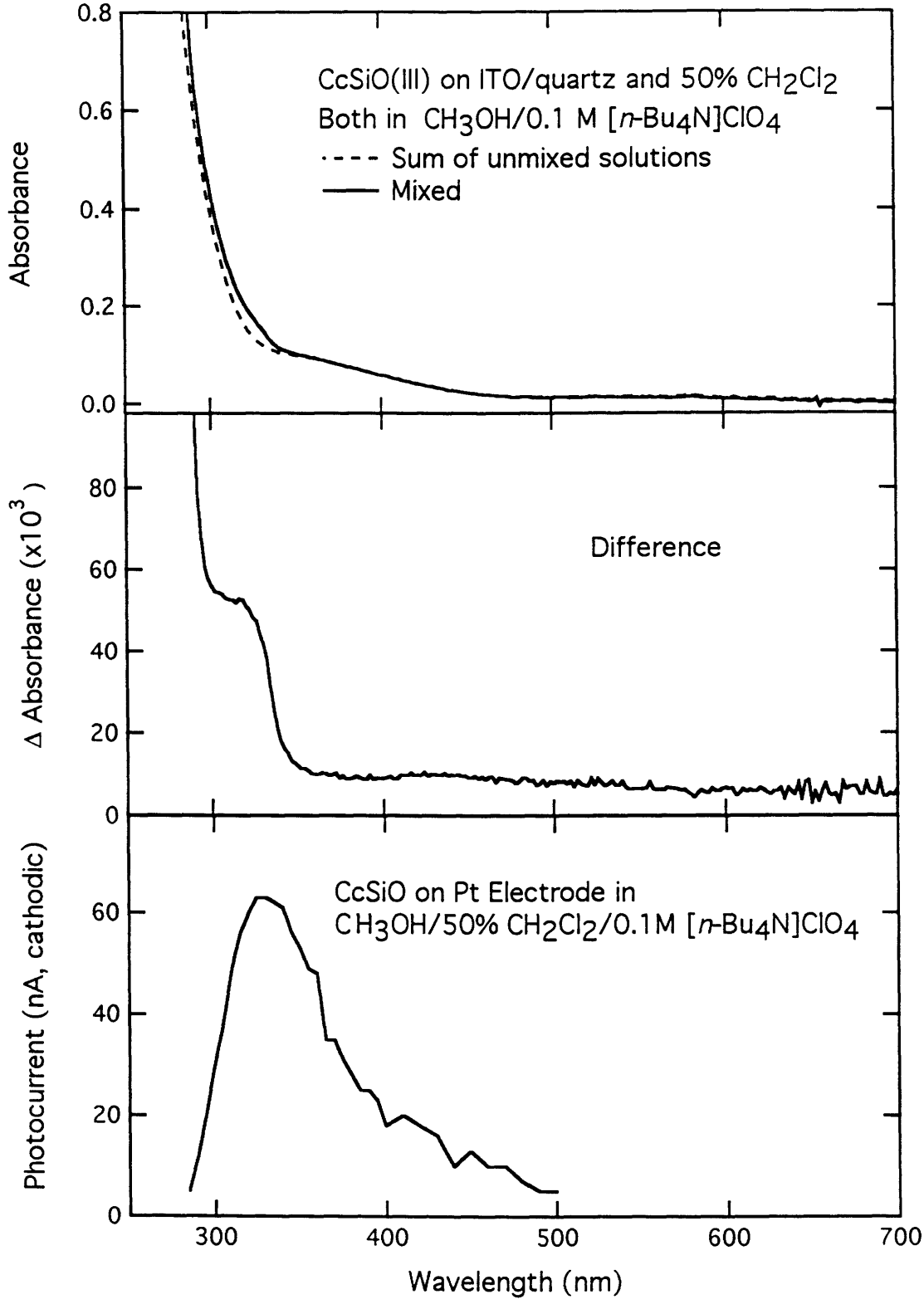

Figure 7. Variation of photocurrent with CCl_4 concentration for an FcEMA derivatized electrode in CH_3CN/0.1 M [*n*-Bu_4N]PF_6. Irradiation was provided by a 250 W Hg lamp. Ferrocene coverage of the electrode was 3 x 10^{-8} mol/cm^2

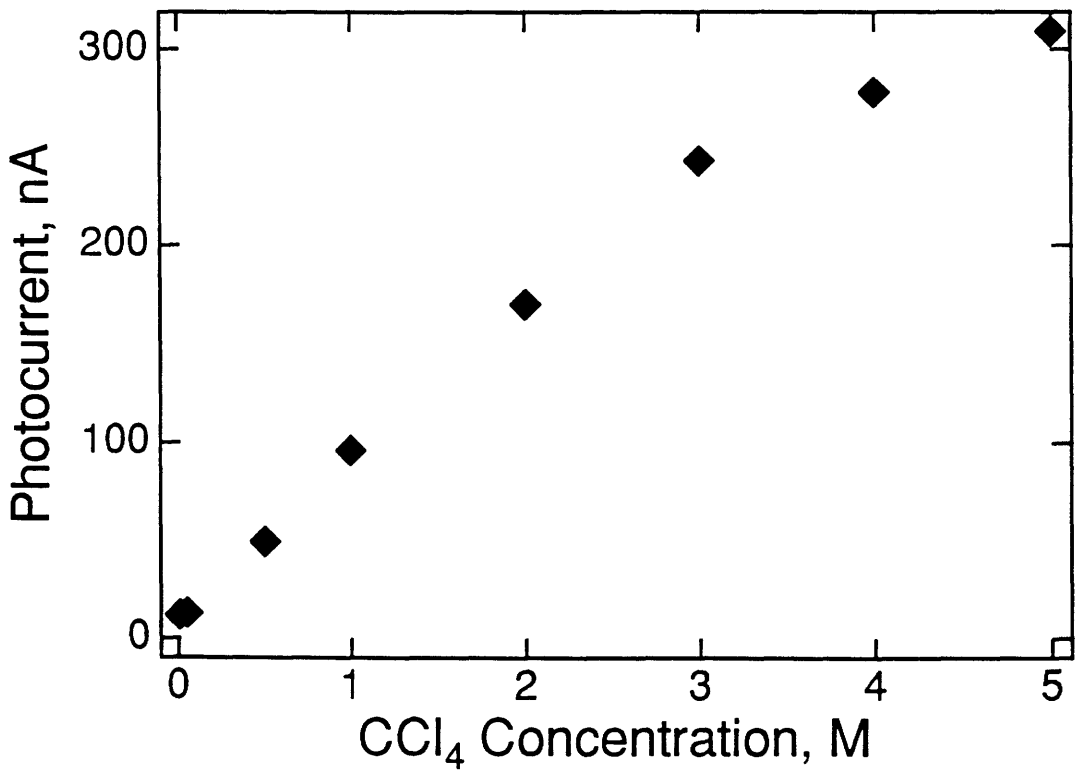
Photocurrent, nA
300
200
100
0
0
1
2
3
4
5
CCl4 Concentration, M

Photocurrent is linear with CCl_4 concentration from approximately 0.1 to 3 M.

The potential dependence of photocurrents in the FcEMA-CCl_4, Me_8FcPMA-CCl_4, and CcSiO-CH_2Cl_2 systems is shown in Figure 8. Photocurrent (the difference between the light and dark curves) is higher at more negative potentials, and drops dramatically as the metallocene is oxidized. This indicates that it is, in fact, the reduced form of the metallocene that is responsible for the photocurrent. The variation in redox potential of the metallocene centers is paralleled by a shift in the potential of the onset of photocurrent. The potential dependence of photocurrents resulting from irradiation of FcEMA in $CHCl_3$, CBr_4, $CHBr_3$ are similar to that shown for CCl_4 in that photocurrent is only observed when the metallocene is present in its reduced state.

In order to demonstrate that the photoreaction is catalytic in ferrocene, electrodes with varying coverages of FcEMA were irradiated for extended time periods. Soon after its initial onset, the photocurrent begins to decay under intense (250 W Hg lamp) irradiation. This parallels a loss of ferrocene coverage. An electrode with a relatively high coverage (1×10^{-8} mol/cm^2) passed photocurrent corresponding to oxidation of all of the ferrocene centers 6.5 times in 270 min and exhibited a ~90% coverage loss. However, an electrode with a relatively low coverage (2.9×10^{-9} mol/cm^2) passed current corresponding to 100 turnovers of each

Figure 8. Current resulting from scanning the potential of an electrode derivatized with (a) FcEMA. (b) Me_8FcPMA or (c) CcSiO through the oxidation wave of the metallocene centers with and without irradiation by a 250 W Hg lamp.

Potential Dependence of Photocurrent

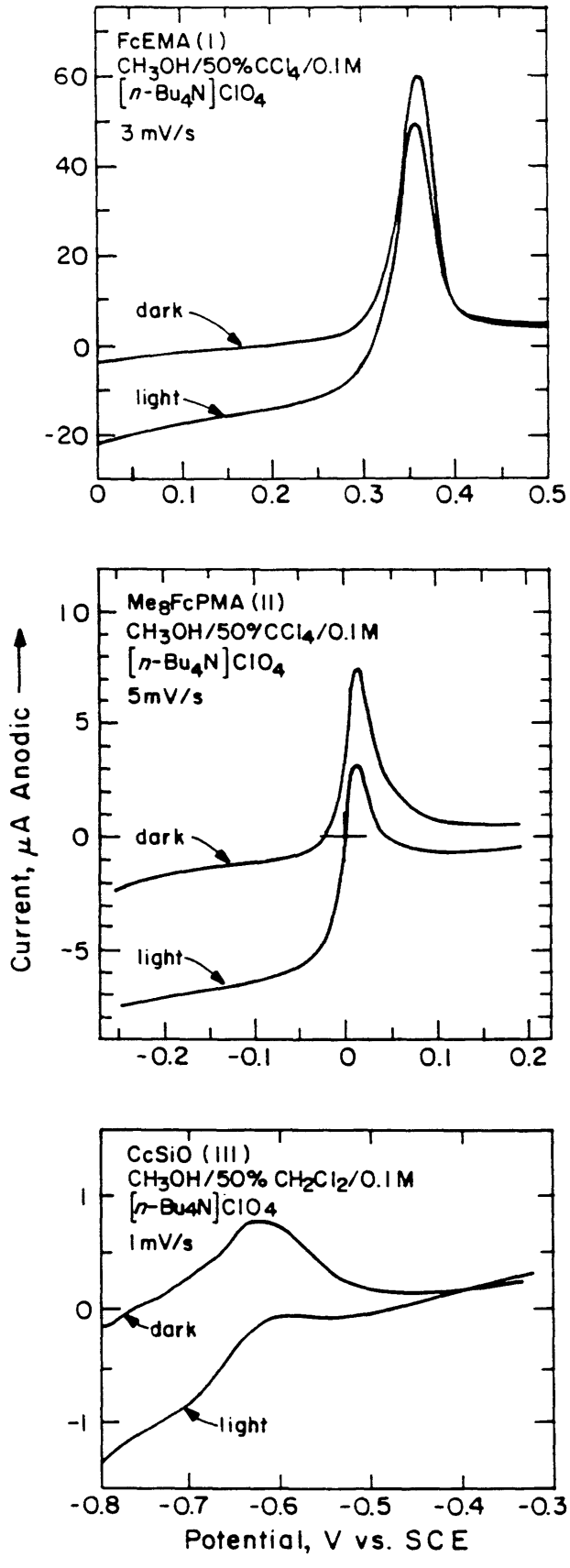

ferrocene in 150 min, Figure 9. This is accompanied by ~80% coverage loss.

The difference in durability of films of different thicknesses is likely the result of the rate of migration of charge through the polymers. Electron hopping between redox centers in such redox "conductors" is known to be relatively slow (on the order of 10^{-9} cm^2/s).[11] In thicker films where a large portion of the ferrocene is distant from the electrode surface and cannot be reduced rapidly, there is more opportunity for side reactions to occur which result in ferrocenium decomposition. When films are thinner, however, photogenerated ferrocenium can be reduced more rapidly, is less susceptible to decomposition and yields a larger number of turnovers. Thicker, longer-lived films could perhaps result if the metallocene centers were attached to a conducting polymer, so that the metallocene reduction would not be hindered by slow charge transport through the film. However, the effectiveness of such a polymer may be limited, because most conducting polymers are not optically transparent, and they often undergo photochemistry that would interfere with or mask the effect of CTTS processes.

Figure 9. Current resulting from extended irradiation of an FcEMA derivatized Pt electrode in CH_3CN/50% CCl_4/0.1 M [*n*-Bu_4N]PF_6 by a 250 W Hg lamp. Starting ferrocene coverage was 2.9×10^{-9} mol/cm^2.

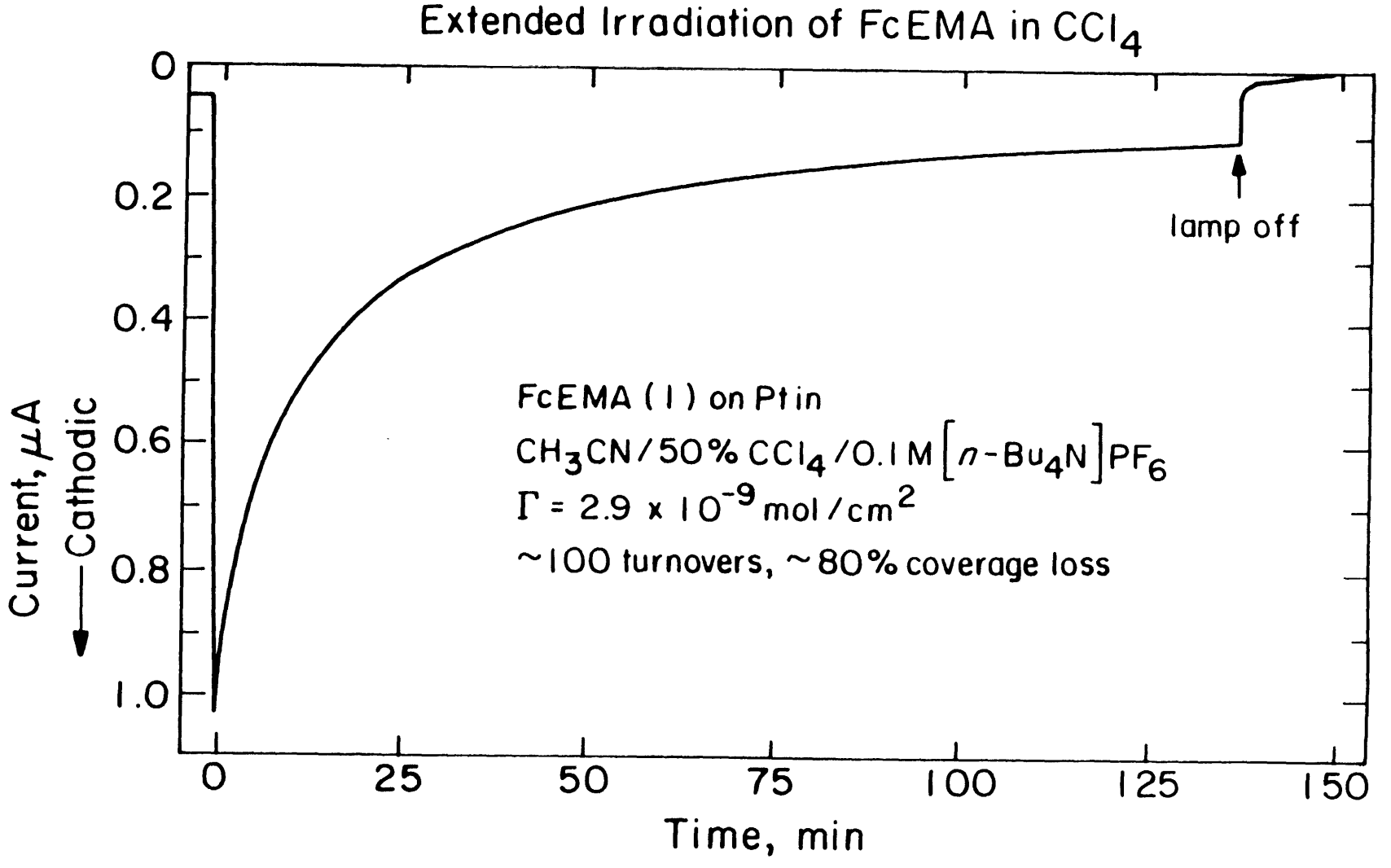
Extended Irradiation of FcEMA in CCl_4
Current, μA
Cathodic
0
0.2
0.4
0.6
0.8
1.0
lamp off
FcEMA (1) on Pt in
CH_3CN/50% CCl_4/0.1 M $[n\text{-}Bu_4N]PF_6$
$\Gamma = 2.9 \times 10^{-9}$ mol/cm^2
~100 turnovers, ~80% coverage loss
0
25
50
75
100
125
150
Time, min

Conclusions

We have demonstrated that confinement of metallocenes to electrode surfaces allows regeneration of the reduced metallocene following photochemical oxidation. CTTS excitation also results in reduction of a halocarbon electron acceptors in solution at a potential positive of the onset of its reduction in the dark. Irradiation of a metallocene confined to the surface of an electrode which is held at a reducing potential yields a photocurrent whose potential and wavelength dependence is consistent with reduction of the metallocenium following oxidation by CTTS. We have shown the photoassisted reduction of CCl_4 by CTTS from ferrocene to be catalytic in ferrocene.

The potential of the halocarbon photoreduction is, in fact, dependent only ond the formal potential of the metallocene. In the case of FcEMA and Me_8FcPMA, changing to the metallocene with a more negative formal potential moves the onset of photoreduction closer to the potential where the halocarbon is reduced in the dark, but also shifts the CTTS absorbance to lower energy. There is a tradeoff, then, between photoreduction of the halocarbon at a more positive potential and using lower energy excitation. More positive potential of reduction is gained at the cost of higher energy excitation. Thus, systems for catalytic photoreduction of halocarbons at a specified potential or wavelength could be designed by judicious choice of the metallocene component.

Acknowledgments. This work was supported in part by the United States Department of Energy, Office of Basic Energy Science, Division of Chemical Sciences. We thank Dr. James R. Valentine for preparation of **II**, and we thank Ivan Lorkovic for preparation of **III**. The work described chapter is the result of a collaborative effort with Dr. Lawrence F. Hancock and will be submitted for publication in the *Journal of Physical Chemistry*.

Table I. Metallocene-Halocarbon CTTS

Donor-Acceptor	Photocurrent Peak (nm)	Absorbance Peak (nm)	Metallocene $E^{1/2}$ (V vs. SCE)	Approx. Onset of Halocarbon Reduction (V vs. SCE)
FcEMA-$CHCl_3$	275[a]	284[b]	+0.35[c]	-1.5[c]
FcEMA-CCl_4	335[d]	320[f]	+0.35[c]	-0.6[c]
FcEMA-$CHBr_3$	340[a]	316[b]	+0.35[c]	-0.9[c]
FcEMA-CBr_4	352[a]	372[b]	+0.35[c]	-0.9[c]
Me_8FcPMA-CCl_4	365[d]	350[e]	+0.05[g]	-0.6[g]
CcSiO-CH_2Cl_2	330[h]	320[i]	-0.62[g]	<-0.8[g]

[a] Electrodeposited film of metallocene polymer on Pt in CH_3CN/0.5 M acceptor/ 0.1 M [*n*-Bu4]PF_6.

[b] 6 mM ferrocene and 0.5 M acceptor both in CH_3CN/0.1 M [*n*-Bu4]PF_6.

[c] CH_3CN/0.5 M acceptor/ 0.1 M [*n*-Bu4]PF_6.

[d] Electrodeposited film of metallocene polymer on Pt in CH_3CN/50% acceptor/ 0.1 M [*n*-Bu4]ClO_4.

[e] Cast film of metallocene polymer in CH_3OH/0.1 M [*n*-Bu4]ClO_4 and CH_3CN/50% acceptor/ 0.1 M [*n*-Bu4]ClO_4.

[f] Electrodeposited film on indium-tin oxide/quartz electrode in CH_3CN/0.1 M [*n*-Bu4]ClO_4 with and without 50% acceptor.

[g] CH_3OH/50% acceptor/ 0.1 M [*n*-Bu4]ClO_4.

[h] Electrodeposited film on Pt electrode in CH_3OH/50% acceptor/0.1 M [*n*-Bu4]ClO_4.

[i] Electrodeposited film on indium-tin oxide/quartz electrode in CH_3OH/0.1 M [*n*-Bu4]ClO_4 with and without 50% acceptor.

References

1. (a) Brand, J. C. D.; Snedden, W. *Trans. Faraday Soc.* **1957**, *53*, 894. (b) Geoffrey, G. L.; Wrighton, M. W. *Organometallic Photochemistry*; Academic: New York, **1979**.

2. (a) Jaworska-Augustyniak, A.; Wojtczak, J. *Monat. Chem.* **1979**, *110*, 1113. (b) Jaworska-Augustyniak, A.; Wojtczak, J. *Transition Met. Chem.* **1987**, *12*, 167.

3. Dautartas, M. F.; Mann, K. R.; Evans, J. F. *J. Electroanal. Chem.* **1980**, *110*, 379.

4. (a) Germanova, L. F.; Balabanova, L. V.; Vasil'eva, T. T.; Shvenkhgeimer, M.-G. A.; Kochetkova, N. S.; Nelyubin, B. V. *Izv. Akad. Nauk SSSR, Ser. Khim.* **1985**, *7*, 1490. (b) Jaworska-Augustyniak, A. *Transition Metal Chem.* **1982**, *7*, 16. (c) Velichko, F. K.; Balabanova, L. V.; Vasil'eva, T. T.; Bondarenko, O. P.; Shvekhgeimer, G. A. *Isv. Akad. Nauk SSSR. Ser. Khim.* **1987**, *3*, 711. (d) de Violet, P. F.; Logan, S. R. *J. C. S. Faraday I* **1980**, *76*, 578. (e) Gerbert, E.; Reis, A. H.; Miller, J. S.; Rommelmann, H.; Epstein, A. J. *J. Amer. Chem. Soc.* **1982**, *104*, 4403. (f) Traverso, O.; Scandola, F.; Carassiti, V. *Inorg. Chim. Acta*, **1972**, *6*, 471. (g) Petrova, A. A.; Zver'kov, V. A.; Tsura, A. N.; Vannikov, A. V. *Isv. Akad. Nauk. SSSR, Ser. Khim.* **1991**, 346.

5. (a) Traverso, O.; Scandola, F. *Inorg. Chim. Acta.* **1970**, *4*, 493. (b) Jaworska-Augustyniak, A.; Wojtczak, J. *Transition Met. Chem.* **1984**, *9*, 303. (c) Papsun, D. M.;

Thomas, J. K.; Labinger, J. A. *J. Organomet. Chem.* **1981**, *208*, C36. (d) Bergamini, P.; Di Martino, S.; Maldotti, A.; Sostero, S.; Traverso, O. *J. Organomet. Chem.* **1989**, *365*, 341.

6. Ouchi, T.; Taguchi, H.; Imoto, M. *J. Macromol. Sci. Chem.* **1978**, *A12*, 710.

7. (a) Akiyama, T.; Hoshi, Y.; Goto, S.; Sugimori, A. *Bull. Chem. Soc. Jpn.* **1973**, *46*, 1851. (b) Akiyama, T.; Sugimori, A.; Hermann, H. *Bull. Chem. Soc. Jpn.* **1973**, *46*, 1855. (c) Akiyama, T.; Kitamura, T.; Kato, T.; Watanabe, H.; Serizawa, T.; Sugimori, A. *Bull. Chem. Soc. Jpn.* **1977**, *50*, 1173.

8. Rabek, J. F.; Lucki, J.; Zuber, M.; Qu, B. J.; Shi, W. F. *J. Macromolec. Sci. Pure Appl. Chem.* **1992**, *A29*, 297.

9. Zou, C.; Wrighton, M. S. *J. Am. Chem. Soc.* **1990**, *112*, 7578.

10. Simon, R. A.; Mallouk, T. E.; Daube, K. A.; Wrighton, M. S. *Inorg. Chem.* **1985**, *24*, 3119.

11. (a) Feldman, B. J.; Feldberg, S. W.; Murray, R. W. *J. Phys. Chem.* **1987**, *91*, 6558. (b) Nishihara, H.; Dalton, F.; Murray, R. W. *Anal. Chem.* **1991**, *63*, 2955.